Pharmacokinetics and Physiologically Based Pharmacokinetic Modeling of Xenobiotic Disposition in Special Populations

Jing Jing

A dissertation

submitted in partial fulfillment of the

requirements for the degree of

Doctor of Philosophy

University of Washington

2017

Reading Committee:

Nina Isoherranen, Chair

Thomas Burbacher

Bhagwat Prasad

Program Authorized to Offer Degree:

Pharmaceutics

University of Washington

Abstract

Pharmacokinetics and Physiologically Based Pharmacokinetic Modeling of Xenobiotic Disposition in Special Populations

Jing Jing

Chair of the Supervisory Committee:

Professor, Nina Isoherranen

Department of Pharmaceutics

Due to the alteration of the physiological functions, the disposition of xenobiotics is often changed under disease conditions and during pregnancy compared with the healthy status. Under disease conditions including chronic kidney disease (CKD) and cancer, altered physiological functions including changes in liver and kidney function have critical impact on the pharmacokinetics of xenobiotics. During pregnancy, the changes in organ blood flow, plasma protein binding and the expression of hepatic drug metabolizing enzymes can also affect the intrinsic capacity of the organ to metabolize and excrete xenobiotic. However, little is known on the disposition of vitamin A and its metabolites including all-*trans* retinoic acid (*at*RA) in CKD and cancer patients and the disposition of domoic acid (DA), a shellfish toxin, during pregnancy.

The aims of the thesis project is to better characterize the disposition of retinoids in CKD and cancer patients, evaluate the disposition of DA before and during pregnancy in non-human primates and utilize the obtained in vitro and in vivo information to develop physiologically based pharmacokinetic (PBPK) model to simulate the disposition of *at*RA and DA.

To evaluate the disposition of endogenous retinoids and their carrier proteins in CKD patients in comparison to healthy subjects, retinoids and their carrier proteins such as retinol binding protein (RBP4) concentrations in plasma and urine from 55 adult CKD patients and 21 matched healthy subjects were measured. RBP4 and retinol levels were increased approximately 2-fold in patients with CKD. RBP4 renal clearance was higher in patients with CKD than healthy subjects but not associated with estimated glomerular filtration rate (eGFR). Circulating concentrations of *at*RA increased and concentrations of 13*cis*RA decreased in subjects with CKD with no change in RA-to-retinol ratio. Increases in circulating retinol, RBP4, and *at*RA may be due to increased hepatic RBP4 synthesis, retinyl ester hydrolysis, and/or hepatic secretion of RBP4-retinol.

To better characterize and understand the disposition of therapeutically administered *at*RA in healthy and cancer patients in the presence and absence of inhibitors of *at*RA metabolism, a population based PBPK model of *at*RA disposition incorporated saturable metabolic clearance of *at*RA, induction of CYP26A1 by *at*RA and the absorption and distribution kinetics of *at*RA was developed and verified using in vitro and in vivo data. The developed model can be used for the interpretation of *at*RA disposition and efficacy, design of novel dosing strategies, and development of next-generation *at*RA metabolism inhibitors.

To investigate the disposition of DA, toxicokinetics of DA were characterized in female cynomolgus monkeys, following a single 5 µg/kg IV bolus dose and single 0.075 mg/kg and 0.15

mg/kg PO dose before pregnancy. Following IV dosing, DA had a distribution volume of 145 ± 69 ml/kg, systemic clearance of 139 ± 70 ml/hr/kg and elimination half-life of 1.4 ± 1.0 hours. However, following PO dosing, the average terminal half-life of DA was 11± 3.7 hours, indicating that after PO administration DA disposition follows flip-flop kinetics with slow rate-limiting absorption. The absolute bioavailability of DA was 7 ± 4 %. DA was primarily renally eliminated with renal clearance of 104 ± 47 ml/hr/kg. The developed DA PBPK model in monkeys simulated the flip-flop kinetics observed after oral administration and allowed the simulation of urinary excretion and brain and kidney distribution of DA, following IV and PO dosing. DA toxicokinetics were further characterized in monkeys during pregnancy following chronic dose of 0.15 mg/kg/day DA. Decreased AUC of DA and increased DA renal clearance were observed during pregnancy. DA was detected in both plasma and urine samples of delivered infants.

TABLES OF CONTENTS

LIST OF FIGURES

LIST OF TABLES

ACKNOWLEDGEMENTS

I would like to thank my advisor, Dr. Nina Isoherranen for her guidance, support and encouragement. I am very grateful for being her student to learn from her and be inspired by her. I have always been motivated by her energy, enthusiasm and passion for science. I would like to thank her for the scientific discussion we had on each of my thesis project and the time and effort she put into helping me become a better scientist in pharmacokinetics. She was also very supportive for my professional development and offered many opportunities for me to explore potential career pathways.

I would also like to thank everybody in Dr. Isoherranen's lab. I had great time working with them and they had been very supportive. I enjoyed discussing with them on research projects and learning from each other.

I would like to thank my friends Alenka Jaklic and Zufei Zhang for their support during my time in graduate school.

Additionally, I would like to thank Dr. Thomas Burbacher and Dr. Catherine Yeung for their guidance on my projects. I would also like to thank Dr. Bhagwat Prasad and Dr. Danny Shen for serving on my committee.

DEDICATION

I would like to dedicate this dissertation to my parents, Hui Lei and Jianqi Jing. Thank you for your love, support and encouragement throughout the years.

Chapter 1.

Introduction

1.1 XENOBIOTIC DISPOSITION IN SPECIAL POPULATIONS

Pharmacokinetics is dependent on a variety of physiological variables such as age, ethnicity, genotype or pregnancy, and pathological conditions such as renal and hepatic function. Individuals with altered physiological and pathological conditions are defined as special populations, including geriatrics, pediatrics, various racial or ethnic groups, patients with renal and hepatic impairment, and pregnant women. In comparison with healthy individuals, absorption, distribution, metabolism and excretion (ADME) of xenobiotics can be significantly altered in these special populations due to the changes of physiological parameters (Table 1.1).

In patients with impaired renal function, the elimination of drugs that are excreted primarily through kidney decreases, resulting in the accumulation of drugs in the body. Moreover, changes of plasma binding proteins and hepatic drug metabolizing enzyme and transporters activities have also been observed in certain patients with severe renal disease (Verbeeck and Musuamba, 2009). In patients with liver disease, gastrointestinal dysfunction, reduction of hepatic cytochrome P450 (CYP) enzyme activities including CYP1A2, CYP2C19, CYP2D6 and CYP2E1, decrease of plasma albumin and α1-acid glycoprotein levels and liver blood flow, hepatic transporter expressions and biliary excretion have been reported (Verbeeck, 2008). In pediatric population, the age dependent expression and activity of CYP enzymes, UDP-glucuronosyltransferases (UGTs) and transporters were observed (Fernandez *et al.*, 2011; Prasad *et al.*, 2016). Moreover, compared to adults, gastric pH and emptying time, body fat and plasma binding protein level and glomerular filtration rate (GFR) are different in neonates and infants (Lu and Rosenbaum, 2014). In pregnant women, the activity of CYPs and UGTs and drug transporters, GFR, gastric pH, plasma volume, total body water, body fat, cardiac output and portal vein blood flow are elevated, while the plasma concentrations of albumin and α1-acid

glycoprotein decrease during pregnancy (Isoherranen and Thummel, 2013; Maisa Feghali *et al*., 2015). However, due to the simultaneous changes of multiple physiological properties, it's difficult to predict the effects of physiological changes on pharmacokinetics and drug exposure levels in these special populations.

Due to the increased awareness of pharmacokinetic changes in special populations, specific considerations have been taken in relation to clinical study design, drug dosing and labelling in special populations. Numerous guidance has been established by the FDA and other regulatory agencies to assist industry to conduct studies to assess the influence of physiological and pathological changes such as renal and hepatic impairment on the pharmacokinetics of the investigational drugs. Dosage adjustment caused by the alteration of pharmacokinetics of drugs in specific population is required to be described in labels (FDA, 2016). However, the information of disposition of some xenobiotics and endobiotics in special populations that are under potential risk of changed exposure levels is still missing.

Therefore, in this thesis project, disposition of xenobiotics and endobiotics has been specifically evaluated in patients with chronic kidney disease (CKD) and cancer as well as during pregnancy. The following sections provide the overall background for the current knowledge of the impact of physiological changes on pharmacokinetics in these special populations.

1.2 PHARMACOKINETIC CHANGES IN PATIENTS WITH CHRONIC KIDNEY DISEASE

CKD is defined as kidney damage or GFR < 60 ml/min/1.73 m^2 for 3 months or more, irrespective of cause (Levey *et al.*, 2005). CKD is a common type of renal impairment and different from acute kidney injury. CKD is often not reversible with treatment. CKD progresses

from stage 1 to stage 5 with declining estimated glomerular filtration rate (eGFR) (Figure 1.1). At early stage, stage 1 and 2, patients have normal eGFR, but damaged kidney, often proteinuria occurs in these patients. At stage 5, which is also called end stage renal disease (ESRD), patients often need either dialysis or kidney transplant. For CKD patients, drugs that are eliminated predominately by renal excretion, adjustment of dosage regimen is usually needed to avoid the toxic effects of excessive accumulation of the drug and/or its active metabolite(s) caused by the decreased eGFR (Matzke *et al.*, 2011). FDA has published guidance to assist in the evaluation of pharmacokinetics and established the labelling guidance on dosage adjustment in patients with impaired renal function including patients with CKD (FDA, 2010). Label with dose adjustment is required when renal clearance is predominant and pharmacokinetic changes are clinically significant based on exposure-response of the drug.

Besides the decrease of eGFR, the expression of megalin, an endocytic receptor on the renal proximal tubule, is decreased in CKD based on rat studies (Takemoto *et al.*, 2003). Although more studies are needed to evaluate megalin function and expression in patients with CKD, accumulating evidence suggested that vitamin D deficiency in patients with CKD is likely caused by reduced megalin expression and decreased reabsorption of urinary 25(OH)D via megalin, the precursor of active form of vitamin D, 1,25(OH)2D (Obi *et al.*, 2015). The decreased megalin expression in CKD patients may also contribute to the altered reabsorption of numerous megalin substrates including retinol binding protein 4 (RBP4), albumin and antibiotics such as aminoglycosides, polymyxin B and colistin (Nielsen *et al.*, 2016).

Drugs that are primarily eliminated by non-renal mechanisms can also accumulate in patients with CKD if their dosage regimen is not adjusted. It has been reported that the plasma warfarin S/R ratio increased by approximately 50% in ESRD patients compared with control

subjects indicating reduced CYP2C9 activity in these patients since S-warfarin is metabolized predominately by CYP2C9 and R-warfarin is metabolized by multiple CYP and non-CYP pathways (Dreisbach *et al.*, 2003). Besides CYP2C9, reduced expression and activities of hepatic and intestinal CYP enzymes and transporters such as CYP2C19, organic anion-transporting polypeptide (OATP) and P-glycoprotein (P-gp) have also been shown in animals and humans with CKD (Dreisbach and Lertora, 2008). The impact of CKD on CYP enzymes and transporters is likely caused through direct inhibition by circulating uremic toxins and/or by reduction of hepatic CYP gene expression in patients with CKD (Barnes *et al.*, 2014; Velenosi *et al.*, 2014). Upon incubating human liver microsomes with a combination of the four uremic toxins including benzyl alcohol, p-cresol, indoxyl sulfate and hippuric acid at concentrations similar to those found in CKD patients, greater than 50% inhibition of CYP2E1 and CYP3A4 was observed (Barnes *et al.*, 2014). On the other hand, the downregulation of CYP enzymes may be explained by decreased nuclear receptor binding and histone acetylation. As shown in rat CKD model, the binding of pregnane X receptor (PXR) and hepatic nuclear factor 4α (HNF-4α) to the promoter of CYP3A2 and CYP2C11decreased and histone 3 acetylation in the promoter of CYP3A2 and CYP2C11 diminished (Velenosi *et al.*, 2014), leading to the decreased mRNA expression of CYP3A2 and CYP2C11.

Besides the changes of drug metabolizing enzymes and transporters, the decrease of albumin binding capacity with the progression of CKD was also reported in patients with CKD, which in turn could influence the distribution and elimination of drugs (Klammt *et al.*, 2012). Moreover, due to the presence of uraemic gastritis, diabetic and/or uremic gastroparesis respectively, the gastric acidity and gastric emptying time is usually altered in patients with CKD (Arnouts *et al.*, 2014), which may cause the alteration of the absorption and bioavailability of

drugs. Taken together, these changes suggest that pharmacokinetics of drugs are altered in CKD due to multiple mechanisms that affect ADME of the drugs of interest. Hence, it is critical to characterize the disposition of drugs that are dosed in patients with CKD, to provide appropriate dosing recommendations and better understand the mechanism of pharmacokinetic changes.

1.3 PHARMACOKINETIC CHANGES IN PATIENTS WITH CANCER

Cancer is a major public health problem in the United States and worldwide. In contrast to most other therapeutic areas, clinical trials of anticancer drugs are usually directly conducted in cancer patients due to the toxicity and side effects of anticancer drugs. Notably, the changes of numerous physiological parameters at the presence of tumors can affect the ADME characteristics of anticancer agents. However, the knowledge of how drug disposition is altered between cancer patients and healthy subjects is not well characterized.

The absorption of orally administered drugs in cancer patients can be affected by a variety of sources including previous surgery, radiation or chemotherapy, nausea and/or vomiting, special diet, genetic differences in intestinal drug-metabolizing and drug-transport systems, altered intestinal transit time, gastrointestinal pH and concomitant medications (Argilés, 2005). The differences in amount of body fat and/or concentration of plasma proteins can change drug distribution in cancer patents. In fact, the mean plasma α1-acid glycoprotein concentrations in breast, lung and ovarian cancer patients were two-fold higher than those in the healthy population (Duché et al., 2000). Lower hematocrit and albumin levels were also observed in cancer patients (Cheeti et al., 2013). These changes in plasma proteins suggest that plasma protein binding of drugs is altered in cancer patients in a drug dependent manner.

Moreover, cancer patients, especially individuals having hepatic dysfunction such as liver cancer patients, may also experience reduced drug metabolism due to reduced CYP activities compared to healthy individuals. Indeed, reduced CYP2C19 activity has been reported in patients with advanced metastatic cancer compared with a healthy reference population (Williams et al., 2002). In addition, altered hepatic blood flow and differences in hepatic drug-transport systems can also contribute to altered hepatic clearance. It has been shown that OATP1B1 and OATP1B3 were downregulated in liver tumors (Pressler et al., 2011). Furthermore, myeloma kidney, urinary tract obstruction, drug induced nephropathy or major surgical procedures caused renal dysfunction in cancer patients may also change the renal excretion of drugs (Lameire et al., 2005). Taken together, these altered ADME processes in cancer patients are likely to alter the dosing requirements of drug in cancer patients when compared to healthy subjects.

The differences in the age distribution in cancer patients versus healthy subjects can also contribute to the potential differences in drug dispositions in cancer patients. The age-related changes in physiological conditions can make a significant impact on the disposition of drugs caused by the altered physiological variables including reduced gastric-acid secretion and gastrointestinal motility, increased proportion of body fat, reduced intracellular water and plasma albumin, reduced liver mass and CYP activity and reduced hepatic and renal blood flow as well as GFR (Undevia et al., 2005).

Due to the diversity of tumor types and disease burden, large pharmacokinetic variability of ADME is commonly observed in patients with cancer. However, the impact of changed physiological parameters on drug disposition in specific cancer type is not well evaluated. Therefore, conducting of appropriate pharmacokinetic studies to better understand the

mechanisms underlying pharmacokinetic changes is important for individualized dosing regimen and the improvement of the treatment outcomes in patients with cancer.

1.4 PHARMACOKINETIC CHANGES DURING PREGNANCY

Despite the awareness of the risk to both mother and the fetus of using medications during pregnancy, maternal use of medications during pregnancy is common to treat a variety of preexisting chronic medical conditions such as epilepsy, asthma and hypertension, acute conditions such as influenza, and pregnancy-related conditions such as gestational diabetes. In fact, between 2006 and 2008, about 82% of pregnant women had experiences of taking medications during pregnancy (Mitchell *et al.*, 2011). Interviews conducted among nearly 20,000 U.S. and Canadian women over 25 years showed a mean of 2.3 medications used during pregnancy, excluding vitamins and minerals (Mitchell *et al.*, 2011). However, for large portion of medications taken by pregnant women information on efficacy and safety during pregnancy is incomplete since pregnant women are generally not included in clinical studies. Dynamic physiological alterations during pregnancy including changes of blood and body composition and organ systems such as cardiovascular, hepatic, renal and gastrointestinal systems (Costantine, 2014) can induce profound changes to pharmacokinetic properties of medications in pregnant women.

During pregnancy the concentrations of plasma proteins such as albumin and α1-acid glycoprotein decrease and total body water and fat increase, which can decrease the plasma protein binding and increase the volume of distribution of drugs. Cardiac output and glomerular filtration rate also increase during pregnancy which can have impacts on the rate of distribution and renal excretion, respectively (Thomas and Yates, 2012). Moreover, gastric emptying is delayed and gastric pH increases as pregnancy progresses, which may affect the bioavailability

of drugs. Nausea and vomiting, a common problem in early pregnancy, may also contribute to the alteration of drug bioavailability (Costantine, 2014). Furthermore, activities of drug metabolizing enzymes, such as CYP1A2 is reported to be decreased, while activities of CYP2C9, CYP2D6, CYP3A4, CYP2E1 and UGT1A4 increased during pregnancy as determined using probe drugs (Isoherranen and Thummel, 2013; Tasnif *et al.*, 2016). Besides enzymes, transporters including organic cation transporter 2 (OCT2), P-gp, and organic anion transporter 1(OAT1) activities also increased during pregnancy (Tasnif *et al.*, 2016).

The pharmacokinetic changes during pregnancy can result in toxicity or lack of efficacy of drugs in pregnant women and also leave fetus at potential risk of unintended toxicities, teratogenicity and adverse effects through exposure to drugs and toxins transferred from maternal side. Drugs can passively diffuse across the placenta or be transferred to fetal circulations by transporters expressed on the placenta. The quantitative assessment of fetal exposure to drugs during pregnancy, especially during early gestation cannot be conducted in humans. Animal models are often used for studying fetal exposures and understanding the mechanism of movement of drugs between the maternal and fetal circulations. Taken together, characterization of drug disposition during pregnancy is critical to provide appropriate dosing recommendations to pregnant women to protect maternal and fetal health.

1.5 PBPK MODELING TO CHARACTRIZE DRUG DISPOSITION IN SPECIAL POPULATIONS

PBPK modeling is an approach used for the simulation and prediction of ADME of xenobiotics and endobiotics in humans and in animal species. PBPK models consist of two major components: system-specific component and drug-dependent component (Figure 1.2). System-specific component is independent of drugs and includes physiological parameters such as organ

volume and composition, organ blood flow, enzyme and transporter localization and abundance, and plasma protein concentrations (Maharaj and Edginton, 2014). The system-specific component describes the anatomical arrangement of the tissues and organs that are linked by perfusing blood in humans and animals. Drug dependent component includes parameters that are critical to determine the ADME properties of the drug such as physiochemical properties, plasma-protein binding affinity, membrane permeability and enzyme and transporter kinetics (Rowland *et al.*, 2011). PBPK models are frequently used for internal decision-making in drug development on first in human study, dose predictions, compound selection, food effect assessments drug-drug interaction (DDI) predictions and cases to address regulatory questions in pharmaceutical industry (Jones *et al.*, 2015). According to the review on PBPK modeling of pharmaceutical agents in humans published in English between 2008 and May 2015, PBPK models were most commonly used for the prediction of DDI (28%) and interindividual variability and clinical pharmacokinetics (23%) (Sager *et al.*, 2015).

Due to the incorporation of intrinsic factors such as tissue blood flows and GFR in the system specific component (Figure 1.2) of PBPK model, it is possible to include the physiological and pathological features in PBPK models to simulate and predict pharmacokinetics in specific physiological conditions or in disease states. In fact, PBPK modeling approach has been increasingly used in simulating and predicting the effects of physiological and pathological changes on drug disposition (Sager *et al.*, 2015). A review of the literature reported that PBPK modeling related to the age-related changes in pharmacokinetics and pregnancy accounted for 10% and 2% of the overall published PBPK models between 2008 and May 2015, (Sager et al., 2015). Moreover, FDA suggested the use of PBPK modeling in the latest guidance documents on hepatic and renal impairment populations (Wagner *et al.*, 2015).

However, the confidence of PBPK modeling in special populations remains to be low to moderate due to the limited knowledge of the abundance of CYP, non-CYP enzymes and transporters and poor understanding of physiological changes in special populations (Jones *et al.*, 2015). As such there is a great need to develop PBPK models for variety of compounds to increase the understanding of the system specific changes in pharmacokinetics in special populations and to further develop PBPK modeling to allow better simulation approached for special populations.

1.6 All-TRANS RETINOIC ACID AND DOMOIC ACID AS MODEL COMPOUNDS

In this project, the disposition of xenobiotics in special populations including CKD, cancer and pregnancy was studied using two model compounds, all-trans retinoic acid (*at*RA) and domoic acid (DA).

1.6.1 All-Trans Retinoic Acid

*at*RA is the active metabolite of vitamin A and an endogenous signaling molecule. Vitamin A and *at*RA signaling is essential for growth and development, vision, a healthy immune system, reproduction, and healthy skin and barrier functions. Vitamin A is obtained from the diet either as preformed vitamin A, consisting predominantly of retinol and retinyl esters, or as provitamin A carotenoids, most importantly β-carotene (Bendich A, 1989). Retinyl esters are stored primarily in the liver stellate cells, the lungs and adipose tissues serving as the reservoir of vitamin A in the body. The esterification of retinol and the hydrolysis of the stored esters are regulated by lecithin retinol acyltransferase (LRAT) and retinyl ester hydrolase (REH) respectively (Figure 1.3). Circulating retinol is delivered to target tissues by its transport proteins RBP4 and transthyretin (TTR) and retinol is taken up to target cells mainly by uptake transporter

STRA6 (D'Ambrosio *et al.*, 2011). In target tissues, retinol is oxidized to retinal by or alcohol dehydrogenase or retinol dehydrogenase (ADH or RDH) and retinal can be reduced back to retinol by RDH and dehydrogenase reductase (DHRS) (Kedishvili, 2013). The formation of retinoic acid (RA) requires irreversible oxidation of retinal to RA by aldehyde dehydrogenase 1A (ALDH1A) (Bhat and Samaha, 1999), which appear to lay a critical role in controlling tissue *at*RA concentrations. RA has been reported to exist as at least five isomers, including *at*RA, 9-*cis*RA, 13-*cis*RA, 9,13-*dicis*RA, and 11-*cis*RA (Kane, 2012). Of the RA isomers, *at*RA is considered to be the biologically active and the primary enzymatic product of retinal oxidation. *at*RA regulates the cell cycle by binding to the nuclear retinoic acid receptors (RARs) to control the expression of target genes that are involved in differentiation and apoptosis in a concentration-dependent manner (Okada et al., 2004; Noy, 2010).While the clearance of RA is mediated predominantly by CYP26 in human liver (Thatcher and Isoherranen, 2009), the clearance of retinol may be mediated via metabolism to retinal, by esterification for storage and possible by filtration and megalin mediated reabsorption by the kidneys. The retinol -RBP4 complex can be filtered by the kidney due to its small size (21kDa), but after RBP4 is further bound with TTR in circulation, the complex is too large for filtration (Raghu and Sivakumar, 2004). Despite the filtration of retinol- RBP4, very little retinol or RBP4 ends up in the urine as the filtered retinol- RBP4 complex is reabsorbed in the proximal tubule cells by megalin. The critical role of megalin in maintaining vitamin A homeostasis has been shown in mice with a kidney-specific megalin deficiency. In this study, mobilization of hepatic vitamin A stores was accelerated to maintain normal plasma retinol (Raila *et al.*, 2005). However, the role of tubular cells in retinol metabolism and the role of kidney in maintaining systemic vitamin A homeostasis has not been well studied.

Despite the fact that vitamin A homeostasis is tightly regulated in healthy subjects, vitamin A homeostasis seems to be altered under disease states. In comparison to individuals with normal glucose tolerance, plasma RBP4 and retinol levels were altered in patients with type 2 diabetes (Erikstrup *et al.*, 2009). Similarly, the retinol to RBP4 ratio was reported to be significantly lower in obese subjects than non-obese subjects (Mills *et al.*, 2008). Moreover, serum RA concentrations in patients were shown to be lower in patients with nonalcoholic fatty liver disease (NAFLD) and nonalcoholic steatohepatitis (NASH) compared with control subjects (Liu *et al.*, 2015). However, the mechanisms of altered vitamin A homeostasis under disease conditions are not well understood.

Due to the activity of *at*RA in inducing apoptosis, *at*RA has been also pursued for the treatment of various cancers including non-small-cell lung cancer, head and neck cancer, astrocytoma, and Kaposi's sarcoma (Phuphanich *et al.*, 1997; Saiag *et al.*, 1998; Arrieta *et al.*, 2010; Lim *et al.*, 2012). *at*RA is also an approved drug for the treatment of acute promyelocytic leukemia (APL), in which therapeutic doses of *at*RA can overcome the blockage of differentiation caused by formation of promyelocytic leukemia-RARα fusion protein and trigger RAR-mediated promyelocyte differentiation. However, the use of *at*RA is limited due to the decreased plasma exposure levels and relapse in patients following chronic dosing of 22.5 mg/m^2 BID. Currently, *at*RA combined with arsenic trioxide is often used in the clinical treatment of APL. In the combination therapy, arsenic trioxide 0.15 mg/kg/day IV plus *at*RA 22.5 mg/m^2 BID is recommended (Iland *et al.*, 2012). However, this dosing regimen is designed on an empirical basis without detailed pharmacokinetic characterization or pharmacokinetic and pharmacodynamic rationale.

Due to the lack of intravenous dosage form of *at*RA, *at*RA disposition has never been evaluated following IV dose in humans. The mechanism of *at*RA absorption in gastrointestinal track, the distribution of *at*RA and elimination pathways of *at*RA are not well understood in humans especially in patients with cancer. The observed reduction of the plasma concentrations of *at*RA upon daily dosing explained by the induction of CYP26A1 based on the in vitro experiments (Tay *et al.*, 2010) has never been verified in humans. As *at*RA is dosed to different age groups and the disposition of *at*RA is subject to various nonlinearities, PBPK modeling is well suited to study *at*RA disposition in humans using the available in vitro and in vivo data.

1.6.2 Domoic Acid

Domoic acid (DA) is a water soluble, excitatory amino acid which is usually produced by the microscopic algae Pseudo-nitzschia in marine waters. It acts as a glutamate analog and is excitotoxic in the vertebrate central nervous system and other glutamate receptor-rich organs and affects numerous organisms including sea birds, dolphins and sea lions, as well as humans through food web (Mos, 2001a). The greatest risk of DA exposure for humans and marine wildlife comes from the dietary consumption of DA-contaminated marine organisms such as shellfish and finfish. Multiple DA poisoning incidents have occurred in marine mammals over the last few decades. Over 100 free-ranging adult California sea lions were reported to be intoxicated by DA during three harmful algal blooms between 1998 and 2000 in central and northern California coastal waters (Silvagni *et al.*, 2005). The only reported human DA poisoning incident occurred in Canada in 1987 during which clinical signs of acute toxicity such as gastrointestinal distress, confusion, disorientation, memory loss, coma and death were observed (Perl *et al.*, 1990). Due to the establishment of effective research and monitoring programs for the detection of DA in shellfish and coastal waters, no human DA poisoning has

been documented since this incident. However, DA producing algal blooms are increasing in frequency worldwide due to increased temperature and pollution in seawater posing an increasing threat to not only marine organisms but also human populations that consume relatively large amounts of shellfish and fish on a daily basis (Kathi A. Lefebvre and Robertson, 2010).

Since the two major factors that govern the toxicity of most compounds following oral ingestion are the rate and extent of gastro-intestinal absorption and the rate of elimination, toxicokinetic parameters must be studied in order to gain further insight into factors such as renal impairment and pregnancy that can increase an individual's susceptibility to DA-induced toxicity. However, no DA toxicokinetic information is available in humans due to the lack of sensitive measurement of DA at the time poisoning incidents occurred. Animal models are widely used in the study of DA disposition and toxicity. Studies in rats and monkeys showed that DA was mainly cleared from plasma through the kidneys (Suzuki and Hierlihy, 1993; Truelove J, 1994).

Due to the effective DA monitoring, acute DA intoxications in humans have been avoided, however concern remains about the potential impacts of chronic low-level DA exposure on risk human populations, including pregnant women and elderly patients with impaired and reduced renal function who consume shellfish and fish as the major source of protein. There is no information on the long term safety and effects due to chronic exposure of DA in humans. The complete information on DA elimination pathways, pharmacokinetic profile after chronic oral dosing and pharmacokinetic changes during pregnancy is missing. Therefore, studies of DA disposition in animal models following chronic oral dosing before and during pregnancy are

needed to better understand DA pharmacokinetics, potential risks of DA exposure and the requirements of adjusted tolerable daily intake in special populations.

1.7 HYPOTHESIS AND AIMS

The hypotheses of this thesis projects were: 1) vitamin A homeostasis is altered in patients with CKD and the changes are caused by the increased liver synthesis of retinol and RBP4, downregulation of vitamin A metabolism and altered utilization of dietary vitamin A in CKD patients; 2) The dose- and time- dependent disposition of *at*RA in healthy and cancer populations in the absence and presence of *at*RA metabolism inhibitors can be simulated using PBPK model, and *at*RA PBPK model can help better understand *at*RA pharmacokinetic changes in patients with cancer; 3) The disposition of DA is changed during pregnancy due to the altered physiological condition including increased glomerular filtration and renal blood flow. The long-term low-dose exposure to DA can cause accumulation of DA in monkeys and their fetuses and induce toxicity.

These hypotheses were addressed in the following specific aims:

Aim 1. Determine plasma and urine retinol, RBP4, *at*RA and 13*cis*RA levels and their association with eGFR in patients with CKD in comparison to matched healthy subjects and evaluate the mechanism of altered retinoids disposition in patients with CKD (Chapter 2)

Aim 2. Determine the physicochemical and absorption, distribution, metabolism and elimination properties of *at*RA through in vitro and in vivo experiments and use PBPK model to simulate complex pharmacokinetics and drug interactions with *at*RA in cancer patients (Chapter 3)

Aim 3. Characterize the toxicokinetics of DA in female cynomolgus monkeys following IV and PO dosing and develop PBPK model of DA in monkeys (Chapter 4)

Aim 4. Determine whether the toxicokinetics of DA in female cynomolgus monkeys is altered during pregnancy following chronic PO dosing when compared to non-pregnant animals (Chapter 5)

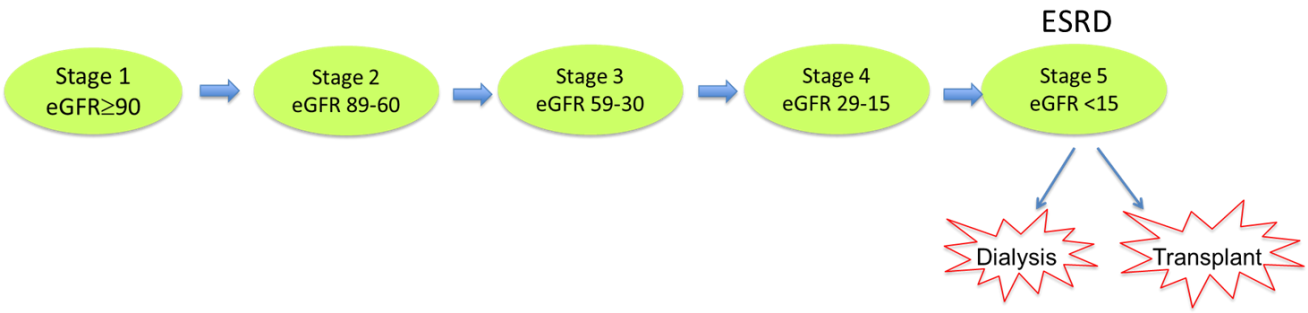

Figure 1.1. Progression of CKD. eGFR is in the unit of ml/min/1.73 m^2

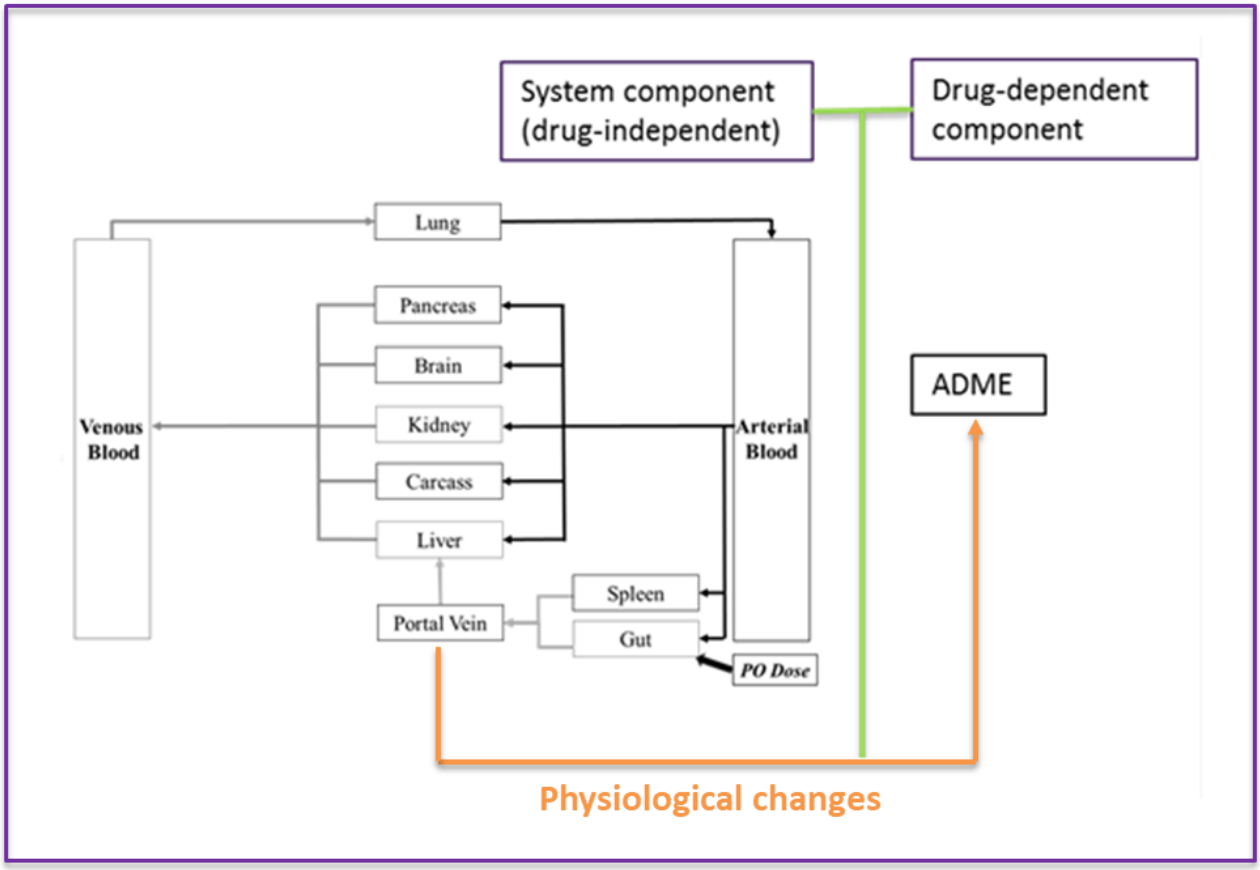

Figure 1.2. **Structure of a PBPK model.** A PBPK model incorporate system-specific component and substrate/drug-dependent component. Physiological changes occurring in the system component can alter ADME of a xenobiotic or endobiotic compound.

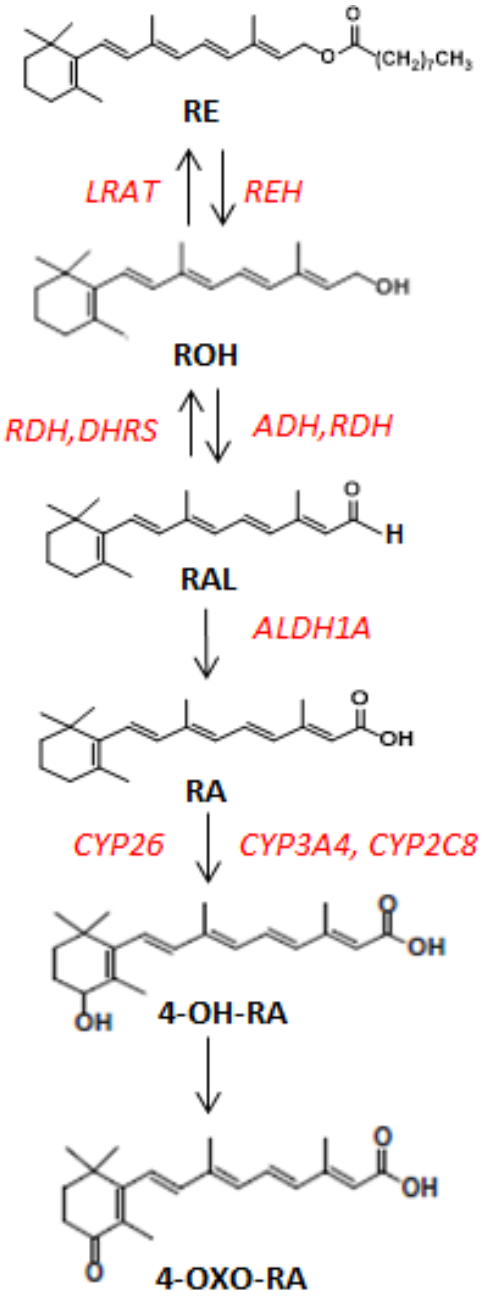

Figure 1.3. Vitamin A metabolism in healthy subjects

Table 1.1. Summary of changed physiological parameter in special populations that affects ADME of xenobiotics

Special populations	Changed physiological parameters
Renal impairment patients	GFR, plasma binding protein level, activity and expression of drug metabolizing enzymes and transporters
Hepatic impairment patients	Gastrointestinal dysfunction, activity and expression of Drug metabolizing enzymes and transporters, plasma binding protein level, liver blood flow and biliary excretion
Pediatrics	Gastric pH and gastric emptying time, GFR, plasma binding protein, body fat, drug metabolizing enzymes and transporters
Pregnant women	Cardiac output, portal vein blood flow, GFR, drug metabolizing enzymes and transporters, plasma binding protein level, gastric pH, plasma volume, total body water, body fat

Chapter 2.

Chronic Kidney Disease Alters Vitamin A Homeostasis via Effects on Hepatic RBP4 Protein Expression and Metabolic Enzymes

This chapter was published in *Clin Transl Sci (2016) 9, 207–215*

2.1 ABSTRACT

Vitamin A, via retinoic acid (RA), is a critical micronutrient. Normally, plasma concentrations are tightly regulated. Concentrations of vitamin A metabolites (13*cis*-RA, *at*RA) and relationships between RBP4 and retinoids have never been fully evaluated in adult patients with CKD. We measured retinoid and RBP4 concentrations in plasma and urine from 55 adult patients with CKD and 21 matched healthy subjects. RBP4 and retinol levels were increased approximately twofold in patients with CKD, with a negative correlation between plasma retinol and eGFR ($p = 0.006$) and plasma RBP4 and eGFR ($p = 0.0007$). RBP4 renal clearance was higher in patients with CKD than healthy subjects but not associated with eGFR. Circulating concentrations of *at*RA increased and concentrations of 13*cis*-RA decreased in subjects with CKD with no change in RA-to-retinol ratio. Increases in circulating retinol, RBP4, and *at*RA may be due to increased hepatic RBP4 synthesis, retinyl ester hydrolysis, and/or hepatic secretion of RBP4-retinol.

2.2 INTRODUCTION

Chronic kidney disease (CKD) is associated with a higher incidence of cardiovascular disease and diabetes, and lower bone mineral density (USRDS 2013 Annual Data Report). Inability to biologically access critical micronutrients may play a role in the development and progression of these comorbid conditions in patients with CKD. This association has been well-established for vitamin D, a fat-soluble micronutrient that requires bioactivation by the kidney in order to regulate circulating levels of calcium and phosphorous (Bosworth and de Boer, 2013). Circulating concentrations of vitamin A (which includes retinol and retinyl esters) and vitamin A metabolites, particularly bioactive all-trans retinoic acid (*at*RA), essential for cellular maintenance, gene regulation, lipid metabolism, and inflammatory response, also seem to be

altered in patients with CKD (Frey *et al.*, 2008; Henze *et al.*, 2010; Manickavasagar *et al.*, 2014). The inability to regulate the bioactivation or transport of vitamin A to target tissues has been associated with fracture risk (Michaëlsson *et al.*, 2003), atherosclerosis/ cardiovascular disease (Lambadiari *et al.*, 2014), and diabetes (Erikstrup *et al.*, 2009), and may contribute to development of these comorbidities in patients with CKD.

In healthy individuals, circulating concentrations of retinol, *at*RA, and retinol binding protein 4 (RBP4) are tightly regulated with plasma concentrations varying less than 20%, 23%, and 3%, respectively, in the healthy population (Chen *et al.*, 1996; Makimura *et al.*, 2009). Vitamin A is obtained from the diet either as provitamin A carotenoids or as preformed vitamin A (Figure 2.1), the plasma concentrations of retinol and retinoic acids (RAs) are regulated by a complement of enzymes that are responsible for storing and remobilizing vitamin A in the liver and synthesizing RA from the retinol precursor in a tightly controlled manner. In adults with CKD, serum concentrations of RBP4 and retinol have been reported to be elevated but it is unclear whether kidney disease itself or CKD related comorbidities causes altered vitamin A homeostasis (Frey *et al.*, 2008; Henze *et al.*, 2008, 2010; Barazzoni *et al.*, 2011). In pediatric subjects with CKD, but without commonly occurring adult comorbidities (e.g., diabetes and hypertension), circulating concentrations of retinol, its metabolites, and carrier proteins are dysregulated, suggesting that decreased kidney function, and not the presence of other medical conditions, is the primary driver of altered vitamin A homeostasis (Manickavasagar *et al.*, 2014). Despite this, the role of the kidneys in regulating vitamin A homeostasis is uncharacterized and, therefore, in contrast to the well understood mechanisms of how CKD decreases the active metabolite of vitamin D, the mechanisms by which decreased kidney function alters vitamin A homeostasis, and the concentrations of these tightly regulated compounds are completely

unknown. The observed accumulation of circulating RBP4 and retinol in patients with CKD might be explained by the impaired ability of the kidneys to excrete RBP4 and retinol by decreased metabolism of retinol to its active metabolite, *at*RA, or by activation of a yet uncharacterized renal-hepatic signaling pathway resulting in increased hepatic synthesis and secretion of RBP4 with accompanying mobilization of retinol from hepatic stores. We hypothesize that circulating concentrations of RBP4, retinol, and *at*RA are elevated in subjects with CKD due to alterations in hepatic mechanisms of retinoid regulation. Thus, the objectives of this study were to evaluate circulating vitamin A, *at*RA, and RBP4 in individuals with CKD in comparison with matched healthy adults and to differentiate the role of altered renal clearance and hepatic metabolic processes in driving altered vitamin A homeostasis in CKD.

2.3 MATERIALS AND METHODS

2.3.1 Study Population

The study population comprising of 55 patients with CKD and 21 matched healthy subjects was obtained from the Seattle Kidney Study or Healthy Kidney Study (Bosworth *et al.*, 2012).The Seattle Kidney Study is a nephrology clinic-based prospective cohort study of patients with CKD based in Seattle, WA, USA, designed to evaluate long-term complications of CKD. Healthy subjects were matched to these subjects based on gender, age, and body mass index (BMI; ±10%). Institutional review boards at the University of Washington and Veterans Affairs Puget Sound Health Care System approved the Seattle Kidney Study and Healthy Kidney Study and all participants provided written informed consent.

2.3.2 Dietary Vitamin A Intake

Food diaries were administered to the participants in this study. These subjects received approximately 1 h of training from a dietician on how to record all dietary intake, including specific ingredients and brand names, snacks, fruits, coffee, and tea. Participants were instructed to complete the prospective diary every other day for 5 days to include at least one weekend day. Diaries were returned to the dietician who entered all recorded items into the Nutrition Data Recall System for Research software system (Minneapolis, MN, USA). Plasma and urine sample collections were obtained concurrently with the participants' diet records.

2.3.3 Analytical Measures

Clinical data including age, gender, race, BMI, estimated glomerular filtration rate (eGFR), urine albumin, history of diabetes mellitus, and history of dialysis were collected from the Seattle Kidney Study and Healthy Kidney Study data repository. The eGFR was determined using the serum creatinine based CKD-EPI equation (Levey *et al.*, 2006). Urine albumin-to-creatinine ratio was determined from a 12-h urine collection. RBP4 renal clearance was calculated using the equation 2.1:

$$\text{Renal clearance} = \frac{Rate\ of\ urinary\ excretion}{Plasma\ concentration} = \frac{dA_e/dt}{C} \qquad \text{Equation 2.1}$$

where A_e is the amount of RBP4 excreted in urine in a given time t, and C is the RBP4 plasma concentration.

2.3.4 Bioanalytical Methods

Blood and urine samples were stored at −80°C. All sample processing, preparation, and extraction were conducted on ice under red light to minimize degradation of retinoids. For retinoid measurement, 80 µl acetonitrile was added to 40 µl plasma and urine with 20 µM retinyl

acetate (for retinol measurement) or 40 nM 13*cis*-RA-d_5 as internal standard, and the samples were centrifuged at 3,010 × g at 4°C for 40 min. The supernatant was collected for analysis. Plasma retinol was measured with an Agilent 1200 Series HPLC System, equipped with an Agilent extend-C18 column (5μm, 2.1 × 150 mm; Agilent Technologies), mobile phase consisting of acetonitrile/H2O/glacial acetic acid-90/10/2 at a flow rate of 0.4 mL/min for 7.5 min. Retinol was detected at a wavelength of 325 nm. A retinol standard curve for quantification was constructed in DC MASS SPECT GOLD human serum (Golden West Biologicals, Temecula, CA, USA) at concentrations of 0.25–16 μM and detection was linear for this range. Retinal, *at*RA, and 13*cis*-RA were measured by LC-MS/MS, as described previously (Arnold *et al.*, 2012), using an AB Sciex 5500 qTrap Q-LIT mass spectrometer (AB Sciex, Foster City, CA, USA) equipped with an Agilent 1290 UHPLC (Agilent, Santa Clara, CA, USA) and an Ascentis Express RP Amide column (2.7 μm, 15 cm ×2.1 mm; Sigma). Compound-dependent mass spectrometer parameters used for detection of retinal were collision energy -13, collision cell exit potential -4, declustering potential -66, and entrance potential -10. Gradient elution with a flow rate of 0.5 mL/min using (A) H2O (B) acetonitrile with 40% methanol and 0.1% formic acid in A and B was used. The gradient was from an initial 60% A for 2 min to 5% A over 13 min and then to 60% A for 2 min. Analytes were detected using positive ion APCI mode. MS/MS transitions for retinal, atRA, 13*cis*-RA, and 13*cis*-RA-d_5 were m/z 285 > 161, m/z 301 > 205, m/z 301 > 205, and m/z 306 > 116. Plasma and urine RBP4 and transthyretin (TTR) were measured by enzyme-linked immunosorbent assay kits according to the manufacturer's protocol (R&D Systems, Minneapolis, MN, USA, and Abnova, Taipei, Taiwan, respectively). RBP4 and TTR standard curves were constructed at concentrations of 0–100 ng/mL and 0–31.25 ng/mL, respectively.

2.3.5 Statistical Analyses

Baseline characteristics were tabulated according to four categories of kidney function: CKD stages 1–2 (eGFR ≥60 mL/min/1.73 m^2), CKD stages 3–5 (eGFR <60 mL/min/1.73 m^2, not yet on dialysis), participants who had initiated dialysis, and healthy subjects. Descriptive statistics are presented as mean and SD or median (interquartile range [IQR]) for continuous variables and number and proportion for categorical variables. Retinoid and binding protein concentrations were reported as medians (25th and 75th percentile). Linear regression was used to evaluate associations of kidney function and retinol and RBP4 and to estimate p values. The P for trend statistics were obtained using the Wald test for the four ordinal categories of kidney function, among all participants. Vitamin A metabolite concentrations were log-transformed in order to examine linear associations of eGFR with the metabolites. Secondarily, analyses were stratified by diabetes status. All p values were two-tailed ($\alpha = 0.05$). Analyses were performed using STATA (release 13.1; StataCorp, College Station, TX, USA) or Prism software (GraphPad, La Jolla, CA, USA).

2.4 RESULTS

Among participants with CKD, the mean (SD) eGFR was 44.18 (20.86) mL/min/1.73m^2, mean age was 54.73 years, and mean BMI was 32.54 kg/m^2. Similar demographics were observed in matched healthy control subjects (Table 2.1).

Plasma concentrations of RBP4 (Figure 2.2 a, b) and retinol (Figure 2.2 c, d) were significantly higher as eGFR (categorized by CKD stage and as a continuous variable) declined. There was greater variability in subjects with CKD than healthy subjects; variability was highest among patients on dialysis (Table 2.2). In healthy subjects, the median plasma retinol binding

protein (RBP) concentration was 1.3 (25th and 75th percentile 1.1, 1.5) μM (15% difference between the median and 75th percentile), whereas in patients receiving dialysis, the median RBP concentration was significantly higher, 2.9 (2.3, 5.9) μM (103% difference between median value and 75th percentile).

Plasma retinol concentrations were higher in patients with CKD at all stages, compared with healthy subjects (Figure 2.2c). The highest retinol levels were observed in patients with CKD at stages 3–5 and dialyzed patients (Table 2.2). Among patients with CKD, lower eGFR was associated with higher plasma retinol ($p = 0.006$; Figure 2.2d) and this association was unaffected by diabetes status. A significant difference in plasma retinol concentration ($\beta = 6.09$; 95% confidence interval = 0.83–11.35 μM per 10 mg/mL/1.73m^2 decrease in eGFR) was observed. This association was not altered when adjusted for the presence of diabetes ($\beta = 6.10$; 95% confidence interval = 0.79–11.42 μM per 10 mg/mL/1.73m^2 decrease in eGFR; Table 2.2). Circulating retinol concentrations were less variable in healthy subjects (IQR = 0.53) than in patients with CKD (IQR = 2.65). CKD was not associated with molar ratios for retinol: RBP4 (Table 2). Plasma retinol concentrations were correlated with RBP4 in healthy subjects and in those with CKD (Figure 2.3).

The *at*RA concentrations were higher in CKD and dialysis patients compared with healthy subjects ($p < 0.001$; Figure 2.4a), the *at*RA/retinol ratio was not significantly different from controls in any of the groups with CKD (Figure 2.4b). The 13*cis*-RA concentrations and the 13*cis*-RA/*at*RA ratio (Figure 2.4c, d) were lower in patients with CKD at all stages and on dialysis ($p < 0.001$) compared with healthy subjects.

RBP4 renal clearance ($p = 0.3093$; Figure 2.4e) was not associated with eGFR despite higher urine RBP4 concentrations among patients with CKD ($p = 0.0001$; Figure 2.4f). Similarly,

among CKD participants, macroalbuminura (urine albumin-to-creatinine ratio >300 mg/g) was associated with higher urine RBP4 levels, relative to normoalbuminuric participants (Figure 2.5). In a random subset of 14 patients with CKD, we were able to detect retinol in the urine of the subjects at concentrations ranging from 50 nM to 800 nM (data not shown). These concentrations were extremely low in comparison to the RBP4 concentrations measured (1–400 uM). We were unable to detect RBP4 in the urine of healthy subjects.

Plasma concentrations of TTR were unaltered in patients with CKD (Figure 2.5a) with an increased plasma RBP4/TTR ratio with increasing CKD stage (Figure 2.5b). Among patients with CKD, mean (IQR) vitamin A intake based on total vitamin A activity was 6,649 (5,575) IU or 766 (372) μg retinol activity equivalents. Mean (IQR) retinol intake was 520 (304) μg and the intake of provitamin A carotenoid derived β-carotene equivalent was 2,949 (2,801) μg. RBP4, retinol (Figure 2.5c, d), *at*RA, and 13*cis*-RA (Figure 2.6) concentrations were not associated with vitamin A intake in patients with CKD (all p values > 0.3). Among subjects with CKD, BMI (Figure 2.5e) was not associated with higher circulating RBP4 concentrations ($p = 0.35$). Similarly, when healthy subjects were included in the analysis of the association between BMI and plasma RBP4 concentration, no association between BMI and RBP4 plasma concentration was observed ($p = 0.94$).

2.5 DISCUSSION

This study unequivocally demonstrates that vitamin A homeostasis is altered in adults with CKD and that the increased RBP4 and retinol concentrations observed in CKD also result in increased concentrations of the active metabolite of vitamin A, RA. This suggests that in patients with CKD, RA concentrations in retinoid target tissues, such as the immune system, liver, and skin, are also altered as serum RA concentrations have been shown to correlate with tissue

concentrations and reflect altered retinoid metabolism in target tissues (Arnold *et al.*, 2015).Increased retinol, RBP4, and RA concentrations may lead to adverse outcomes; chronically elevated plasma retinoid concentrations have been associated with osteoporosis/osteopenia (Penniston and Tanumihardjo, 2006), cardiac events (Desai *et al.*, 2014), and hypertriglyceridemia (and other dyslipidemias) (Brelsford and Beute, 2008), which are distressingly common in patients with CKD. Normalizing retinoid homeostasis in this population could play a major role in reducing these coincident conditions. Plasma concentrations of retinol, *at*RA, 13*cis*-RA, RBP4, and TTR, and the retinol:RBP4 and RBP4:TTR ratios were within twofold of the values reported in children with CKD (Manickavasagar *et al.*, 2014). Additionally, our reported values for RBP4 and RBP4:TTR were also similar to those previously reported in adult CKD populations (e.g., our reported RBP4 concentration of 2.6 μM in subjects with CKD vs. 3.8 μM and 3.75 μM, respectively) (Frey *et al.*, 2008; Henze *et al.*, 2010).

The findings of increased RBP4 and retinol are in agreement with previous studies that quantified RBP4 and/or retinol concentrations in patients with CKD with renal insufficiency (Frey *et al.*, 2008; Henze *et al.*, 2008), and a variety of comorbidities (Michaëlsson *et al.*, 2003; Frey *et al.*, 2008; Erikstrup *et al.*, 2009; Henze *et al.*, 2010; Barazzoni *et al.*, 2011; Lambadiari *et al.*, 2014). This increase in circulating RBP4 exists despite the inevitable loss of RBP4 due to proteinuria that is common, and is a defining diagnostic feature, in patients with CKD. In previous studies, the underlying mechanisms for the aberrant vitamin A homeostasis in this population were not resolved and it remained unclear whether the altered vitamin A homeostasis was a result of comorbidities associated with CKD (such as diabetes) vs. CKD itself. Most importantly, the relationship among CKD, diabetes, and altered vitamin A homeostasis has not been established. The elevated RBP-to-retinol ratio and RBP4 concentration in subjects with

type 2 diabetes mellitus has been reported without controlling for declining kidney function frequently observed in this population (Cho *et al.*, 2006; Erikstrup *et al.*, 2009). On the other hand, RBP4 and retinol were reported to be elevated in CKD without ascertaining the diabetes status of the subjects (Frey *et al.*, 2008). Our data show that the differences observed in retinol and RBP4 concentrations are most likely due to CKD and not diabetes, and suggest that the changes in circulating RBP4 concentrations observed in patients with diabetes were mainly due to renal impairment associated with diabetes. This interpretation is in agreement with previous findings that children with CKD (without diabetes) have similar alterations in vitamin A homeostasis (Manickavasagar *et al.*, 2014) as observed here in adult patients. Several preclinical models have also suggested that obesity alters RBP4 and retinol secretion as adipose tissue (in addition to the liver) can synthesize RBP4 (Tsutsumi *et al.*, 1992; Yang *et al.*, 2005). To address this, we demonstrated that, in individuals with CKD, obesity has a minimal effect of RBP4 concentrations. RBP4 is synthesized mainly in the liver and adipose tissue; the liver secretes only RBP4 bound to retinol (Conaway *et al.*, 2013).This was not a factor in our population as plasma RBP4 concentrations were not associated with BMI and, hence, the effects observed are likely predominantly due to CKD itself.

The elevated RBP4 and retinol concentrations in CKD have largely been proposed to be due to decreased renal clearance of RBP-retinol. Accumulation of circulating RBP4 and retinol in our CKD study population is explainable by either the impaired ability of the kidneys to excrete RBP4 and retinol or increased hepatic synthesis of RBP4 with accompanying release of retinol from hepatic stores. Because the TTR-RBP4 complex is too large to be filtered, whereas RBP4 is filtered by the glomerulus, an alteration in the TTR to RBP4 ratio could result in altered RBP4 renal clearance. Plasma and urinary RBP4 in patients with CKD may also be affected by

impaired megalin-mediated reabsorption of many proteins in the diseased proximal tubule, despite the fact that filtration is decreased.

Our results show that, in CKD, the RBP4 concentrations in the urine are increased with no change in the renal clearance of RBP4 suggesting altered renal clearance of retinol, and RBP4 and retinol are not responsible for the increased plasma concentrations. In addition, the TTR/RBP4 ratio was unchanged in CKD. Hence, we hypothesized that the increased retinol concentrations may be due to decreased metabolism of retinol to *at*RA. If metabolism of retinol to *at*RA by aldehyde dehydrogenase 1A1 (ALDH1A1) and ALDH1A2 was decreased, the *at*RA/retinol ratio should be decreased in patients with CKD. However, we found that this ratio was unchanged in patients with CKD suggesting that the etiology of increased retinol and RBP4 concentrations is increased synthesis (de-esterification) of retinol in the liver and not decreased metabolism to *at*RA.

We detected extremely low concentrations of retinol in the urine in comparison to RBP4 concentrations, with an RBP4- to-retinol ratio ranging from 200 to 1,000, confirming that holo-RBP4 is not excreted in urine. At present, it is impossible to differentiate whether the retinol in urine is a result of approximately 1% of RBP4 in urine being in the holo form or excretion of retinol directly into the urine. Our observation is interesting given that plasma RBP4 is reported to be present as 86% and 67% holo protein in healthy controls and patients with CKD, respectively (Frey *et al.*, 2008).Clearly, the kidneys play a role in homeostatic regulation of both the retinoids and associated binding proteins, and the loss of megalin-mediated reasbortive function in patients with CKD results in the urinary loss of albumin in tandem with other proteins, including RBP4 (Figure 2.7).

The 13*cis*-RA is formed in humans either via ALDH1A1 mediated synthesis from 13*cis*-retinal (Arnold *et al.*, 2015) or via isomerization from *at*RA via glutathione S-transferase and glutathione mediated processes. However, the native precursor for 13*cis*-RA is not known, therefore, the mechanism for the significantly decreased 13*cis*-RA concentration and decreased 13*cis*-RA/*at*RA ratio cannot be determined. Given that 13*cis*-RA and *at*RA can be generated by largely independent pathways, further work is required to evaluate the importance of this observation. Possible mechanisms include altered isomerization from *at*RA to 13*cis*-RA due to increased oxidative stress, or that ALDH1A1, the only ALDH1A enzyme forming 13*cis*-RA (Arnold *et al.*, 2015), is downregulated in the liver. Collectively, all the data point to altered liver retinoid handling and homeostasis in CKD.

We propose that altered signaling between the kidneys and liver in CKD affects liver RBP4 and retinol synthesis and results in elevated circulating RBP4 and retinol concentrations. The effect of kidney disease on hepatic function has been well-described for hepatic cytochrome P450 enzymes and hepatic drug transporters (Yeung *et al.*, 2014). Uremic toxins, which accumulate in patients with CKD, have been shown to both directly inhibit enzyme activity as well as interfere with transcriptional activation, resulting in downregulation of gene expression mediated by proinflammatory cytokines (Yeung *et al.*, 2014). Further research is necessary to determine if uremic toxins can also affect enzymes in the retinoid metabolism pathway, however, we believe that uremia is not solely responsible for the observed changes as altered retinoid metabolism is observed in even stages 1 and 2 CKD when the uremic burden is minimal. As such, it is plausible that CKD directly affects liver RBP synthesis and retinol ester release as retinol, and at the same time decreases 13*cis*-RA synthesis by ALDH1A1 or by glutathione mediated mechanisms from retinol and *at*RA.

This study has several limitations. First, we have used a commercial enzyme-linked immunosorbent assay kit for quantifying RBP4; some investigators have expressed concern that enzyme-linked immunosorbent assay is less accurate than conventional Western blotting (Graham *et al.*, 2007). However, we believe that our methodology, which includes a standard curve that is linear within the relevant range, is sufficient for accurate measurement of RBP4. Second, we measured total RBP4 and did not distinguish between holo-RBP4 and apo-RBP4; this may be relevant for future studies as apo-RPB4 can be regulated by a feedback mechanism that regulates mobilization and release of holo-RBP4 from hepatic retinoid stores (Frey *et al.*, 2008). A related source of confounding may be that below some GFR threshold (which has not been determined), the filtered load of apo-RBP may exceed the maximum transport capacity by the proximal tubule, which would result in a nonlinear relationship between the excretion rate and concentration of plasma apo-RBP. However, despite these limitations, we believe that our results implicate changes in hepatic synthesis and that secretion of RBP4/retinol is involved in the dysregulation observed in patients with CKD.

Normalizing retinoid homeostasis in patients with CKD could play a major role in reducing coincident osteoporosis/osteopenia (Penniston and Tanumihardjo, 2006), cardiac events (Desai *et al.*, 2014), and hypertriglyceridemia (and other dyslipidemias) (Brelsford and Beute, 2008). A clearer understanding of the pathophysiologic mechanism of elevated RBP4 and retinoids is critical in order to develop pharmacologic and dietary interventions to reduce circulating retinoid concentrations and avoid common comorbid conditions.

The observation that retinoid homeostasis is significantly altered even in stages 1 and 2 CKD suggests that altered retinoid status may be an early and sensitive marker of impaired

kidney function or may be a predictor of the rate of decline in GFR. Based on this study, further longitudinal study associating retinoid homeostasis with clinical outcomes is warranted.

In summary, we have shown that circulating retinol and its carrier protein levels are elevated in patients with CKD and that this effect is independent of vitamin A dietary intake and diabetes status. This effect is due to increased hepatic synthesis and secretion of RBP4 and retinol mediated by an uncharacterized signaling pathway between the kidneys and liver. Further study is required in order to define the mechanisms by which kidney disease affects hepatic protein expression and activity. This study highlights the necessity to redefine CKD not as an isolated disease, but as a global condition that affects many organ systems.

a

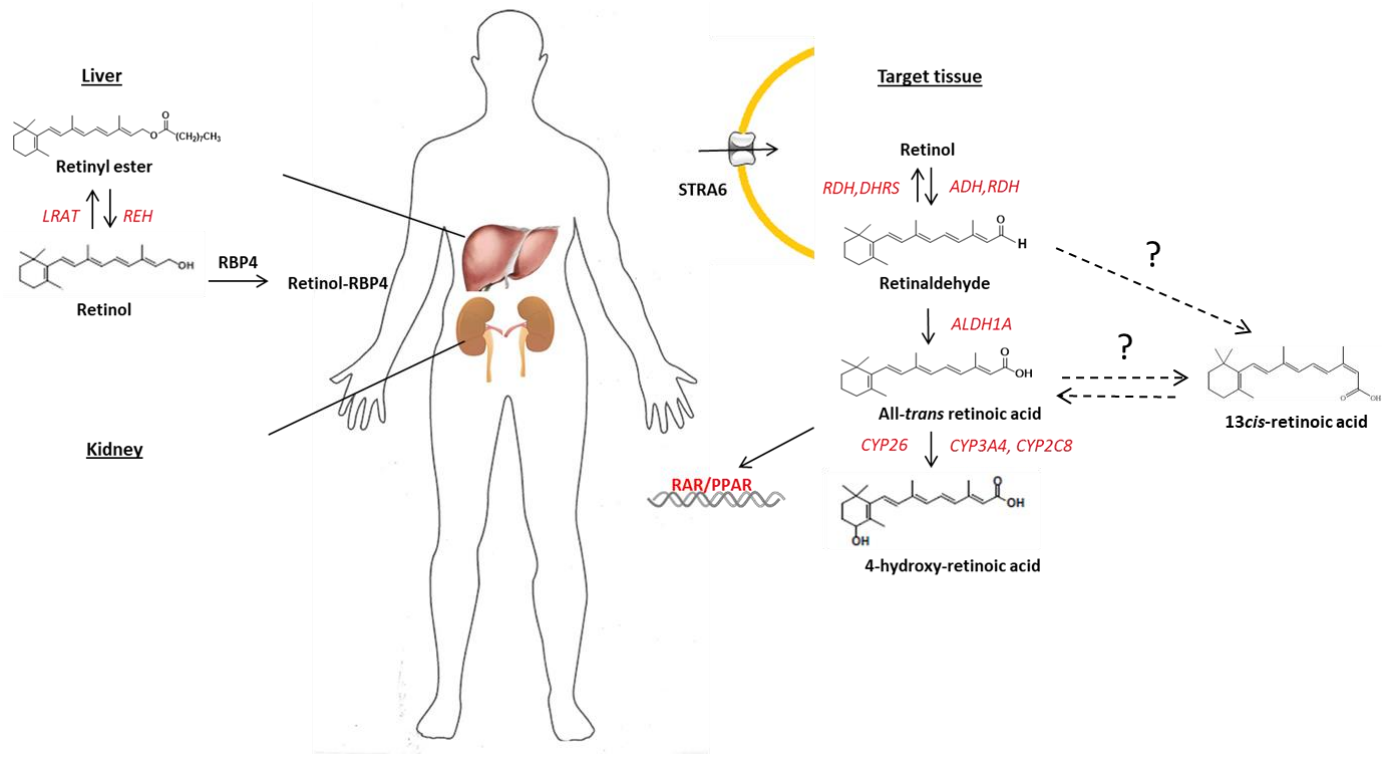
Liver
Retinyl ester
LRAT
REH
Retinol
RBP4
Retinol-RBP4
Kidney
STRA6
Target tissue
Retinol
RDH,DHRS
ADH,RDH
Retinaldehyde
ALDH1A
All-trans retinoic acid
13cis-retinoic acid
CYP26
CYP3A4, CYP2C8
4-hydroxy-retinoic acid
RAR/PPAR
?
?

b

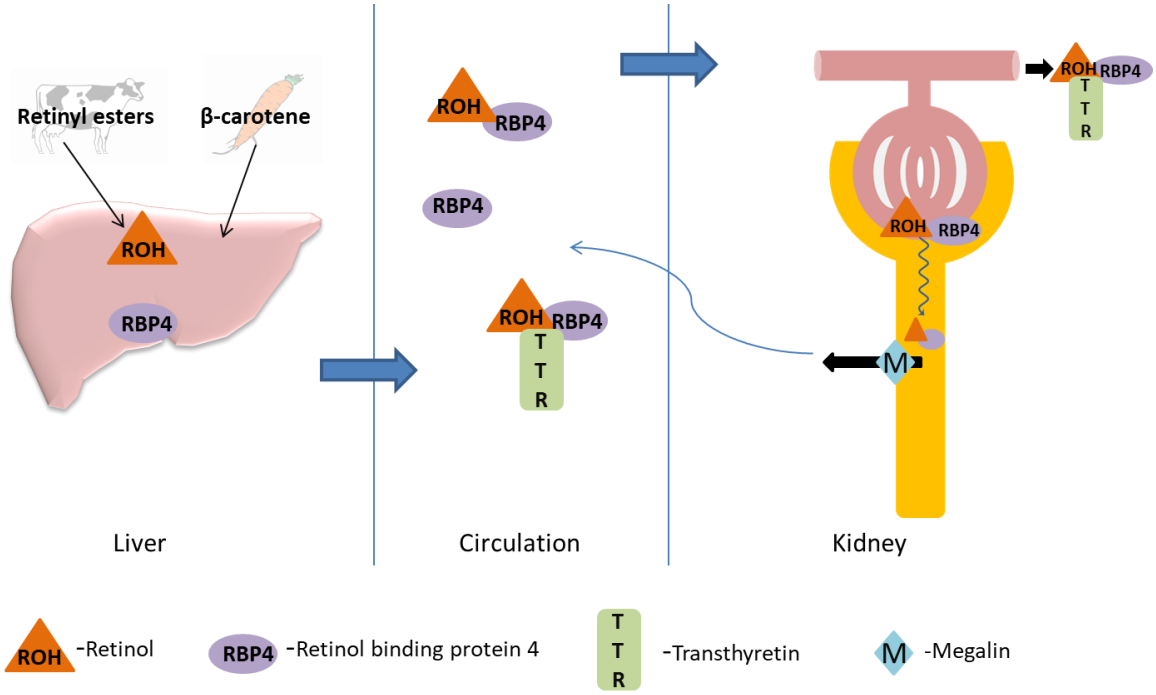

Figure 2.1. Vitamin A metabolism in healthy subjects (a) In the liver, the esterification of retinol and the hydrolysis of the stored esters are regulated by lecithin retinol acyltransferase (LRAT) and retinyl ester hydrolase (REH), respectively. Circulating retinol is delivered to target tissues by retinol binding protein 4 (RBP4) and transthyretin (TTR, not shown) and retinol is taken up into target cells by uptake transporter STRA6. In target tissues, retinol is oxidized to retinaldehyde (retinal) by alcohol dehydrogenase (ADH) or retinol dehydrogenase (RDH); retinaldehyde can be reduced back to retinol by RDH and dehydrogenase reductase (DHRS). The formation of all-trans retinoic acid (*at*RA) requires irreversible oxidation of retinaldehyde to *at*RA by aldehyde dehydrogenase 1A (ALDH1A). The clearance of retinoic acid (RA) is mediated predominantly by cytochrome P450 family 26 enzymes (CYP26). The 13*cis*-RA is likely formed from retinaldehyde via an unknown intermediate or via isomerization from *at*RA. (b) The retinol-RBP4 complex is filtered by the kidneys; the retinol-RBP4-TTR complex is too large for filtration. The filtered retinol-RBP4 complex is reabsorbed in the proximal tubule cells by megalin.

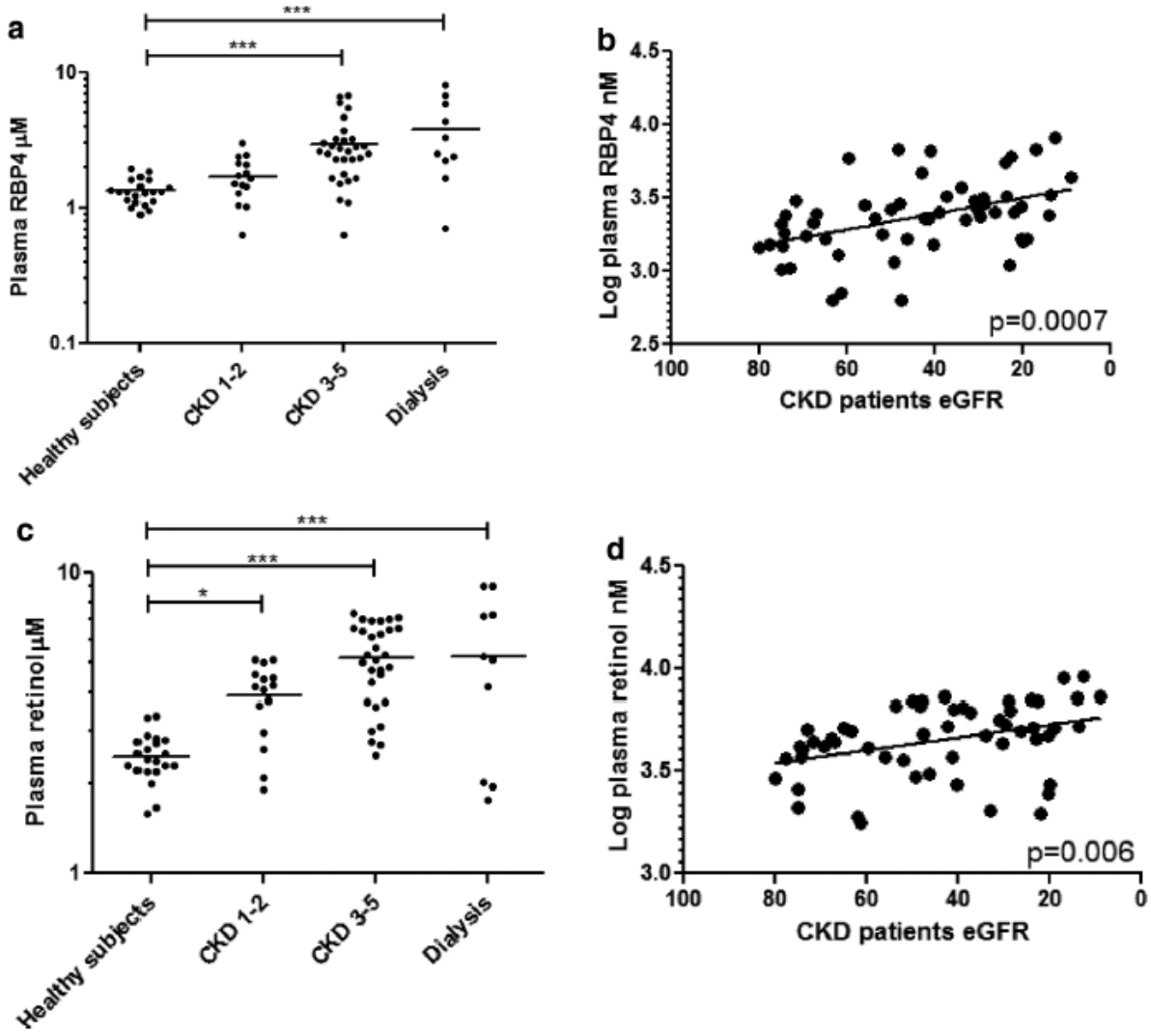

Figure 2.2. Plasma retinol and RBP4 levels and their correlation with eGFR in CKD patients. Patients with chronic kidney disease (CKD) exhibit elevated (a, b) plasma retinol binding protein 4 (RBP4) concentrations and (c, d) plasma retinol concentrations analyzed categorically by CKD stage and as continuous variables. *$p \leq 0.05$; ***$p \leq 0.001$.

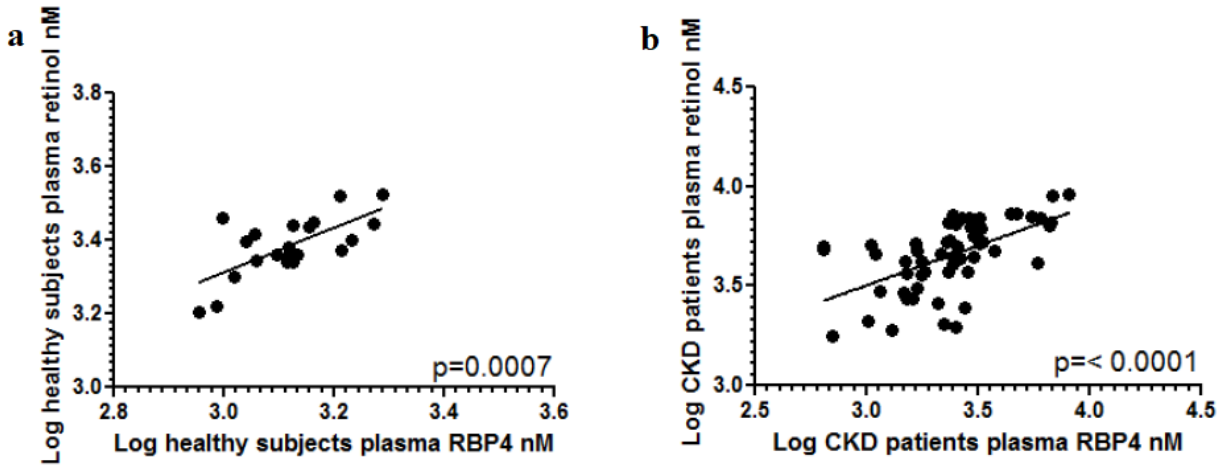

Figure 2.3. Plasma retinol concentrations and their association with plasma RBP4 in healthy subjects and CKD patients. Plasma retinol concentrations are associated with RBP4 concentrations in (a) healthy subjects and in (b) patients with CKD.

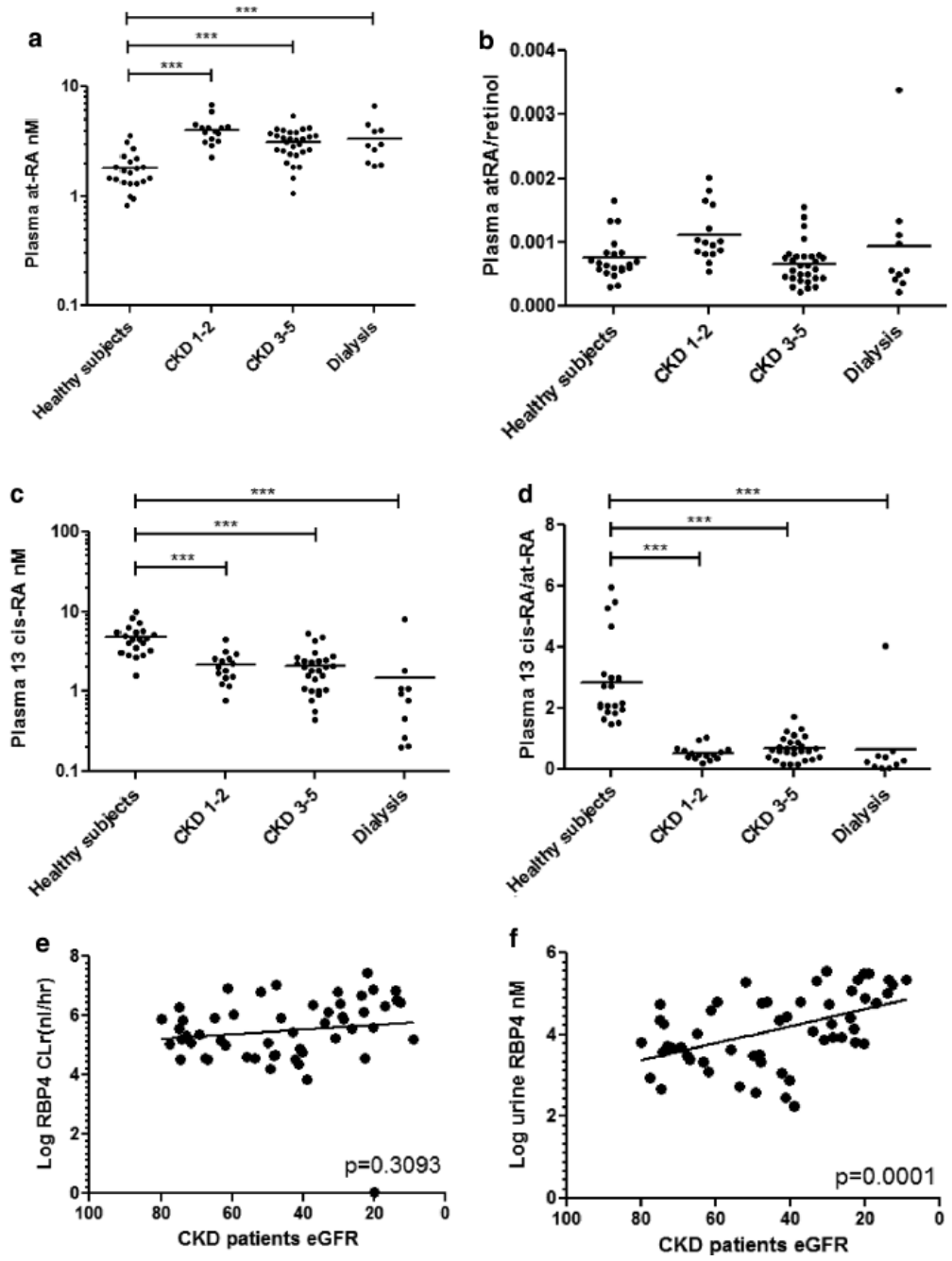

Figure 2.4. Plasma RA levels and RBP4 renal clearance in CKD patients. (a) All-trans retinoic acid (*at*RA) concentrations are higher in patients with chronic kidney disease (CKD) and undergoing dialysis compared with healthy subjects, but the (b) *at*RA/retinol ratio does not change in patient with CKD. (c) The 13*cis*-RA concentrations are lower in patients with CKD at all stages and on dialysis compared with healthy subjects and the (d) 13*cis*-RA/*at*RA ratio was lower in all patients with CKD compared with healthy controls. (e) Retinol binding protein 4 (RBP4) renal clearance does not change in patients with declining estimated glomerular filtration rate (eGFR) despite (f) higher urine RBP4 concentrations among patients with CKD. ***p ≤0.001.

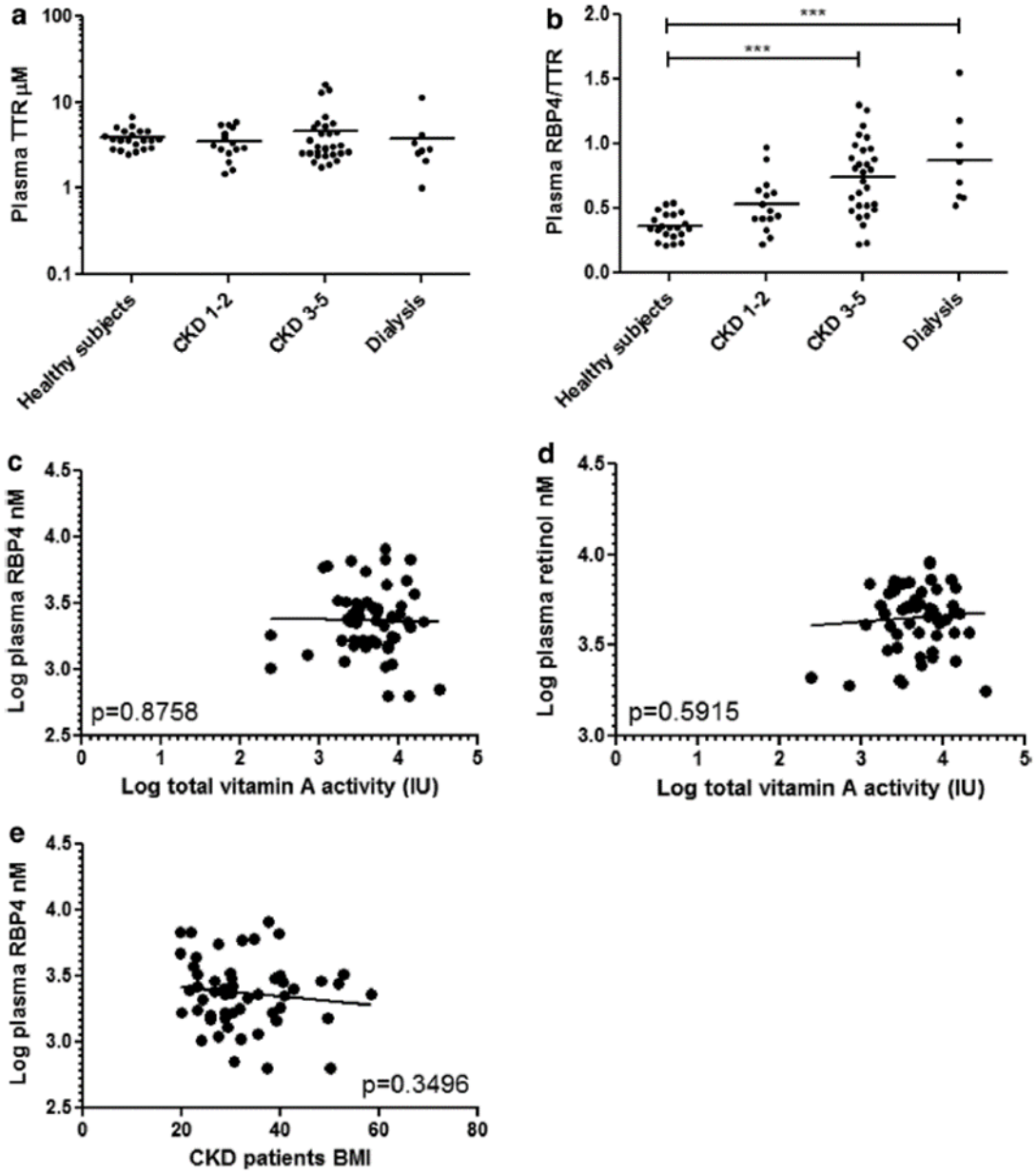

Figure 2.5. Plasma TTR levels and the association between plasma RBP4 and retinol with vitamin A activity. (a) Plasma transthyretin (TTR) concentrations are not associated with stage of chronic kidney disease (CKD) and (b) the retinol binding protein 4 (RBP4)/TTR ratio is higher in subjects with CKD than in healthy subjects and highest among patients on dialysis. (c) RBP4 and (d) retinol are not associated with intake of vitamin A activity units in patients with CKD ($p > 0.3$). (e) Body mass index (BMI) is also not associated with plasma RPB4 concentration. ***$p \leq 0.001$.

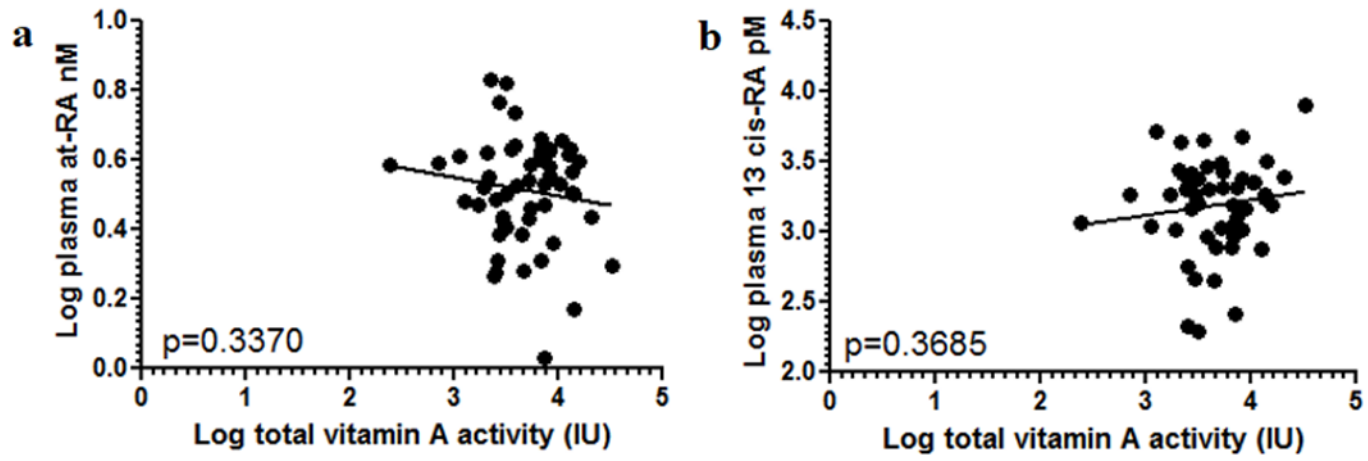

Figure 2.6. Plasma RA levels and their association with vitamin A activity. Plasma concentrations of (a) *at*RA and (b) 13*cis*-RA are not associated with intake of vitamin A activity units in CKD patients.

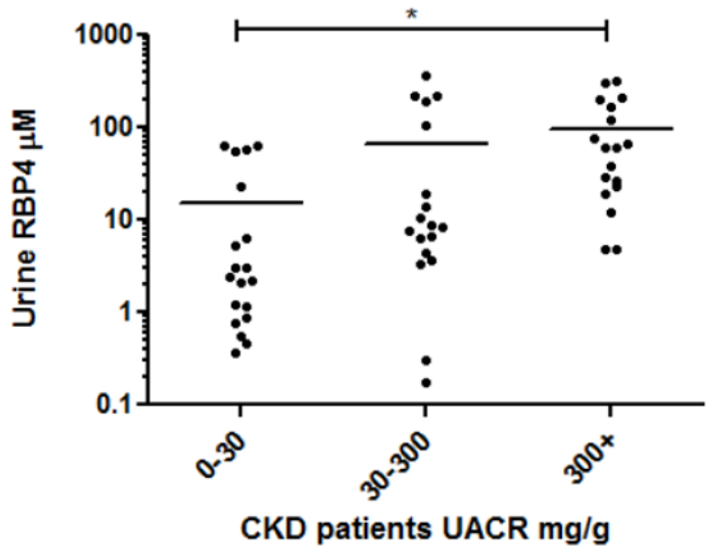

Figure 2.7. Albuminuria and its association with urine RBP4 levels. Among CKD patients, albuminuria (UACR >300+) is associated with higher urine RBP4 levels, relative to normal albuminuric participants. * $P \leq 0.05$

Table 2.1. Demographic and clinical features of the study population

	Healthy subjects $n = 21$	CKD 1–2 $n = 15$	CKD 3–5 $n = 30$	Dialysis $n = 10$
Male	15 (72)	9 (60)	13 (43)	6 (60)
Female	6 (28)	6 (40)	17 (57)	4 (40)
BMI	28 (7)	30 (6)	34 (11)	31 (6)
Age, y	57 (14)	50 (11)	57 (8)	54 (15)
White	15 (71)	9 (60)	16 (53)	2 (20)
African American	4 (19)	5 (33)	11 (37)	5 (50)
Diabetes	6 (19)	5 (33)	15 (50)	6 (60)
UACR median (IQR)	N/A	25 (4–107)	71 (12–371)	853 (217–1,848)
eGFR	N/A	71 (5)	36 (11)	N/A

BMI, body mass index; CKD, chronic kidney disease; eGFR, estimated glomerular filtration rate; IQR, interquartile range; N/A, not available; UACR, urine albumin-to-creatinine ratio. Descriptive statistics are presented as means (SD) for continuous variables and N (%) for categorical variables except where specified.

Table 2.2. Plasma retinoid and retinol binding protein concentrations (median [25th and75th percentile])

	Plasma retinol (μM)	Plasma retinal (nM)	Plasma *at*RA (nM)	Plasma *13 cis*-RA (nM)	Plasma total RA (nM)	Plasma RBP4 (μM)	Plasma TTR (μM)	Plasma ratio retinol:RBP4	Plasma ratio RBP4:TTR
Healthy subjects, $n = 21$	2.4 (2.2–2.8)	8.2 (6.8–9.5)	1.7 (1.4–2.1)	4.4 (3.3–5.5)	5.9 (5.0–7.6)	1.3 (1.1–1.5)	3.7 (2.9–4.6)	1.8 (1.7–1.9)	0.4 (0.3–0.5)
CKD 1–2, $n = 15$	4.2 (3.0–4.6)	6.2 (4.9–6.7)	4.0 (3.2–4.4)	2.0 (1.5–2.6)	5.8 (4.9–7.3)	1.6 (1.3–2.1)	3.2 (2.6–5.1)	2.1 (1.7–2.8)	0.5 (0.4–0.6)
CKD 3–5, $n = 30$	5.2 (3.7–6.6)	6.9 (5.6–8.2)	3.3 (2.6–3.8)	2.0 (1.1–2.5)	5.2 (4.1–6.5)	2.6 (1.8–3.2)	3.0 (2.5–5.1)	1.9 (1.6–2.4)	0.8 (0.5–1.0)
Dialysis, $n = 10$	5.2 (2.0–7.2)	7.3 (4.1–8.5)	3.0 (2.1–4.1)	0.9 (0.3–1.1)	4.6 (3.2–5.7)	2.9 (2.2–5.9)	2.8 (2.3–3.8)	1.5 (0.9–2.5)	0.8 (0.6–1.1)
P-for trend	< 0.0001	0.013	0.001	< 0.0001	0.006	< 0.0001	0.562	0.776	< 0.0001
Percent difference in analyte concentration per 10 mg/mL/1.73m^2 lower eGFR (beta, 95% CI), among participants with non-dialysis CKD,[a] $n = 45$	6.09 (0.83–11.35) 0.024	–	−4.28 (−9.73, 1.17) 0.121	−0.08 (−9.70, 8.16) 0.863	−2.21 (-5.14, 0.71) 0.136	11.10 (3.20, 19.00) 0.007	2.57 (−6.01, 11.16) 0.548	−5.01 (−12.15, 2.14) 0.165	8.29 (1.42, 15.17) 0.019
Percent difference in analyte concentration per 10 mg/mL/1.73m^2 lower eGFR (beta, 95% CI)[a] adjusted for diabetes among participants with non-dialysis CKD,[a] $n = 45$	6.10 (0.79–11.42) 0.025	–	−4.27 (−9.40, 0.86) 0.100	−0.07 (−9.74, 8.25) 0.868	−2.53 (−5.44, 0.38) 0.088	11.15 (3.30, 19.00) 0.006	2.68 (−5.77, 11.13) 0.525	−5.04 (−12.17, 2.07) 0.160	8.25 (1.32, 15.18) 0.021

*at*RA, all-trans retinoic acid; CI, confidence interval; CKD, chronic kidney disease; eGFR, estimated glomerular filtration rate; RA, retinoic acid; RBP4, retinol binding protein 4; TTR, transthyretin.

[a]Linear regression was used to evaluate associations of kidney function and retinol and RBP4 and to estimate p values. Analyte concentrations were logtransformed in order to examine linear associations with eGFR. Values indicate the slope of the regression line per 10 units of eGFR. P-for trend statistics were obtained using the Wald test for the four ordinal categories of kidney function among all participants.

Chapter 3.

Physiologically Based Pharmacokinetic Model of all- *trans*-Retinoic Acid with Application to Cancer Populations and Drug Interactions

This chapter was published in *J Pharmacol Exp Ther. 2017 May; 361(2):246-258*

3.1 ABSTRACT

All-trans retinoic acid (*at*RA) is a front-line treatment for acute promyelocytic leukemia (APL). Due to its activity in regulating the cell cycle, it has also been evaluated for the treatment of other cancers. However, the efficacy of *at*RA has been limited by *at*RA inducing its own metabolism during therapy, resulting in a decrease of *at*RA exposure during continuous dosing. Frequent relapse occurs in patients receiving *at*RA monotherapy. In an attempt to combat therapy resistance, inhibitors of *at*RA metabolism have been developed. Of these, ketoconazole and liarozole have shown some benefits but their usage is limited by side effects and low potency towards CYP26A1, the main *at*RA hydroxylase. The aim of this study was to determine the pharmacokinetic basis of therapy resistance to *at*RA, and to test whether the complex disposition kinetics of *at*RA could be predicted in healthy subjects and in cancer patients in the presence and absence of inhibitors of *at*RA metabolism using physiologically based pharmacokinetic (PBPK) modelling. A PBPK model of *at*RA disposition was developed and verified in healthy individuals and in cancer patients. The population based PBPK model of *at*RA disposition incorporated saturable metabolic clearance of *at*RA, induction of CYP26A1 by *at*RA and the absorption and distribution kinetics of *at*RA. It accurately predicted the changes in *at*RA exposure after continuous dosing and when co-administered with ketoconazole and liarozole. The developed model will be useful in interpretation of *at*RA disposition and efficacy, design of novel dosing strategies and development of next generation *at*RA metabolism inhibitors.

3.2 INTRODUCTION

*at*RA is an active metabolite of vitamin A (retinol), circulating at endogenous plasma concentration of about 2 nM in healthy humans (Jing *et al.*, 2016). One of the main biological activities of *at*RA is regulating cell cycle by binding to the nuclear retinoic acid receptors

(RARs). Via RAR activation *at*RA controls the expression of target genes involved in differentiation, cell cycle arrest and apoptosis in a concentration-dependent manner. Due to its activity in inducing apoptosis, *at*RA has been pursued for the treatment of various cancers including non-small-cell lung cancer, head and neck cancer, astrocytoma and Kaposi's sarcoma (Phuphanich *et al.*, 1997; Saiag *et al*., 1998; Arrieta *et al.*, 2010; Lim *et al.*, 2012). In APL, promyelocyte differentiation is blocked due to the formation of PML-RARα fusion protein caused by the chromosomal translocation between chromosomes 15 and 17. Therapeutic doses of *at*RA resulting in peak plasma concentration of 1 μM (Adamson, 1996) can overcome the blockage and trigger RAR mediated promyelocyte differentiation (Ablain and De The, 2011). As monotherapy, *at*RA induces clinical remissions in 70-90% of APL patients, but relapses are observed if *at*RA is continued as a single agent, so combination therapies are required for long term disease control (Coombs *et al.*, 2015). The loss of *at*RA efficacy is believed to be largely due to the 42-62% reduction of plasma concentrations of *at*RA upon chronic dosing caused by autoinduction of *at*RA clearance (Muindi *et al.*, 1992a; Regazzi *et al.*, 1997; Russo *et al.*, 1998; Ozpolat *et al.*, 2003). This induction is likely due to increased expression of CYP26A1, the main *at*RA hydroxylase in human liver (Tay *et al.*, 2010; Topletz *et al.*, 2015).

To overcome the autoinduction of *at*RA clearance and increase systemic *at*RA concentrations, inhibitors of *at*RA metabolism have been developed. The decline of *at*RA area under plasma concentration-time curve (AUC) after continuous oral treatment was attenuated by ketoconazole, a pan-CYP inhibitor, in advanced lung cancer patients (Rigas *et al*., 1993). Liarozole, an inhibitor of *at*RA metabolism, was found to partially reverse the decline of *at*RA AUC after chronic administration to patients with solid tumors (Miller *et al.*, 1994). Despite these promising clinical results, the use of *at*RA metabolism inhibitors in cancer therapy has

been limited due to the adverse effects and lack of satisfactory potency and selectivity for the primary *at*RA metabolizing enzymes (Njar *et al.*, 2006; Nelson *et al.*, 2013). To develop more potent and selective inhibitors and efficient dosing strategies, a better understanding of *at*RA disposition and kinetics of induction of *at*RA metabolizing enzymes is needed.

CYP26A1 is predicted to be responsible for more than 90 % of hepatic *at*RA clearance, although CYP2C8, CYP3A4 and CYP3A5 also metabolize *at*RA (Thatcher *et al.*, 2010). The induction of *at*RA metabolism upon multiple dosing is likely caused by increased CYP26A1 enzyme expression, since *at*RA treatment significantly induces CYP26A1 mRNA and activity in HepG2 cells and human hepatocytes (Tay *et al.*, 2010; Topletz *et al.*, 2015). However, the quantitative findings of CYP26A1 activity, *at*RA concentration dependent induction of *at*RA metabolism and the magnitude of pharmacokinetic changes in different populations receiving *at*RA have not been integrated into a model of *at*RA disposition in humans that could be applied to designing better inhibitors of *at*RA metabolism or improved dosing regimens in *at*RA therapy. We hypothesized that PBPK modeling and simulation could be used as a mechanistic tool to comprehensively understand the dose- and time- dependent disposition of *at*RA in different populations in the presence and absence of inhibitors of *at*RA metabolism.

PBPK modeling which integrates physiological parameters such as blood flow, tissue sizes and composition with drug-specific parameters is widely applied to simulate drug disposition in plasma and tissues (Jones *et al.*, 2015). Uniquely, altered physiologic parameters in different populations and disease states can be integrated into PBPK models to investigate variable drug disposition in humans. PBPK modeling also provides the possibility to simulate population variability and time varying phenomena including induction and saturation of clearance pathways. Therefore, PBPK modeling is exceptionally well suited to study *at*RA disposition.

Surprisingly, existing *at*RA PBPK models (Clewell *et al.*, 1997; Louisse *et al.*, 2015) have not incorporated the induction of *at*RA metabolism, multiple dosing scenarios or been applied to any disease population. The aim of the present work was to develop a full *at*RA PBPK model incorporating human physiology and *at*RA specific pharmacokinetic parameters to predict *at*RA disposition in humans after single and multiple doses of *at*RA in the absence and presence of *at*RA metabolism inhibitors in both healthy subjects and in cancer patients.

3.3 MATERIALS AND METHODS

3.3.1 Chemicals and Reagents

Ketoconazole, *at*RA and acitretin were purchased from Sigma-Aldrich (St. Louis, MO). *at*RA-d_5 was purchased from Santa Cruz Biotechnology, Inc. (Santa Cruz, CA). 4OH-*at*RA and 4oxo-*at*RA-d_3 were purchased from Toronto Research Chemicals (North York, ON). Liarozole was purchased from Tocris Bioscience (Bristol, U.K.). CYP3A4 and CYP2C8 supersomes co-expressed with reductase and b_5 were purchased from BD Gentest (BD Biosciences, San Jose, CA). NADPH and HPLC-grade ethyl acetate were purchased from EMD Millipore (Billerica, MA). CYP26A1 was expressed in Sf9 insect cells and microsomes containing CYP26A1 were prepared as previously described (Lutz *et al.*, 2009). CYP26A1 content was measured by CO spectrum. Rat cytochrome P450 oxidoreductase was expressed in E. coli and purified as previously described (Lutz *et al.*, 2009). LC-MS/MS mobile phase solvents (water, acetonitrile, and methanol) were Optima grade and purchased from Fisher Scientific (Pittsburgh, PA).

3.3.2 *at*RA and 4OH-atRA Quantification

All analyses were done using AB Sciex 5500 qTrap Q-LIT mass spectrometer (Foster City, CA) equipped with an Agilent 1290 UHPLC (Santa Clara, CA) using previously described

validated analytical methods (Arnold *et al.*, 2012, 2015; Jing *et al.*, 2016) . Sample preparation methods are described for each type of sample below. For analysis of *at*RA-d_5 and *at*RA concentrations in mouse serum and tissue samples, human blood and plasma samples, Caco-2 cell permeability assay and *at*RA depletion in CYP26A1 inhibition assay, *at*RA-d_5 and *at*RA were separated using an Ascentis Express RP-Amide column (2.7 μm, 15cm ×2.1mm; Sigma). A gradient elution with aqueous (A) and acetonitrile (B) with 0.1% formic acid and 40% methanol in both A and B was used. The gradient was from initial 60% A for 2 minutes to 45% A over 8 minutes, then to 10% A over 7 minutes and finally held at 5% A for 3 minutes before re-equilibration. Mobile phase flow was 0.5 mL/min. Analytes were detected using positive ion APCI mode. MS/MS transitions for *at*RA, *at*RA-d_5 (internal standard for *at*RA assay) and acitretin (internal standard for *at*RA-d_5 assay) were m/z 301>205, m/z 306.1>127.2 and m/z 327.0>77 respectively. The declustering potential, collision energy and collision exit potential were 80, 17, and 10 for *at*RA, 46, 23, and 8 for *at*RA-d_5 and 46, 77 and 14 for acitretin. A minimum of 6 quality control samples prepared in the relevant matrix were included in each LC-MS/MS run.

The formation of *at*RA metabolite 4OH-*at*RA in CYP2C8 and CYP3A4 inhibition assays was measured as previously described (Topletz *et al.*, 2015). 4OH-*at*RA was separated using an Agilent Zorbax Extend C18 column (3.5 μm, 2.1 ×100mm; Agilent Technologies) with a gradient elution at a flow rate of 0.3 ml/min. The gradient was from initial 95% of aqueous with 0.1% formic acid (A) and 5% of acetonitrile (B) to 5% A over 5.5 minutes, then held for 1 minute before re-equilibration to initial conditions. Analytes were detected using positive ion ESI mode. The declustering potential, collision energy and collision exit potential were set to 80, 30 and 13 for 4OH-*at*RA and 80, 35 and 2 for 4oxo-*at*RA-d_3 (internal standard). MS/MS transitions for 4OH-*at*RA and 4oxo-*at*RA-d_3 were m/z 299.2 > 197.2 and m/z 300.0 > 226.0.

3.3.3 *at*RA Blood to Plasma Ratio

The blood to plasma ratio of *at*RA was measured in fresh human blood collected into EDTA containing tubes to avoid clotting. *at*RA-d_5 was spiked into 600 µl aliquots of blood in triplicate with 25 nM final concentration. Samples were mixed and incubated at 37°C for 2 hr. After incubation, 120 µL whole blood was removed and protein precipitated with 120 µL acetonitrile. The remaining sample was centrifuged at 16,100 g for 5 minutes at room temperature to pellet red blood cells and isolate plasma. Then 120 µL acetonitrile was added to 120 µL plasma to precipitate plasma proteins. Two µL of 10 µM acitretin was added to all samples as internal standard. Samples were centrifuged at 3,000 g for 15 minutes at 4°C, 100 µL of supernatant was transferred to glass vials and samples were analyzed using LC-MS/MS as described above.

3.3.4 *at*RA Permeability in Caco-2 Cells

Caco-2 cells were cultured at 37˚C in a humidified atmosphere of 5% CO_2 using DMEM supplemented with 10% FBS, 1% L-glutamine, 1% NEAA, and 5% antibiotic-antimycotic solution. Cells were routinely subcultured at 90% confluency with trypsin-EDTA. Caco-2 cells were plated onto cell culture inserts (3.0 µm pores, 0.9 cm^2 growth area) at a density of 6.4 x 10^4 cells/insert. The culture medium (0.8 mL in the insert and 2.0 mL in the well) was replaced with fresh medium at day 5 after initiation of cell culture and every 48 h thereafter. After 21 days in culture, the Caco-2 monolayer was used for the permeability experiments. Cell monolayers were preincubated in transport medium (Hank's balanced salt solution; 0.952 mM $CaCl_2$, 5.36 mM KCl, 0.441 mM KH_2PO_4, 0.812 mM $MgSO_4$, 136.7 mM NaCl, 0.385 mM Na_2HPO_4, 25 mM D-glucose, and 10 mM HEPES, pH 7.4) for 30 min at 37˚C. After preincubation, the transepithelial electrical resistance (TEER) was measured routinely with a Millicell®-ERS system (Millipore Corporation, Bedford, MA) to ensure cell monolayer integrity. The cell monolayers that exhibited TEER values

higher than 500 $\Omega \cdot cm^2$ were used for experiments. Permeability measurement was initiated by adding test compounds (10 µM) to the donor side and transport medium to the receiver side. Transfer of test compounds was observed in two directions, apical to basolateral and basolateral to apical. Samples were obtained from the donor side at 5 min for measurement of initial concentration and from the receiver side at 30, 60, 90, 120 and 180 min. Permeability experiments were performed under no pH gradient condition (apical pH = basal pH = 7.4) at 37˚C. After all experiments, TEER was measured to ensure cell monolayer integrity, and data generated in cell monolayers in which viability had not been adversely affected by the experimental conditions were accepted. The apparent permeability (P_{app}, cm/s) of test compounds across cell monolayers was calculated using the equation 3.1:

$$P_{app} = \frac{dQ}{dt} \cdot \frac{1}{A \cdot C_D} \qquad \text{Equation 3.1}$$

Where Q is the amount of compound transported over time t (therefore, dQ/dt is the amount of compound transported within a given time period [µmol/s]). C_D is the initial concentration of compound in the donor compartment (µM), and A is the membrane surface area (cm^2). The concentration of *at*RA was analyzed by LC-MS/MS as described above. For all transport assays, atenolol and metoprolol were used as controls and the LC-MS/MS methods for these compounds are described in supplemental data.

3.3.5 Tissue Distribution of *at*RA-d_5 in C57BL/6J Mice

Disposition of *at*RA was characterized and tissue to plasma partition coefficients (K_p) were determined in C57BL/6J mice. Animal experiments were approved by the University of Washington's Institutional Animal Care and Use Committee. For the study, 12 male C57BL/6J mice were dosed with 1 mg/kg *at*RA-d_5 IP and blood, liver, kidney and pancreas were collected at

0.5, 1, 2 and 4 hours after dosing under yellow light. Three mice were sacrificed at each time point. In addition, three mice were dosed with vehicle and sacrificed immediately after vehicle administration. At each time point serum was separated from blood by centrifugation, samples were protected from light, and each tissue sample was snap frozen in liquid nitrogen and stored in -80˚C until analysis. Tissue homogenization and *at*RA-d_5 extraction were done as previously described (Arnold *et al.*, 2015). In brief, 100 mg of tissue per sample was homogenized in a 1:1 volume of 0.9% NaCl and *at*RA-d_5 was extracted with 10 mL hexanes after addition of 10 µM acitretin as internal standard. After evaporation of the organic layer under nitrogen, sample was reconstituted with 65 µl of 60:40 acetonitrile /H_2O and the concentration of *at*RA-d_5 was measured using LC-MS/MS as described above.

For pharmacokinetic analysis, area under the tissue or serum concentration versus time curve from time 0 to infinity ($AUC_{0-\infty}$) was calculated by standard non-compartmental analysis with Phoenix (St. Louis, MO) using linear trapezoidal method. K_p was calculated using equation 3.2 with conversion of serum AUC from h*pmol /ml to h*pmol /g, assuming 1 ml serum=1 g.

$$K_p = \frac{AUC_{0-\infty}\text{tissue} \quad h*pmol/g}{AUC_{0-\infty\, serum} \quad h*pmol/g} \qquad \text{Equation 3.2}$$

3.3.6 Development of *at*RA PBPK model in Healthy Humans

A PBPK model of *at*RA was constructed using Simcyp™ population-based ADME simulator v.14 (Certara, Sheffield, UK) using a full PBPK model (Figure 3.1A) and the model was developed and verified according to the workflow shown in Figure 3.1B. The absorption kinetics of *at*RA was simulated with first-order absorption model using the Caco-2 cell permeability data and absorption kinetics of *at*RA observed in healthy volunteers. In brief, fraction absorbed (F_a) and a nominal flow in gut model (Q_{gut}) were predicted using *at*RA Caco-2

cell permeability data within Simcyp. k_a and lag time were estimated using the observed concentration–time profiles from 3 studies in healthy volunteers administered with a single oral dose of *at*RA (Ozpolat *et al.*, 2003; Thudi *et al.*, 2011; Peng *et al.*, 2014). The reported concentration-time profiles were digitized using Plot Digitizer software (http://plotdigitizer.sourceforge.net/) and one compartment pharmacokinetic model with first order absorption was fitted to the data using Phoenix WinNonlin 6.4 (Pharsight Corporation, Cary, NC).

For *at*RA distribution, a full PBPK model was used. Since intravenous *at*RA studies are not available in humans, steady state volume of distribution (V_{ss}) in humans was first predicted using allometric scaling from studies in adult Wistar rats and Macaca fascicularis monkeys after administration of *at*RA intravenously (Sandberg *et al.*, 1994; Saadeddin *et al.*, 2004). V_{ss} of *at*RA in adult humans was estimated using the allometric equation 3.3:

$$Y = a \times W^b \qquad \text{Equation 3.3}$$

where Y is V_{ss} (L), W is body weight (kg) and a and b are the allometric coefficient and exponent respectively. The K_p values were independently predicted in Simcyp using the method described by Rodgers and Rowland (Rodgers and Rowland, 2006). K_p values for liver, kidney and pancreas were then refined based on data from the mouse pharmacokinetic study described above. For lung and brain, K_p values were refined based on reported literature values (Wang *et al.*, 1980). To achieve concordance between the allometric scaling V_{ss} and in silico predicted V_{ss}, a K_p value of 0.2 was assigned to all other tissues except those mentioned above.

The hepatic clearance of *at*RA was predicted using previously reported enzyme kinetic data for CYP2C8, CYP3A4, CYP3A5, CYP3A7 and CYP26A1 (Thatcher *et al.*, 2010). Inter system

extrapolation factor (ISEF) of CYP2C8, CYP3A4, CYP3A5 and CYP3A7 used Simcyp default values for BD supersomes as 0.43, 0.24, 0.24 and 0.24 respectively. For CYP26A1, the ISEF value of 0.14 was calculated based on the reported ratio between the predicted *at*RA clearance (171.0 ± 99.5 µL/min/mg) from recombinant insect cell microsome data and the observed clearance (23.2 ± 20.4 µL/min/mg) obtained in human liver microsomes (HLM) (Thatcher *et al.*, 2010). As the standard Simcyp population file does not have CYP26A1, CYP26A1 was incorporated into the population profile as CYP2J2 in the liver and GI tract. In the liver, the protein abundance of 1.6 pmol/mg protein (63% CV) was assigned for CYP26A1 enzyme abundance according to literature (Thatcher *et al.*, 2010). CYP26A1 turnover half-life was estimated between 24 -48 hours with turnover rate constant (k_{deg}) of 0.029-0.014 h^{-1} based on the in vitro data (Topletz *et al.*, 2015). A sensitivity analysis of k_{deg} in the range of 0.029-0.014 h^{-1} was conducted with less than 20% difference on the predicted *at*RA AUC. Based on this, a turnover rate constant for CYP26A1 was estimated at 0.014 h^{-1} and used in this model. Since both the CYP26A1 mRNA and protein levels were low in human intestine (Topletz *et al.*, 2012), 0 was assigned to CYP26A1 enzyme abundance in the GI tract.

*at*RA is known to induce the mRNA and protein expression of CYP26A1. The induction parameters determined previously in HepG2 cells were incorporated into the model. The maximum fold induction (E_{max}) of CYP26A1 by *at*RA was estimated between 22 - 44-fold based on the observed increase in formation of RA metabolites from *at*RA-d_5 in HepG2 cells after treatment with 1 µM *at*RA (Topletz *et al.*, 2015), and an E_{max} of 33 was used for the model. A sensitivity analysis of E_{max} in the range of 22–44 was conducted with less than 15% difference in the predicted *at*RA AUC. Therefore, E_{max} of 33 was considered acceptable. *at*RA concentration (0.09 µM) that supports half maximal induction (EC_{50}) was taken from the dose response

analysis of CYP26A1 induction by *at*RA after 24-hour treatment in HepG2 cells (Tay *et al.*, 2010). fu_{inc} (fraction of unbound drug in the in vitro incubation) of 0.4 was used in the model based on the literature (Topletz *et al.*, 2015).

3.3.7 Simulation of *at*RA Disposition in Healthy Humans

To compare the simulated *at*RA disposition with the reported studies in healthy humans, PubMed searches were conducted using the search terms "retinoic acid pharmacokinetics" and "retinoic acid" in the title or abstract of the manuscript. Three papers were found on *at*RA disposition in healthy volunteers (Ozpolat *et al.*, 2003; Thudi *et al.*, 2011; Peng *et al.*, 2014). The observed concentration–time profiles from these publications were digitized using Plot Digitizer software (http://plotdigitizer.sourceforge.net/). *at*RA pharmacokinetics were simulated using the Simcyp healthy volunteer profile with the modifications described earlier.

For one study (Peng *et al.*, 2014) that was reported in Chinese, Simcyp Chinese healthy volunteer profile was used with the modifications of the population as described earlier. The population profile was also modified to match the clinical study population for the age range and proportion of females.

For each study, 10 trials were simulated with the number (n) of subjects per trial matching that reported for that clinical study using random seed. The mean and standard deviation of the trials are reported. The dosing regimen was set identical to observed clinical studies. In the healthy volunteer studies, *at*RA was dosed either in mg basis or in mg/m2 basis. All the studies were simulated using the same dosing units as reported in the clinical studies, and the data are reported with the matching dosing regimen as was originally reported. The validity of the model

for healthy volunteers was evaluated by comparing the observed and simulated data using unpaired t test and by calculating the fold difference between the observed and predicted data.

3.3.8 Development of *at*RA PBPK model in Cancer Patients

The model of *at*RA disposition in cancer population was built based on the healthy population model with modifications on absorption kinetics and population parameters. To optimize the *at*RA PBPK model in adult cancer patients, F_a was estimated using bioavailability (F) calculated from published clinical studies in adult healthy subjects and cancer patients using equation 3.4:

$$\frac{F_1\ Dose_1}{AUC_1} = \frac{F_2\ Dose_2}{AUC_2} \qquad \text{Equation 3.4}$$

in which F_1 is the bioavailability in healthy subjects. $Dose_1$ and AUC_1 are from a published clinical study in healthy subjects (Ozpolat *et al.*, 2003). $Dose_2$ and AUC_2 are the mean values from published clinical studies in cancer patients with the same dosage (Muindi *et al.*, 1992a; Muindi *et al.*, 1992b; Rigas *et al*., 1993; Miller *et al.*, 1994; Muindi *et al.*, 1994; Adamson *et al.*, 1995; Lee *et al.*, 1995; Rigas *et al.*, 1996; Russo *et al.*, 1998). Clearance of *at*RA was assumed to be identical in patients since the observed elimination half-life and t_{max} of *at*RA in healthy subjects matched the half-life and t_{max} observed in cancer patients with same single oral dose, but the maximum plasma concentration (C_{max}) and AUC were both altered in cancer patients. Therefore, F_a of 0.14 was used in the cancer population model. Due to the limited information on *at*RA disposition in healthy children and children with cancers, the F_a of 0.14 calculated from adult population was also used for the pediatric cancer population model.

The adult cancer population file was built based on the healthy adult population file with modifications of demographic parameters including age, sex, height, body weight and blood

composition including albumin, alpha-1-acid glycoprotein and hematocrit to match previously described population parameters (Cheeti *et al.*, 2013). For pediatric population demographic parameters were kept the same as healthy children. CYP26A1 expression was incorporated in the cancer populations identically to that described above for healthy population.

To compare the simulated *at*RA disposition with the reported studies in adult and pediatric cancer patients, PubMed searches were conducted using the search terms "retinoic acid pharmacokinetics" and "retinoic acid" in the title or abstract of the article, and studies that were conducted in cancer patients with sufficient pharmacokinetic data for evaluation were selected. Design of simulation trials was the same as described above for healthy subjects. In all of the reported *at*RA studies in patients the dose was reported as mg/m^2 basis, so the *at*RA dose in all the simulations was also set in mg/m^2 units. All the data are also reported for mg/m^2 dosing.

3.3.9 Model Verification

AUC was the primary variable used for model verification. For all populations for which only a single study existed at a given dosage level of *at*RA, unpaired t-test was used to compare whether the observed and predicted AUCs were significantly different from one another. For studies that were conducted at the same dosage level of *at*RA, acceptance criteria with the consideration of sample size and variance of the parameter of interest in reported studies was used. A prediction was considered acceptable if the predicted AUC was within the calculated upper and lower verification range of the observed AUC. The acceptance range of the mean simulated AUC was calculated as previously described (Abduljalil *et al.*, 2014) according to equations 3.5, 3.6 and 3.7,

$$\sigma = \sqrt{\ln[\left(\frac{CV\%}{100}\right)^2 + 1]} \qquad \text{Equation 3.5}$$

$$A\bar{x} = \exp[\ln(\bar{x}) + 4.26\ \frac{\sigma}{\sqrt{N}}\ ]$$ Equation 3.6

$$B\bar{x} = \exp[\ln(\bar{x}) - 4.26\ \frac{\sigma}{\sqrt{N}}\ ]$$ Equation 3.7

where the calculated values A and B are the boundary values for fold difference between the predicted and observed AUC in a given study, $\bar{x}$ is the mean of the AUCs of *at*RA in all clinical studies giving the same dosing regimen, N is the sample size, σ is the standard deviation of the AUC on the natural log scale. Due to the dose difference in reported clinical studies and dose and time dependent kinetics of *at*RA the acceptance criteria (acceptable fold difference between observed and predicted) was calculated separately for each dose strength.

3.3.10 Determination of CYP Inhibition by Ketoconazole and Liarozole

In order to determine the inhibition potency of ketoconazole and liarozole towards *at*RA metabolism, the inhibition of *at*RA hydroxylation by ketoconazole and liarozole was evaluated using recombinant CYP3A4 and CYP2C8 as previously described (Thatcher *et al.*, 2011). Inhibition of CYP26A1 was tested by measuring the inhibition of *at*RA depletion. In brief, 5 pmol CYP3A4 and CYP2C8 supersomes were preincubated with ketoconazole or liarozole (≥ 7 concentrations of 0 – 100 μM) and 1 μM *at*RA for 5 minutes at 37°C in 1 ml 100 mM potassium phosphate buffer (KPi; pH 7.4). The reactions were initiated with addition of 1 mM NADPH and allowed to proceed for 10 min. Reactions were terminated by addition of 3 mL ethyl acetate containing 100 pmol internal standard (4oxo-*at*RA-d_3). After centrifugation for 2 minutes to separate the organic and aqueous layers, the organic layer was collected, dried under nitrogen gas and the sample was reconstituted with 100 μl of acetonitrile and analyzed by LC-MS/MS as described above.

To determine inhibition of CYP26A1 by ketoconazole and liarozole, 0.1 pmol CYP26A1 was pre-incubated with 0.2 pmol reductase at room temperature for 5 minutes to allow reductase incorporation into the membrane. CYP26A1 with reductase was then preincubated with ketoconazole or liarozole (≥ 6 concentrations of 0 – 100 μM) and 2.5 nM *at*RA for 5 minutes at 37°C. Incubations (1 mL) were initiated by addition of 1 mM NADPH and quenched after 5 minutes with 5 ml ethyl acetate. 15 pmol *at*RA-d_5 was added as internal standard. Samples were centrifuged to separate the organic layer, dried under nitrogen and reconstituted with 100 μl of acetonitrile prior to analysis with LC-MS/MS as described above. Depletion of *at*RA was determined in comparison to samples incubated in the absence of NADPH.

All experiments were performed in triplicate. IC_{50} values were estimated by fitting equation 3.8 to the data using nonlinear regression in GraphPad Prism (Graphpad Software, San Diego, CA)

$$\text{Activity remaining \%} = \frac{total\ activity}{1+10^{([I]-\log(IC50))}} \qquad \text{Equation 3.8}$$

The total activity is the % activity in the absence of inhibitor, [I] is the concentration of ketoconazole or liarozole, and the IC_{50} is the concentration of inhibitor that causes 50% of the total measured inhibition.

3.3.11 Determination of Unbound Fraction of Ketoconazole and Liarozole in Supersomes and Plasma

The protein binding of the inhibitors was determined using ultracentrifugation as previously described (Nakai *et al.*, 2004; Shirasaka *et al.*, 2013). To determine the unbound fraction in in vitro incubations and in plasma, 100 μM of ketoconazole or liarozole was added to CYP3A4, CYP2C8 or CYP26A1 (5 pmol/mL) microsomes in KPi buffer or to plasma and the samples split into two aliquots. One aliquot was incubated at 37°C for 90 min, while the other

aliquot was centrifuged in a Sorvall Discovery M150 SE Ultracentrifuge at 100,000 rpm (435,630 × g) for 90 min at 37°C to precipitate protein. After centrifugation, 100 µL aliquots were transferred to a 96-well plate containing 100 µL acetonitrile.

A standard curve of each inhibitor was prepared in 50:50 KPi: acetonitrile (v: v) and analyzed in parallel. The samples were centrifuged using a Beckman Coulter Allegra 25R centrifuge at 3,000 × g for 15 min at 4°C. Following centrifugation, 100 µL from each well was transferred to a clean 96-well plate for LC-MS/MS analysis.

Samples were separated using a Shimadzu Prominence UFLC (Columbia, MD) equipped with a Thermo Hypersil Gold C18 column (2.1 × 100 mm, 1.9 µm) using gradient elution with (A) H_2O (0.1% formic acid) and (B) acetonitrile at a flow rate of 0.5 ml/min. The gradient was from an initial 95% A to 10% A over 3 min, stayed at 10% A for 1.5 min and then returned to 95% A for 2 min. Analytes were detected by an AB Sciex QTRAP® 3200 mass spectrometer operated in electrospray positive mode with detection of m/z MRM transition of 531.1/82.2 for ketoconazole and 309.14/241.1 for liarozole. The declustering potential, entrance potential, cell entrance potential, collision energy and collision exit potential were set to 86, 5.5, 20, 73 and 6 for ketoconazole and 26, 4.5, 16, 17 and 4 for liarozole.

3.3.12 Development of Minimal PBPK Models for Ketoconazole and Liarozole

For the ketoconazole minimal PBPK model, ketoconazole-400 mg QD compound file in Simcyp was first verified with clinical observations. However, oral clearance (CL_{po}) (7.4 L/h) assigned in the compound file was generally lower than the reported average CL_{po} value (9.5 L/h) (Daneshmend *et al*., 1981; Daneshmend *et al.*, 1984; Baxter *et al.*, 1986). Therefore, CL_{po} was optimized to 9.5 L/h with 30% CV. Since CL_{po} (14.4 L/h) in Simcyp ketoconazole-200 mg QD file was similar to the average CL_{po} (13.5 L/h) reported in the literature (Daneshmend *et al*., 1981;

Daneshmend *et al.*, 1984; Huang *et al.*, 1986), this file was used without modification on CL_{po}. For both models the inhibition potency of ketoconazole towards CYP3A4, CYP2C8 and CYP26A1 as determined in the in vitro experiments was incorporated into the compound file.

Liarozole minimal PBPK model was built using information from literature (Bryson and Wagstaff, 1996; De Buck *et al.*, 2007) and in vitro experiments. The absorption of liarozole was described with first-order absorption model with Simcyp predicted absorption parameters. Elimination of liarozole was characterized using CL_{po} reported in humans (Bryson and Wagstaff, 1996). Liarozole distribution was described using a minimal PBPK model with V_{ss} estimated from reported clinical data as 1.08 L/kg (Bryson and Wagstaff, 1996; Denis *et al.*, 1998) and the elimination rate constant was calculated from equation 3.9 :

$$\frac{C_{ss,max}}{C_{ss,min}} = e^{k\tau} \qquad \text{Equation 3.9}$$

in which $C_{ss,\,max}$ and $C_{ss,\,min}$ are the peak and trough concentrations at steady state, k is elimination rate constant and τ is dosing interval. The K_p value of liver was predicted using method 2 (Rodgers and Rowland, 2006) in Simcyp. In vitro measurements of fu_{mic} and K_i of liarozole for CYP2C8, CYP26A1 and CYP3A4 were incorporated into the interaction module. Since inhibition experiments were done at $S << K_m$, the IC_{50} can be assumed to be approximately equal to K_i, and IC_{50} values determined in the inhibition assay were used as K_i (Lutz and Isoherranen, 2012).

3.4 RESULTS

3.4.1 *at*RA PBPK Model in Healthy Humans

The *at*RA PBPK model in Simcyp was first developed in healthy humans based on obtained experimental and literature data. In order to develop the PBPK model, the blood to

plasma ratio of *at*RA was measured. The blood to plasma ratio of *at*RA measured in human blood was 2.3 indicating significant partitioning into blood cells. To develop the PBPK model and establish tissue K_p values, *at*RA disposition in mice was determined (Figure 3.2). The elimination of *at*RA from serum after IP dosing was efficient with elimination half-life of 0.5 hours. Similar half-lives of 0.4-0.6 hours were observed in liver, kidney and pancreas indicating fast metabolism of *at*RA in tissues and a rapid distribution equilibrium. The AUCs in liver, kidney and pancreas were higher than the AUC in serum (Table 3.1), indicating efficient partitioning of *at*RA into tissues. The measured K_p values of 3.79 and 2.06 in liver and kidney were similar to K_p values calculated from reported concentration-time data in mice after IV dosing with 10 mg/kg *at*RA (Wang *et al.*, 1980). K_p values predicted using Rodgers and Rowland method were 16.78, 10.14, 17.34, 2.28 and 26.90 for liver, kidney, pancreas, lung and brain respectively with predicted V_{ss} of 28.10 L/kg. These values greatly exceeded the K_p values obtained from mouse studies. Similarly, the predicted V_{ss} significantly exceeded the V_{ss} of 0.46 L/kg predicted via allometric scaling. Therefore, the experimental K_p values were used to refine the distribution model (Table 3.2).

To predict the F_a and Q_{gut} in the first-order *at*RA absorption model, the permeability of *at*RA was measured in Caco-2 cells. In Caco-2 cells, a permeability of 3.58×10^{-6} cm/s was measured for *at*RA. *at*RA permeability ratio (apical to basolateral / basolateral to apical) was 1.1 indicating that no active transporters were involved (Figure 3.3, Table 3.3). The F_a and Q_{gut} values of 0.48 and 3.5 L/h indicating a low permeability for *at*RA in the gut were predicted based on Caco-2 cell permeability data. A k_a of 0.90 1/hour with a 0.84-hour lag time for absorption was obtained from fitting the observed clinical data into one compartment model.

Due to the lack of dosage form, systemic *at*RA clearance has never been evaluated in humans. Clinical studies in humans after oral administration of *at*RA reported that urinary excretion of unchanged *at*RA is negligible and *at*RA is not found in human urine after β-glucuronidase incubation (Muindi *et al.*, 1992b; Conley *et al.*, 1997). Therefore, renal clearance and UGT mediated elimination were not incorporated into the model and the clearance of *at*RA was all assigned to the hepatic P450 enzymes (Table 2). The complete model parameters are summarized in Table 3.2.

To verify the model, *at*RA disposition was first simulated in healthy subjects after administration of a single oral dose of *at*RA. Three different studies with *at*RA dosed at 10 mg, 20 mg and 22.5 mg/m^2 PO were simulated. The observed mean concentration- time curves were within the 5th and 95th percentile of the simulated, and the mean simulated AUCs were 1.5-, 1.2- and 0.9- fold of the observed ones (Figure 3.4). The predicted AUCs for two of the three studies (70%) met the predefined acceptance criteria (simulated AUC not significantly different from observed, p=0.4 and 0.7) and predicted C_{max} and t_{max} were similar to observed values (Table 3.4). The developed PBPK model successfully simulated the dose dependent kinetics of *at*RA following a single dose administration with the oral clearance decreasing from 140 ± 136 L/h following 10 mg dose to 87 ± 72 L/h after 20 mg dose and to 65 ± 63 L/h after 22.5 mg/m^2 dose of *at*RA.

To test whether the induction parameters for CYP26A1 would accurately predict the autoinduction of *at*RA clearance, the disposition of *at*RA following 22.5 mg/m^2 oral doses BID for 15 days was simulated (Figure 3.4C). The predicted AUCs after multiple doses were not significantly different from the observed AUCs (p=0.1 and 0.2) (Table 3.4). The simulated mean AUCs on day 9 and day 15 were 0.6- and 0.5- fold of the observed ones. The predicted 64% and

65% decreases in *at*RA AUC after multiple dosing were in good agreement with the observed 42% and 37% reductions of *at*RA AUC on day 9 and day 15. Hence the developed model successfully simulated the saturation kinetics and autoinduction of *at*RA clearance, and based on these results the model was considered verified.

3.4.2 *at*RA PBPK Model in Adult and Pediatric Cancer Patients

*at*RA disposition in cancer patients was first simulated using the PBPK model developed in healthy population. Using the *at*RA drug file developed in healthy subjects over-predicted the AUC and C_{max} by about 5- and 3-fold whereas the t_{max} and half-life were accurately predicted. This suggested that F_a is decreased in cancer patients without changes in k_a, CL and V. Therefore, F_a was optimized in the PBPK model from 0.48 to 0.14 and the population profile was modified according to published changes in cancer patients (Cheeti *et al.*, 2013).

*at*RA disposition was then simulated in 11 clinical studies conducted in cancer patients with *at*RA dosed at 40 mg/m^2 (2 studies) and 45 mg/m^2 (9 studies). The predicted AUC for 9 of the studies (82%) was within the predefined acceptance range with mean simulated AUCs within 0.5- and 1.1-fold of the observed ones (Table 3.5). The observed mean AUC values in the two studies that were not accurately predicted were more than 2-fold different from the mean AUC of the other observed studies (Table 3.5). The observed AUC in the study conducted in large cell carcinoma and squamous cell carcinoma patients was <50% of the AUC values observed in the other studies with the same dosing regimen (Table 3.5). None of the other studies in cancer patients had a mean AUC that would have met the calculated acceptance range for the study in large cell carcinoma and squamous cell carcinoma patients. The observed AUC in one of the studies conducted in solid tumor patients had an observed AUC that was 2.7-fold to 3- fold higher than the AUC observed in other studies in solid tumor patients, and none of the other studies in solid tumor patients had a

mean AUC that would have met the calculated acceptance range for this study (Table 3.5). As such, neither the model nor the other clinical studies predicted the *at*RA AUCs in 2 of the 11 studies within the acceptance criteria. Unfortunately, the reported information on study populations was not sufficient to evaluate potential mechanisms of why these two studies showed discrepant disposition compared with other cancer studies.

The PBPK model in cancer population also successfully simulated the dose dependent kinetics of *at*RA with the simulated mean oral clearance decreasing from 335 L/h (2 studies) to 276 L/h (9 studies) as the dose increased from 40 mg/m^2 to 45 mg/m^2 *at*RA. Similarly, the predicted AUCs of *at*RA were within the acceptance range on both day 1 and day 7 of dosing when compared to the observed data of multiple dosing study in chronic myeloid leukemia patients dosed with 40 mg/m^2 *at*RA BID (Table 3.5). The model predicted a 57% decrease in *at*RA AUC over the 7-day dosing which is in good agreement with the observed 62% reduction in *at*RA AUC on day 7.

Because *at*RA is frequently used in pediatric population, the PBPK model was applied to a pediatric cancer population to simulate *at*RA disposition in pediatric patients. The *at*RA disposition after a single oral dose was simulated for 3 different studies with 30 and 40 mg/m^2 dose of *at*RA to pediatric cancer patients. The simulated mean AUC was 1.0-, 0.4- and 0.5- fold of the observed values. The predicted AUC for 2 of the studies was within the predefined acceptance range (Table 3.6). For the third study with higher dosing regimen the predicted AUC was not significantly different from the observed ($p=0.1$) and was within 2-fold of the observed. Similar to what was observed in adult clinical studies, large variability in *at*RA kinetics was also observed in pediatric patients. The simulation of *at*RA disposition in adult and pediatric population successfully captured this large variability (Tables 3.5 and 3.6).

3.4.3 PBPK modeling of Effects of Ketoconazole and Liarozole on *at*RA Disposition

To predict the drug-drug interactions (DDI) between *at*RA and ketoconazole and liarozole, the inhibition of *at*RA metabolism by ketoconazole and liarozole was first characterized in vitro (Figure 3.5) and the results were incorporated into ketoconazole and liarozole models (Tables 3.7 and 3.8).

Ketoconazole had the highest inhibition potency towards CYP3A4 (IC_{50} 0.015 µM, 95% CI 0.010-0.023 µM) followed by CYP26A1 (IC_{50} 0.47 µM, 95% CI 0.25–0.91 µM) and CYP2C8 (IC_{50}: 6.7 µM; 95% CI 1.4–31 µM) (Figure 4A). In contrast, liarozole had similar affinity to all three CYPs with IC_{50}s of 3.3 µM (95% CI 2.1–5.0 µM) for CYP26A1, 1.2 µM (95% CI 0.92–1.6 µM) for CYP3A4 and 1.3 µM (95% CI 0.77–2.3 µM) for CYP2C8 (Figure 3.5B).

The ketoconazole PBPK models for different ketoconazole dosages were verified with clinical ketoconazole pharmacokinetic studies (Figure 3.6 and Table 3.9) and the ketoconazole 200 mg PO dosing model and 400 mg PO dosing model were considered acceptable for DDI simulation. A liarozole PBPK model was also developed based on existing in vivo data (Table 3.8) and liarozole disposition was simulated and compared to reported clinical studies (Table 3.10). Due to the lack of information on the variability in liarozole disposition in the reported study, liarozole model could not be verified using the acceptance criteria described. However, the predicted pharmacokientic parameters were within the 2-fold range of the observed values and therefore considered to be similar to the reported parameters and acceptable for DDI simulation.

After model verification, a multi-phase DDI study between ketoconazole and *at*RA was simulated. In the clinical study, cancer patients were treated with 45 mg/m^2 *at*RA on days 1, 2, 28, and 29 of treatment and with 45 mg/m^2 *at*RA BID for the remaining days 3-27. A single dose of 200 mg or 400 mg ketoconazole was given on days 2 and 29, 1 hour prior to *at*RA (Rigas *et al*.,

1993). The study was simulated using the verified ketoconazole PBPK model in the cancer population, and the simulation successfully predicted the DDI between *at*RA and ketoconazole in adult cancer patients (Table 3.11 and Figure 3.7). The predicted AUC of *at*RA on each kinetic day in the presence and absence of ketoconazole met the acceptance criteria and was also within 2-fold of the observed (Table 3.11). The observed AUC on the first day was not available for the individual ketoconazole dosing groups and hence a single control group for *at*RA disposition was simulated.

The predicted decrease in *at*RA AUC between day 1 and day 28 of dosing was about 61% and in excellent agreement with the observed 61% decrease in *at*RA AUC. The inhibition of *at*RA clearance by ketoconazole was also well predicted. The simulation predicted a 1.4-fold increase in *at*RA AUC following ketoconazole administration on day 2, a fold increase similar to the observed average 1.1-fold increase in *at*RA AUC. The simulation also predicted a 2.0 and 2.7-fold increase in *at*RA AUC following 200 mg and 400 mg ketoconazole administration on day 29, a fold increase in excellent agreement with the observed 1.5 and 2.2-fold increases in *at*RA AUC between days 28 and 29. In context of predicting the efficacy of ketoconazole in combating therapy resistance, the model accurately predicted that 400 mg ketoconazole would restore the *at*RA exposure on day 29 to the levels observed on day 1.

Similar to the DDI study between ketoconazole and *at*RA, a DDI study between liarozole and *at*RA was simulated according to a reported study (Miller *et al.*, 1994). In the reported study, cancer patients were treated with 45 mg/m^2 *at*RA on days 1, 2, 28, and 29 and with 45 mg/m^2 b.i.d. for the remaining days 3-27. A single dose of 75 mg, 150 mg or 300 mg liarozole was given on days 2 and 29, 1 hour prior to *at*RA. The simulation successfully predicted the DDI between *at*RA and liarozole in adult cancer patients with the exception of 150 mg liarozole dosing where the

observed studies reported *at*RA AUCs that had acceptance ranges that excluded all other clinical observations as well (Table 3.11 and Figure 3.7). The other predicted AUCs of *at*RA on each reported study day in the presence or absence of liarozole were within the predefined model acceptance criteria.

The simulation predicted about 61% decrease in *at*RA AUC between day 1 and day 28, a prediction in good agreement with the observed 58-84% decrease in *at*RA AUC. The simulation also correctly predicted that on day 2 despite the liarozole administration, the AUC of *at*RA would be lower or not different when compared to that on day 1 of treatment. Similarly, the simulation predicted a 1.2-1.5-fold increase in *at*RA AUC by liarozole dosing between day 28 and day 29 which is in excellent agreement with the 1.7- 2.2-fold observed increase in *at*RA AUC (Table 3.11). The simulation also accurately predicted the efficacy of liarozole in combatting therapy resistance to *at*RA. The simulated data predicted that 300 mg liarozole would restore *at*RA AUC to 58% of the initial AUC after a single dose. This is in excellent agreement with the observed efficacy of liarozole restoring *at*RA AUC to 61% of that observed after single dose (Table 3.11).

3.5 DISCUSSION

*at*RA is widely used as a therapeutic agent in the treatment of APL and has shown promise in the treatment of other malignancies. However, the therapeutic use of *at*RA is limited due to its dose- and time- dependent kinetics. Although the dose- and time- dependent kinetics of *at*RA have been observed in animals and humans, the mechanisms and kinetics of saturation and induction of *at*RA metabolism have not been well characterized in vivo. The PBPK model of *at*RA disposition presented here provides a mechanistic framework for understanding the time- and dose-dependent kinetics of therapeutically administered *at*RA. Complex *at*RA kinetics were incorporated in the PBPK model and successfully simulated clinical studies after single and multiple doses of *at*RA

both in healthy volunteers and in cancer patients. The simulations strongly support the hypothesis that the dose dependent, nonlinear kinetics of *at*RA are due to saturation of CYP26A1 mediated clearance of *at*RA, and that the time dependent increase in *at*RA clearance is due to induction of hepaticCYP26A1 by *at*RA. It is possible that CYP26A1 is induced in other metabolic sites as well, but at present CYP26A1 expression appears to be restricted predominantly to the liver (Topletz *et al.*, 2012). Taken together, the developed *at*RA PBPK model demonstrates a unique application of PBPK modeling to a complex clinical scenario of drug disposition including time and concentration dependent changes in clearance. The presented data shows that in vitro data can successfully be used to develop PBPK models of such complex systems and incorporate new eliminating enzymes into existing models when adequate physiological data is available.

At present, there is no appropriate dosage form of *at*RA to allow IV administration to humans, and therefore the absorption and distribution kinetics of *at*RA are poorly understood. The studies presented here show that despite its high lipophilicity, *at*RA has relatively low permeability and a restricted volume of distribution similar to many other lipophilic acidic compounds that are highly bound to plasma albumin. The Caco-2 cell assay suggested that passive diffusion is the primary mechanism of *at*RA absorption in gut, and that transporters do not contribute to *at*RA absorption. The distribution volume of *at*RA appears to be predictable between species and it is likely that the individual organ tissue to plasma partition ratios are similar between species. However, at present the distribution component of the PBPK model is not adequate to allow simulation of *at*RA distribution to specific organs or drug target sites except the liver, kidney, lung, pancreas and brain.

The in vivo clearance of *at*RA was predicted from in vitro enzyme kinetic data with the addition of the in vivo information of lack of renal elimination of unchanged *at*RA and detection

of conjugated metabolites such as glucuronides in human urine. The enzyme kinetic data and the dynamic model predicted approximately 90% clearance of *at*RA by hepatic CYP26A1 metabolism following a single dose of *at*RA, a value in good agreement with the previously predicted >90% contribution based on static prediction (Thatcher *et al.*, 2010). Uniquely, this model also accurately predicted the saturation kinetics of *at*RA based on the in vitro enzyme kinetic values and the time dependent induction of CYP26A1 based on HepG2 cell and hepatocyte induction data. In addition to *at*RA disposition when administered alone, the model also accurately predicted the complex DDIs between *at*RA and ketoconazole and *at*RA and liarozole.

The inhibition of *at*RA clearance has been an attractive therapeutic target for combatting therapy resistance to *at*RA in treatment of APL and possibly other cancers. However, the development of inhibitors of *at*RA metabolism has been hindered by lack of understanding of the necessary potency and pharmacokinetic characteristics of novel inhibitors, especially in the target cancer population. The developed model together with the DDI simulations provides insight to the shortcomings of the clinical studies conducted with ketoconazole and liarozole as CYP26 inhibitors, and it will allow design of future dosing regimens that can restore *at*RA exposures to the levels observed following single doses. In addition, the model can be used to design *at*RA dosing regimens that achieve maximum exposure and efficacy.

It is well recognized that patient demographics and physiological features are different for cancer patients and healthy subjects. To address these differences, a previously developed adult cancer population model (Cheeti *et al.*, 2013) was adapted to test whether the healthy population PBPK model for *at*RA could be applied to cancer patients. Based on model verification and sensitivity analysis, all the data collectively suggested that *at*RA absorption is significantly decreased in cancer patients, while all the physiological features reported in the previous cancer

population model were applicable to the cancer populations included in the *at*RA clinical studies. The decrease in *at*RA absorption is not entirely surprising, as malnutrition, anorexia and cachexia and alterations in nutrient absorption and nutritional status are commonly reported in cancer patients (Argilés, 2005). As *at*RA is also the active form of vitamin A it is possible that alterations in its absorption are related to the general poor absorption of nutrients in cancer patients and will not reflect absorption processes for cancer medications. However, further studies are needed to investigate potential effects of cancer on drug absorption.

With the modification of the absorption of *at*RA in cancer patients, the developed PBPK model accurately predicted *at*RA disposition in this challenging patient population for which it is often difficult to obtain sufficient pharmacokinetic data. In addition, the developed PBPK model could be applied to predict *at*RA disposition in pediatric cancer patients, a uniquely vulnerable population. As such, the data obtained supports the use of PBPK models developed in healthy populations to predict disposition in patient populations including pediatrics.

In summary, a mechanistic PBPK model predicting *at*RA disposition in both healthy volunteers and cancer patients has been developed. The model was successfully applied to simulate the pharmacokinetic profiles of *at*RA after single and multiple doses and to quantitatively predict the interaction between *at*RA and *at*RA metabolism inhibitors (ketoconazole and liarozole). Therefore, it could be used to investigate *at*RA disposition, to design drug -drug interaction studies in the development of novel *at*RA metabolism inhibitors and to predict *at*RA pharmacokinetics in cancer patients.

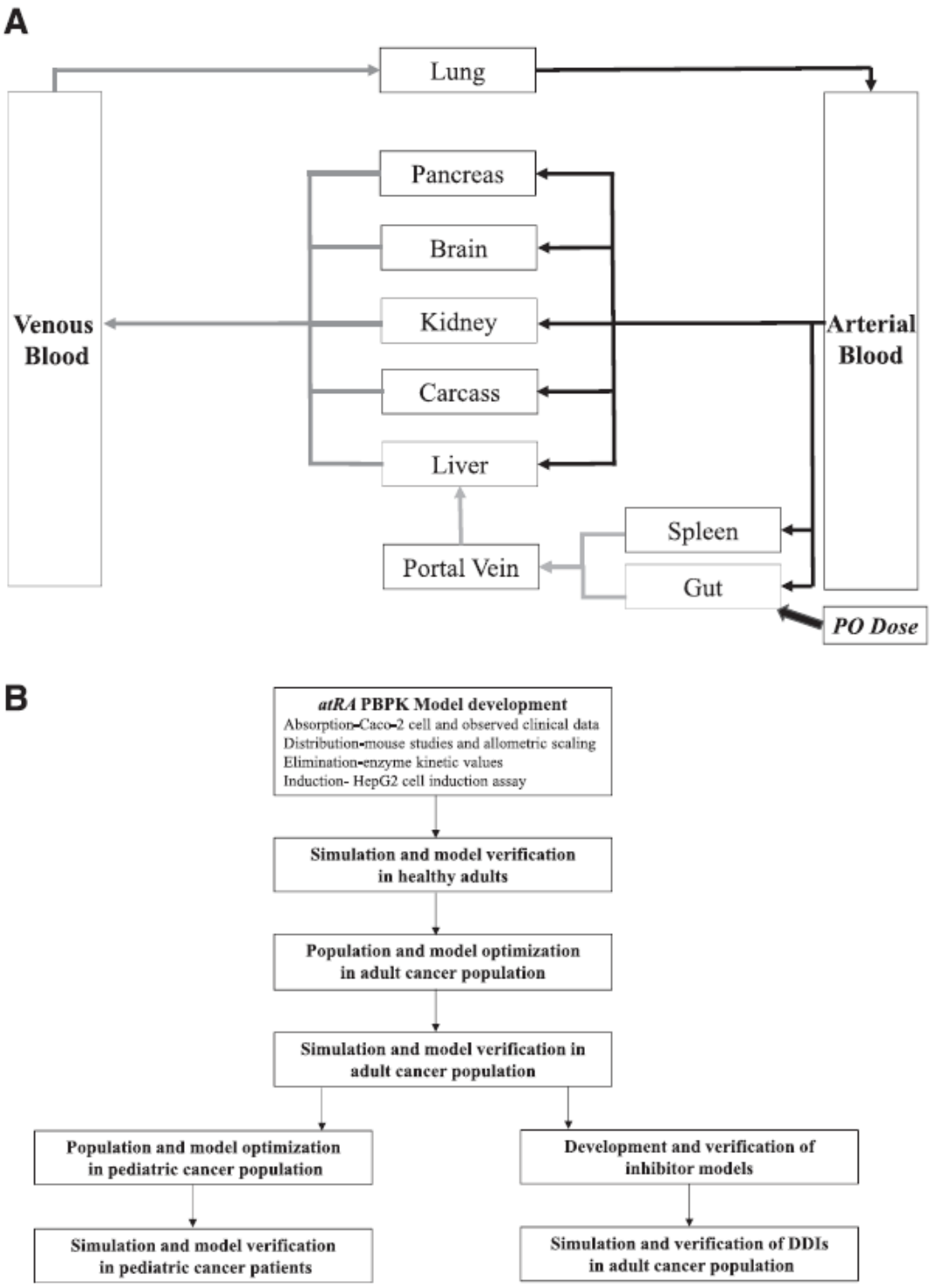

Figure 3.1. **Development of the *at*RA PBPK model.** (A) The *at*RA PBPK model structure. (B) Workflow of model development and verification.

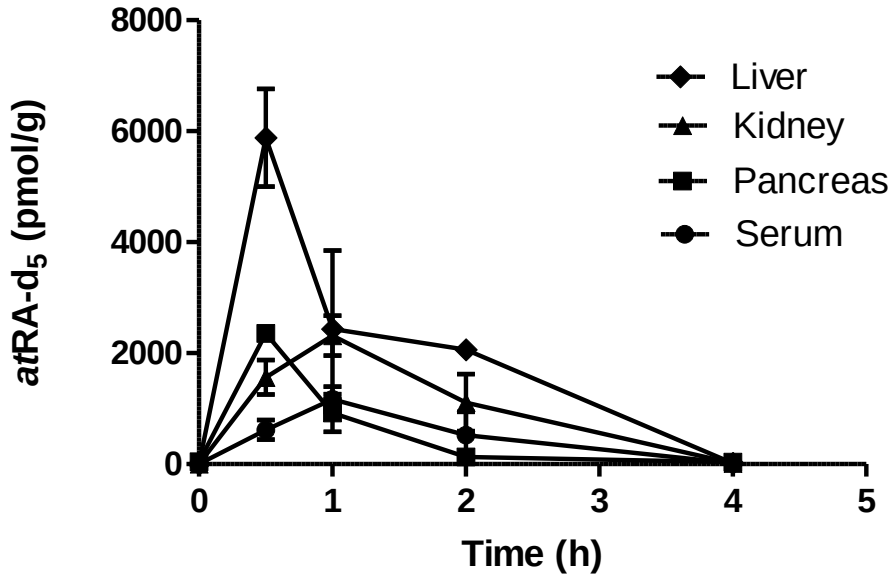

Figure 3.2. Concentration–time profiles of *at*RA in C57BL/6J mouse (n = 12) serum, liver, kidney, and pancreas after administration 1 mg/kg *at*RA-d_5 IP.

Data are shown as mean ±S.D.

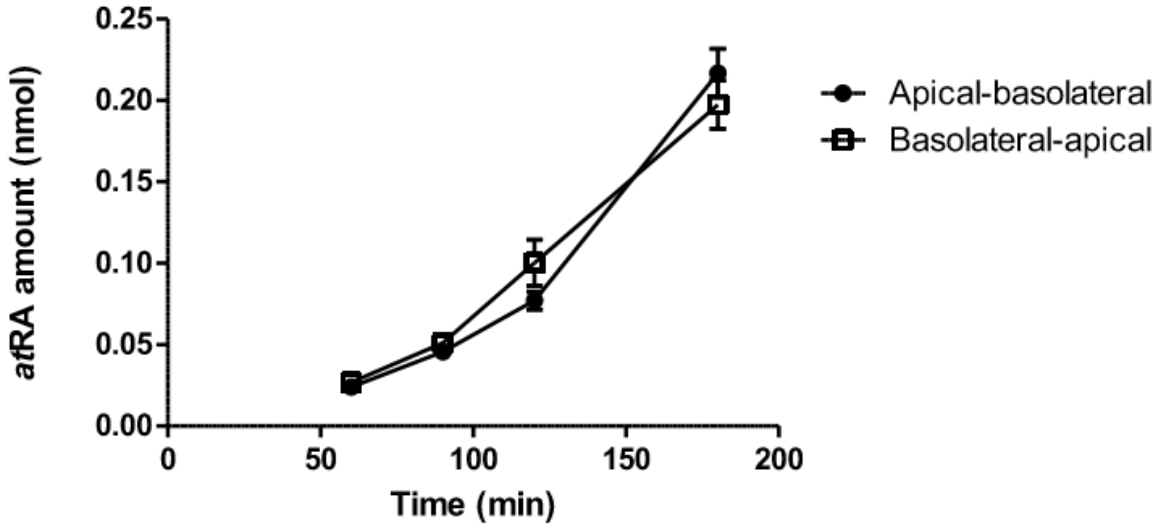

Figure 3.3. Transcellular transport of *at*RA in Caco-2 Cells

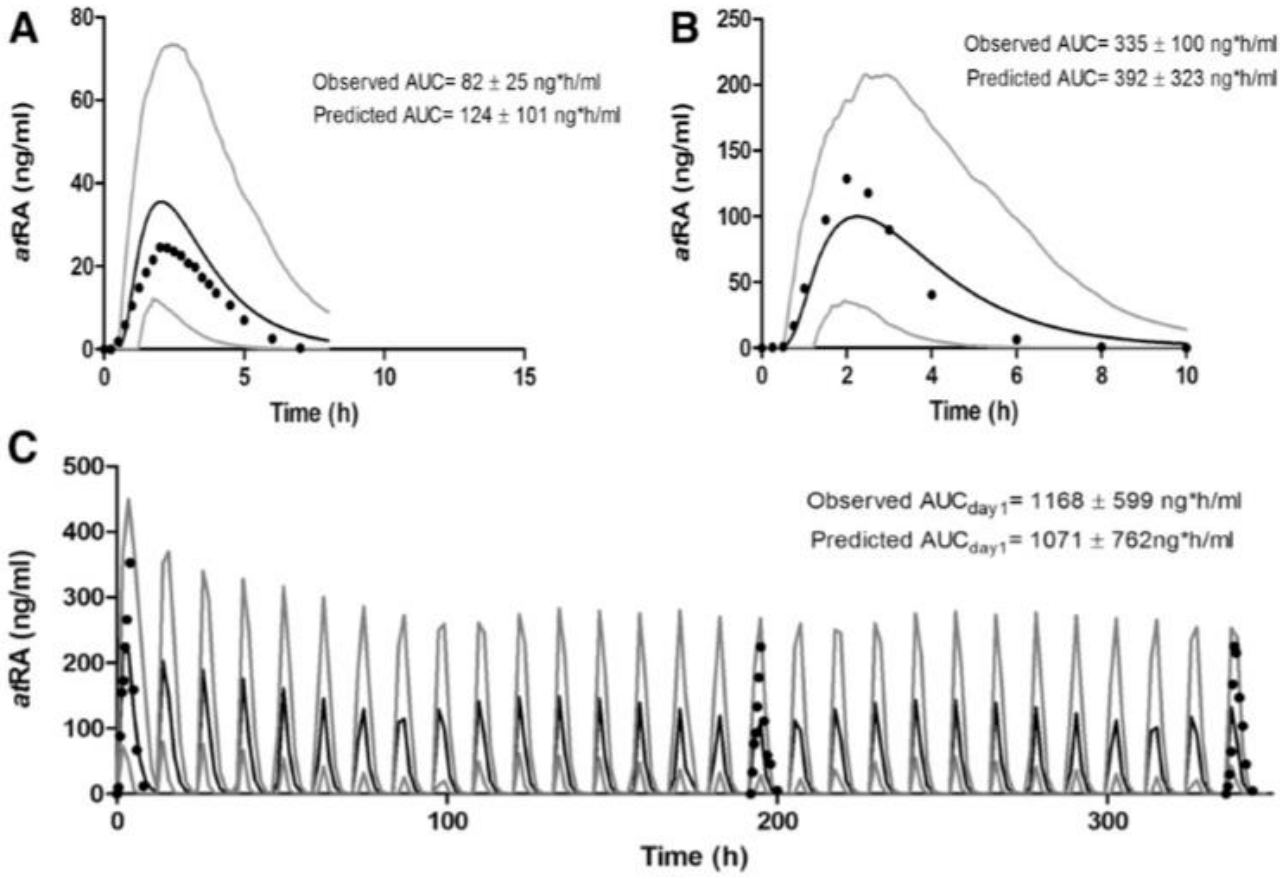

Figure 3.4. Predicted and observed mean plasma concentration–time profiles of *at*RA in healthy volunteers. (A) Administration of 10 mg *at*RA PO (as described inThudietal., 2011). (B) Administration of 20 mg *at*RA PO (as described in Peng et al., 2014). (C) Administration of 22.5 mg/m^2 *at*RA PO BID (as described in Ozpolat et al., 2003). The solid line depicts the mean of the simulated data with 5th and 95th percentile shown with light gray line. Solid circles show the observed data in the study.

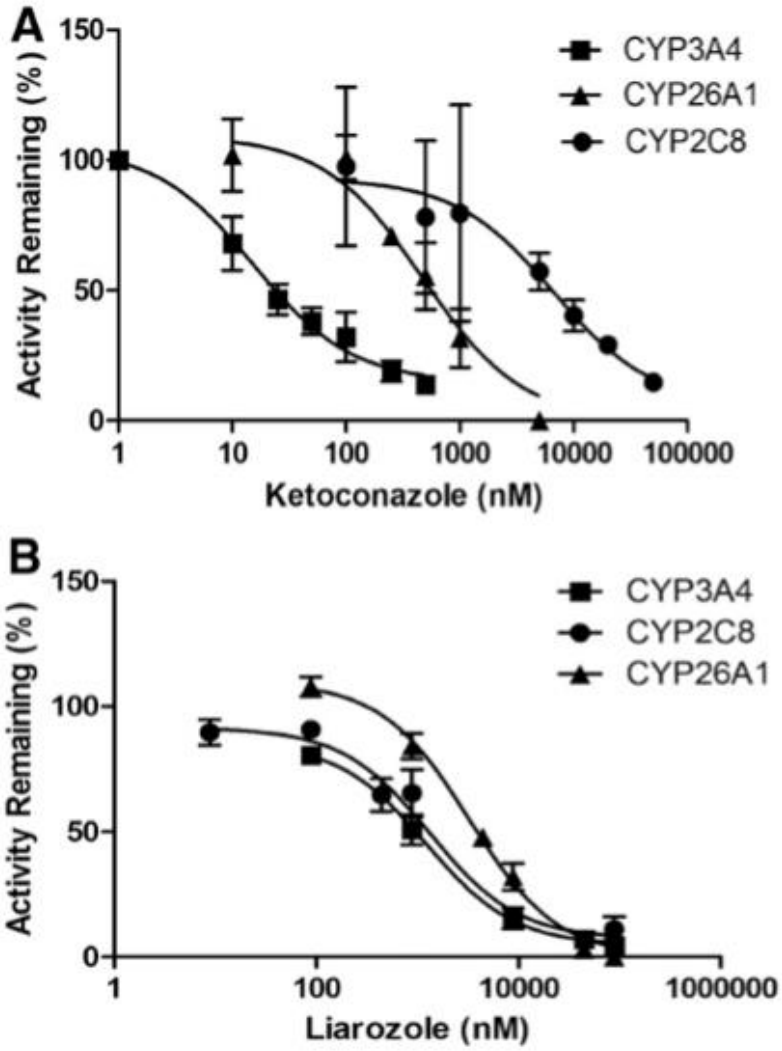

Figure 3.5. In vitro IC50 curves for CYP26A1, CYP3A4, and CYP2C8 with *at*RA as substrate and ketoconazole and liarozole as inhibitors. Data are shown as mean ± S.D. (A) Ketoconazole CYP3A4 IC_{50}: 0.015mM; CYP26A1 IC_{50}: 0.47 mM; CYP2C8 IC_{50}: 6.65 mM. (B) Liarozole CYP3A4 IC_{50}: 1.22 mM; CYP26A1 IC_{50}: 3.26 mM; CYP2C8 IC_{50}:1.33mM.

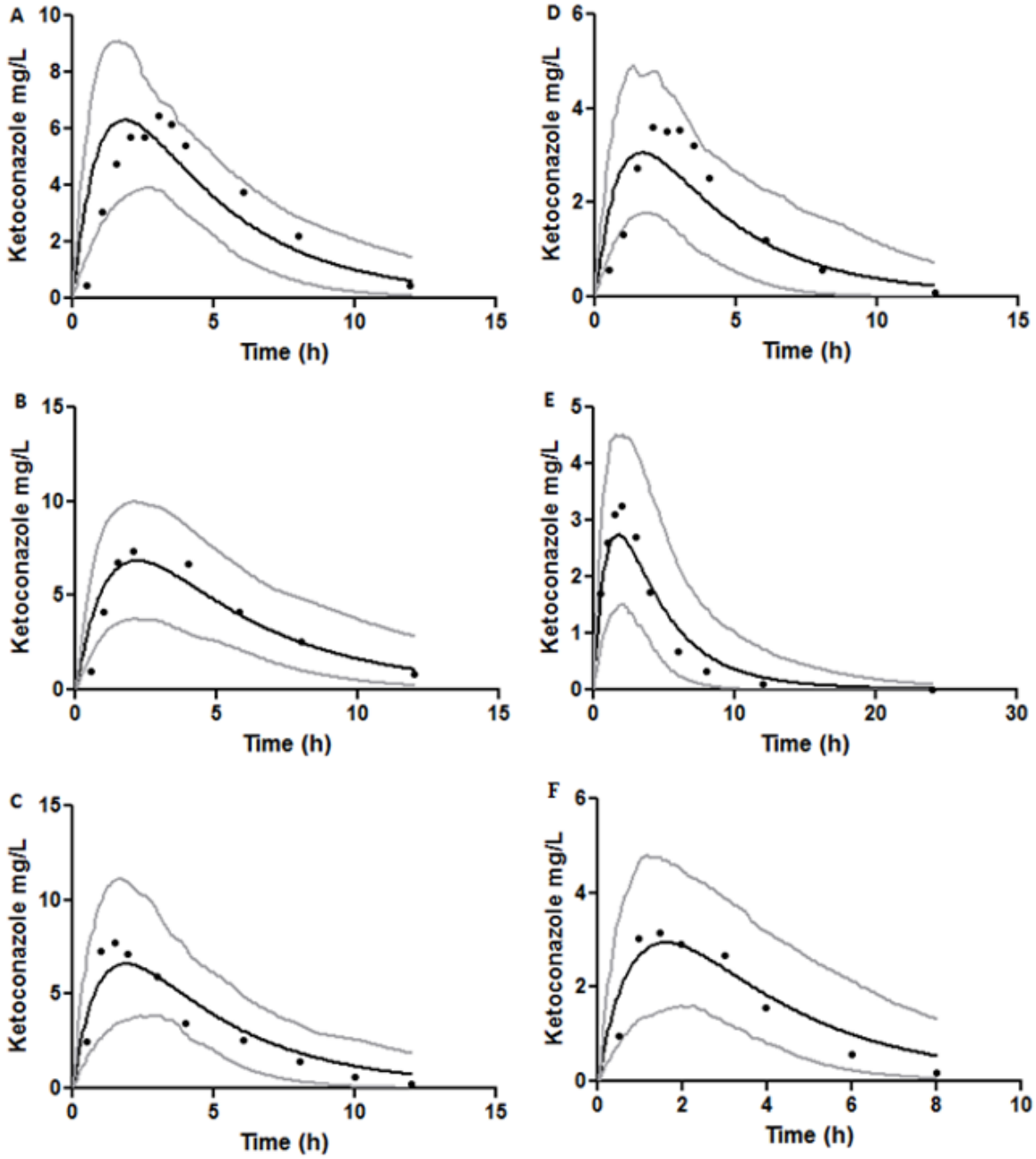

Figure 3.6. Predicted and observed mean plasma concentration–time profiles of ketoconazole in healthy volunteers. The solid line depicts the mean of the simulated data with 5th and 95th percentile shown with light grey line. Solid circles show the observed data in the reported studies. Panels A-C show the data for ketoconazole after a 400 mg PO dose and panels D-F show the data for ketoconazole after a 200 mg PO dose. The observed data is from Daneshmend et al., 1981; Baxter et al., 1986; Daneshmend et al., 1984 and Huang et al., 1986.

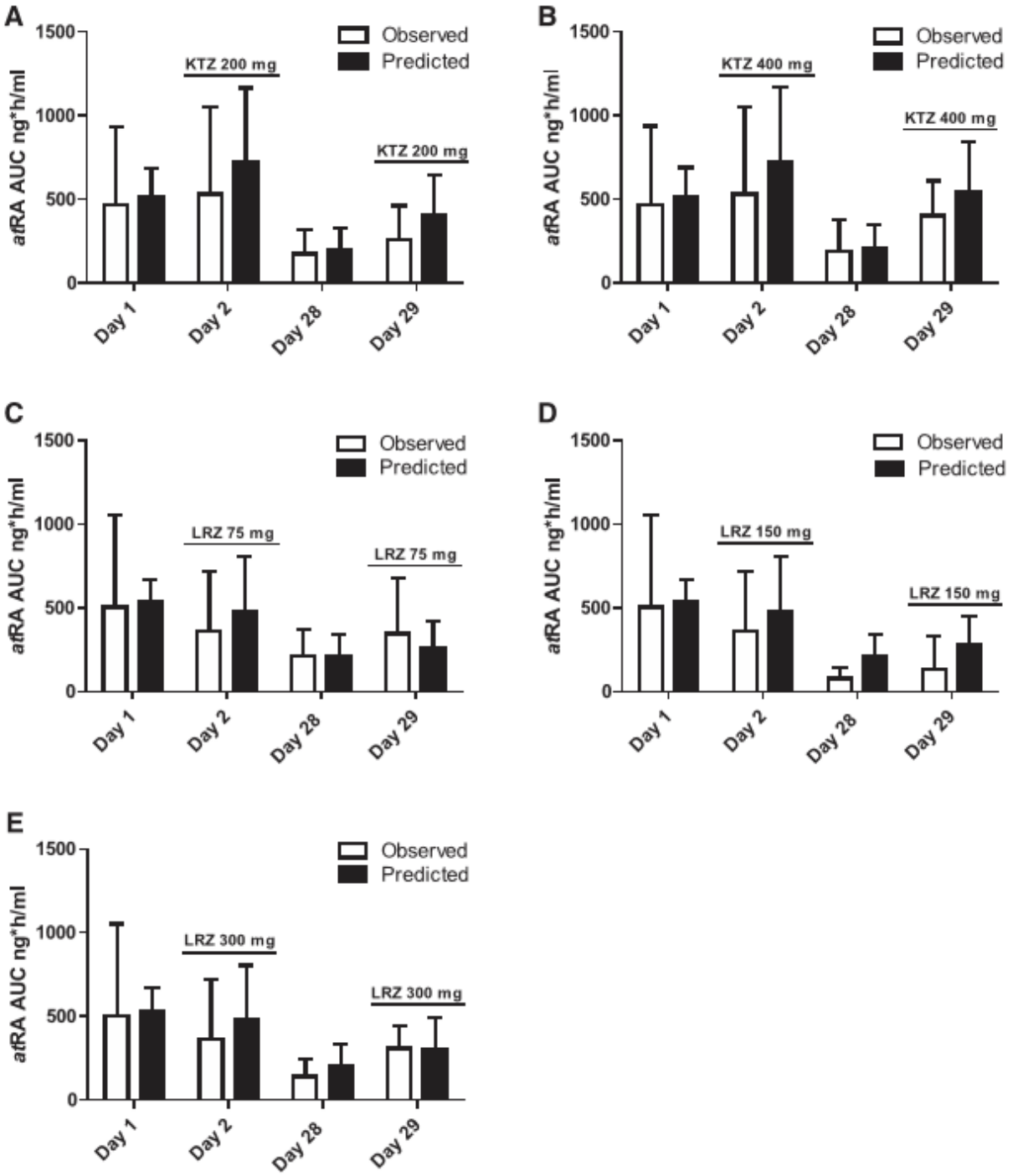

Figure 3.7. Predicted (black bars) and observed (white bars) *at*RA AUC in cancer patients dosed with a single dose of 45 mg/m^2 of *at*RA on days 1, 2, 28, and 29, and twice a day for the rest of the days. A single dose of ketoconazole or liarozole was given on days 2 and 29 1 hour before *at*RA. Ketoconazole was dosed at (A) 200 mg and (B) 400 mg, and liarozole at (C) 75 mg, (D) 150 mg, and (E) 300 mg. The observed data are from Miller et al. (1994) and Rigas et al. (1993).

Table 3.1. Pharmacokinetic parameters of *at*RA obtained in male C57BL/6J mice (n = 12) dosed with 1 mg/kg *at*RA-d5 IP.

	$AUC_{0-\infty}$	C_{max}	t_{max}	$t_{1/2}$	K_p
	(h*pmol/g)	(pmol/g)	(h)	(h)	
Serum	1717	1168	1.0	0.5	
Liver	6503	5884	0.5	0.4	3.79
Kidney	3531	2316	1.0	0.4	2.06
Pancreas	1949	2358	0.5	0.6	1.13

Table 3.2. Summary of parameter input values for *at*RA PBPK model

Parameters	Input Values	Reference/Comment
Molecular weight (g/mol)	300.4	PubChem
log$P_{o:w}$	6.3	Drug bank
Compound type	Monoprotic acid	
pK_a	5	Drug bank
Blood-to-plasma ratio (B/P)	2.3	Measured
$f_{u,p}$	0.05	Muindi et al., 1992b
Absorption	1st order absorption model	
F_a		
Healthy population	0.48	Predicted
Cancer population	0.14	Predicted
k_a (1/h)	0.9	Assigned
Lag time (h)	0.84	Assigned
$f_{u,Gut}$	1	Simcyp default value
Q_{Gut} (l/h)	3.5	Predicted
$P_{eff,\ man}$ (10^{-4}cm/s)	0.5	Predicted
Distribution	Full PBPK model	
V_{ss} (l/kg)	0.46	Predicted
K_p		
Liver	3.79	Measured
Kidney	2.06	Measured
Pancreas	1.13	Measured
Lung	1.53	Wang et al., 1980
Brain	3.39	Wang et al., 1980
Other tissue	0.2/each	Assigned
Elimination	Enzyme kinetics: recombinant	
CYP3A4		
V_{max} (pmol/min/pmol p450)	4.0	Thatcher et al., 2010
K_m (μM)	19.4	Thatcher et al., 2010
$f_{u,mic}$	0.37	Thatcher et al., 2010
CYP2C8		
V_{max} (pmol/min/pmol p450)	4.8	Thatcher et al., 2010
K_m (μM)	13.4	Thatcher et al., 2010
$f_{u,mic}$	0.54	Thatcher et al., 2010
CYP26A1		
V_{max} (pmol/min/pmol p450)	11.3	Thatcher et al., 2010
K_m (μM)	0.0094	Thatcher et al., 2010
$f_{u,mic}$	1	Thatcher et al., 2010
CYP3A5		
V_{max} (pmol/min/pmol p450)	4.9	Thatcher et al., 2010
K_m (μM)	11.1	Thatcher et al., 2010
$f_{u,mic}$	0.31	Thatcher et al., 2010
CYP3A7		
V_{max} (pmol/min/pmol p450)	2.3	Thatcher et al., 2010
K_m (μM)	11.3	Thatcher et al., 2010
$f_{u,mic}$	0.3	Thatcher et al., 2010
Interaction	CYP26A1-induction	
Ind_{max}	33 (8.4 CV %)	Tay et al., 2010; Topletz et al., 2015
$IndC_{50}$ (μM)	0.09 (20.4 CV %)	Tay et al., 2010
$f_{u,inc}$	0.4	Topletz et al., 2015

Table 3.3. Permeability of *at*RA and reference compounds atenolol and metoprolol in Caco-2 Cells. These values were incorporated into the final *at*RA PBPK model absorption predictions

Compound	Concentration (μM)	Apical to basolateral ($\times 10^{-6}$ cm/sec)	Basolateral to apical ($\times 10^{-6}$ cm/sec)	Ratio
*at*RA	10	3.58 ± 0.41	3.90 ± 0.46	1.09
Atenolol	10	0.64 ± 0.04	0.63 ± 0.04	0.99
Metoprolol	10	28 ± 1. 1	26 ± 0.3	0.93

Table 3.4. Observed and predicted pharmacokinetic parameters of *at*RA in healthy subjects (mean ±SD) following single dose (s.d.) and multiple doses (dosing regimen and duration specified).

Study dosing schedule (number of subjects)	[a]10 mg s.d. (n=54)	[b] 20 mg s.d. (n=29)	[c] 22.5 mg/m^2 b.i.d. day 1 (n=11)	22.5 mg/m^2 b.i.d. day 9 (n=11)	22.5 mg/m^2 b.i.d. day 15 (n=11)
Observed AUC (ng*h/ml)	82 ± 25	335 ± 100	1168 ± 599	676 ± 427	738 ± 742
Predicted AUC (ng*h/ml)	124 ± 101*	392 ± 323	1071 ± 762	385 ± 243	376 ± 240
Observed C_{max} (ng/ml)	33 ± 9	141 ± 32	508 ± 215	346 ± 235	376 ± 354
Predicted C_{max} (ng/ml)	38 ± 20	106 ± 54	264 ± 122	156 ± 75	154 ± 75
Observed t_{max} (h)	2.4 ± 0.9	2.1 ± 0.4	3.9 ± 2.9	3.1 ± 1.4	2.9 ± 1.5
Predicted t_{max} (h)	2.0 ± 0.4	2.3 ± 0.5	2.5 ± 0.5	2.0 ± 0.3	2.0 ± 0.3

Data from [a]Thudi et al., 2011; [b]Peng et al., 2014; [c]Ozpolat et al., 2003; [*]unpaired t-test $p<0.05$ between the observed and predicted AUC

Table 3.5. Observed and predicted pharmacokinetic parameters of *at*RA in adult cancer patients (mean ±SD) following single and multiple doses.

Diagnosis for study population	n	Dose (mg/m^2)	Observed AUC (ng*h/ml)	Predicted AUC (ng*h/ml)	AUC acceptance range (ng*h/ml)	Reference
CMK day 1	18	40 b.i.d.	678 ± 498	438 ± 323	339 - 1356	Russo et al., 1998
CMK day 7	18	40 b.i.d.	259 ± 272	187 ± 115	130 - 518	Russo et al., 1998
Kaposi's sarcoma	8	40	725 ± 368	389 ± 322	363 - 1450	Adamson et al., 1995
LCC/SCC	21	45	162 ± 119	428 ± 264*	81 - 308	Rigas et al., 1996
Adenocarcinoma	22	45	571 ± 291	499 ± 316	286 - 1085	Rigas et al., 1996
Advanced NSCLC	31	45	467 ± 469	475 ± 329	234 - 887	Rigas et al., 1993
Solid tumors	13	45	1355 ± 1479	525 ± 403*	678 - 2575	Lee et al., 1995
Solid tumors	47	45	454 ± 419	510 ± 377	227 - 863	Muindi et al., 1994
Solid tumors	19	45	504 ± 549	505 ± 409	252 - 958	Miller et al., 1994
APL	10	45	499 ± 200	530± 388	250 - 948	Muindi et al., 1992a
APL	13	45	682 ± 500	545 ± 425	341 - 1296	Muindi et al., 1992b
APL	20	45	603 ± 442	561 ± 406	302 - 1146	Muindi et al., 1994

**Outside of verification range. CMK-chronic myeloid leukemia; LCC- large cell carcinoma ; SCC-Squamous cell carcinoma ; NSCLC- non small cell lung cancer*

Table 3.6. Observed and predicted pharmacokinetic parameters of *at*RA in pediatric cancer patients (mean ±SD) following single dose.

n	Dose (mg/m^2)	Observed AUC (ng*h/ml)	Predicted AUC (ng*h/ml)	AUC acceptance range (ng*h/ml)	Reference
8	30	340 ± 141	340 ± 297	102 - 1020	Smith et al., 1992
5	30	972 ± 990	364 ± 234	292 - 2916	Takitani et al., 1995
8	40	1007 ± 631	535 ± 532*	N/A	Smith et al., 1992

**unpaired t-test p=0.1 between the observed and predicted AUC in the indicated study. Not significantly different from observed AUC*

Table 3.7. Summary of parameter input values for the ketoconazole PBPK model

Parameters	Input values	Reference/comment
Interaction		
CYP2C8		
K_i (µM)	6.65	Measured
fu_{mic}	0.72	Measured
CYP26A1		
K_i (µM)	0.47	Measured
fu_{mic}	0.72	Measured
CYP3A4		
K_i (µM)	0.015	Measured
fu_{mic}	0.72	Measured

Table 3.8. Summary of parameter input values for the liarozole minimal PBPK model

Parameters	Input values	Reference/comment
Molecular weight (g/mol)	308.76	PubChem
$logP_{o:w}$	3.38	De Buck et al., (2007)
Compound type	Neutral	De Buck et al., (2007)
Blood-to-plasma ration (B/P)	0.9	De Buck et al., (2007)
$fu_{,p}$	0.055	Measured
Absorption	1st order absorption model	
F_a	1	Predicted
k_a (1/h)	5.05	Predicted
fu_{Gut}	0.0035	Predicted
Q_{Gut} (L/h)	16.25	Predicted
P_{eff} ,man (10^{-4}cm/s)	12.28	Predicted
Distribution	Minimal PBPK	
V_{ss} (L/kg)	1.08	Calculated
K_p – liver	5.69	Predicted
Elimination		
CL_{po} (L/h)	12.55	Bryson et al., (1996)
Interaction		
CYP2C8		
K_i (µM)	1.33	Measured
fu_{mic}	0.51	Measured
CYP26A1		
K_i (µM)	3.26	Measured
fu_{mic}	0.51	Measured
CYP3A4		
K_i (µM)	1.22	Measured
fu_{mic}	0.51	Measured

Table 3.9. Observed and predicted PK parameters (mean ±SD) of ketoconazole in healthy subjects after given 400 mg and 200 mg ketoconazole PO. The observed data is from Daneshmend et al., 1981; Baxter et al., 1986; Daneshmend et al., 1984 and Huang et al., 1986.

n	Dose	Observed AUC (mg*h/L)	Predicted AUC (mg*h/L)	Observed C_{max} (mg /L)	Predicted C_{max} (mg /L)	Observed T_{max} (h)	Predicted T_{max} (h)	AUC acceptance range (mg*h/L)
6	400	41 ± 11	39 ± 10	7	7 ± 2	3.0	2.0 ± 0.5	21 - 82
5	400	50 ± 15	51 ± 21	9 ± 3	7 ± 2	2.6 ± 1.2	2.3 ± 0.5	25 - 100
8	400	37 ± 24	43 ± 14	9 ± 5	7 ± 2	1.6 ± 0.4	2.1 ± 0.6	19 - 74
6	200	18 ± 5	17 ± 7	4	3 ± 1	2.0	1.9 ± 0.6	11 - 29
8	200	13 ± 4	16 ± 6	4 ± 2	3 ± 1	1.6 ± 0.7	1.8 ± 0.5	8 - 21
23	200	15 ± 9	16 ± 7	3 ± 2	3 ± 1	1.7 ± 0.9	1.9 ± 0.5	9 - 24

Table 3.10. Observed and predicted pharmacokinetic parameters of liarozole after a single oral dose of 300 mg liarozole (mean ±SD). The observed data is from Bryson HM and Wagstaff AJ, 1996.

n	Observed AUC (mg*h/L)	Predicted AUC (mg*h/L)	Observed C_{max} (mg /L)	Predicted C_{max} (mg /L)	Observed t_{max} (h)	Predicted t_{max} (h)
18	24	26 ± 8	4	3 ± 1	1.5	1.3 ± 0.5

Table 3.11. Observed and predicted AUC of *at*RA in adult cancer patients in the presence of ketoconazole and liarozole (mean ±SD). The ketoconazole study data is from Rigas et al., 1993 and Liarozole data is from Miller et al., 1994. In the studies *at*RA was dosed for 29 days and ketoconazole or liarozole administered on days 2 and 29 while the control session PK studies were done on day 1 and 28.

Study	Study day	n	Observed AUC (ng*h/ml)	Predicted AUC (ng*h/ml)	AUC acceptance range (ng*h/ml)
Control (ketoconazole dosing)	1	31	467 ± 469	517 ± 171	234 - 887
Ketoconazole (all dose levels combined)	2	31	531 ± 522	724 ± 443	267 - 1009
Control (ketoconazole 200 mg study)	28	7	176 ± 141	201 ± 130	88 - 334
Ketoconazole 200 mg	29	7	262 ± 200	404 ± 239	131 - 498
Control (ketoconazole 400 mg study)	28	6	185 ± 190	205 ± 139	93 - 352
Ketoconazole 400 mg	29	6	400 ± 211	547 ± 296	200 - 760
control (liarozole dosing)	19	19	504 ± 549	533 ± 138	252 - 958
Liarozole (all dose levels combined)	2	19	363 ± 358	482 ± 323	182 - 726
Control (liarozole 75 mg study)	28	5	210 ± 159	208 ± 134	105 - 399
Liarozole 75 mg	29	5	347 ± 329	257 ± 163	174 - 659
Control (liarozole 150 mg study)	28	8	78 ± 65	208 ± 131*	39 - 156
Liarozole 150 mg	29	8	135 ± 195	278 ± 169*	68 - 270
Control (liarozole 300 mg study)	28	6	140 ± 108	203 ± 130	70 - 280
Liarozole 300 mg	29	6	309 ± 138	307 ± 184	155 - 618

**Outside of the acceptance range.*

Chapter 4.

Toxicokinetics and Physiologically Based Pharmacokinetic Modelling of the Shellfish Toxin Domoic Acid in Non-human Primates

4.1 ABSTRACT

Domoic acid (DA), a neurotoxin, is produced by marine algae and has caused intoxications worldwide in animals and humans. However, the toxicokinetics of DA has not been fully evaluated, and information is missing on the disposition of DA following oral exposures at doses that are considered safe for human consumption and do not cause acute toxicity. In this study, toxicokinetics of DA were investigated in cynomolgus monkeys, following a single 5 µg/kg IV dose and single 0.075 mg/kg and 0.15 mg/kg PO dose. A novel sensitive LC-MS/MS method was developed to measure plasma and urine DA concentrations. Following IV dosing, DA had a systemic clearance of 139 ± 70 ml/hr/kg, volume of distribution at steady state of 145 ± 69 ml/kg and elimination half-life of 1.4 ± 1.0 hours. However, following PO dosing, the average terminal half-life of DA was 11 ± 3.7 hours, indicating that after PO dosing DA disposition follows flip-flop kinetics with slow rate-limiting absorption. DA was primarily renally eliminated with the average renal clearance of 104 ± 47 ml/hr/kg and the average absolute bioavailability of DA was 7 ± 4 %. A novel physiological based pharmacokinetic (PBPK) model was developed for DA in monkeys that replicated the flip-flop kinetics observed after oral administration and allowed simulation of urinary excretion and brain and kidney distribution of DA, following IV and PO dosing. This study is the first to characterize DA disposition at exposure levels close to the current reference intake and to mechanistically model DA disposition in a model species.

4.2 INTRODUCTION

Domoic acid (DA, Figure 4.1) is an analog of kainic acid and glutamate produced by several diatom species of the genus *Pseudo-nitzschia* in seawater (Mos, 2001). As *Pseudo-nitzschia* blooms are initiated by anomalously warm ocean conditions, increasing sea temperatures are predicted to increase algal blooms and consequently DA outbreaks and exposure precipitating a

potential increase in public health risks of exposure. In fact, the largest recorded outbreak of DA along the North American west coast was recorded in 2015 and was shown to be initiated by warm ocean conditions and resulting Pseudo-nitzschia blooms (Mccabe *et al.*, 2016). DA is transferred through marine food webs by ingestion of *Pseudo-nitzschia* cells by pelagic and benthic organisms, marine mammals and sea birds who consume organisms contaminated with DA including mussels and other crustaceans and fish such as anchovies (Lefebvre *et al.*, 2002; Lefebvre and Robertson, 2010). Elevated concentrations of DA in tissues of marine animals and cases of DA intoxication resulting in stranding and deaths of sea mammals are closely tied to the severity of DA producing algal blooms (Scholin *et al.*, 2000; Lewitus *et al.*, 2012; Du *et al.*, 2016). While the incidence and severity of DA producing algal blooms appears to be increasing with warming seawaters (Mccabe *et al.*, 2016; Mckibben *et al.*, 2017), human DA intoxication was already reported in 1987 when 3 individuals died and more than 100 fell ill with signs of DA related amnesic shellfish poisoning including gastrointestinal distress, neurological abnormalities, seizures and autonomic nervous system dysfunction (Perl *et al.*, 1990; Todd, 1993). Based on detailed analysis of nine of these cases, the intoxication was determined to be due to consumption of DA containing mussels, at intake levels of 60-290 mg (0.9-4.1 mg/kg) of DA (Perl *et al.*, 1990).

Following the human poisoning event, the acute toxicity of DA has been extensively studied, and oral acute reference doses and tolerable daily intake (TDI) values of 0.018- 0.1 mg/kg have been proposed (Costa *et al.*, 2010). A TDI of 0.075 mg/kg PO was suggested based on the no observed adverse effect level (NOAEL) in monkeys following a short-term (15 days) exposure to 0.75 mg/kg/day DA orally (Mariën, 1996; Truelove *et al.*, 1997). However, information to establish the chronic TDI for DA is currently not available (Pulido, 2008). Several studies in various model species have suggested that chronic low-level DA exposure at asymptomatic doses

results in adverse effects including epigenetic changes and sensitization of animals to the toxicity of DA (Hiolski *et al.*, 2014; Lefebvre *et al.*, 2017), but the mechanisms underlying these chronic toxicities are not known and the toxicokinetics and target organ exposures at the level of acute oral reference dose of DA have not been characterized. In contrast, the mechanisms causing acute DA toxicity have been extensively studied (Pulido, 2008) and DA has been well characterized as a neurotoxin acting via binding to alpha-amino-3-hydroxy-5-methylisoxazole-4-propionate (AMPA) and kainate receptors resulting in lesions in the hippocampus and amygdala (Pulido, 2008). As such, distribution of DA into the central nervous system (CNS) appears to be key to its acute toxicity.

DA is a very polar compound (log P= -0.23) with four ionized groups at normal physiological pH; three carboxylic acids with pK_a between 1.85 and 4.75 and an amine with a pK_a of 10.6 (Walter *et al.*, 1992). Due to its polarity and highly charged state, DA has limited membrane permeability as shown in Caco-2 cells (Kimura *et al.*, 2011), and DA would be expected to have poor oral bioavailability and limited permeability across physiological barriers such as intestinal epithelium, blood brain barrier and the placenta. However, absorption of DA from the GI tract, distribution to the brain and penetration to the developing fetus in pregnant rodents has been shown (Truelove *et al.*, 1997; Fuquay *et al.*, 2012a; b). Yet, the bioavailability of DA following acute high doses appears to be low (<10%) based on observed excretion of DA into urine following IV and PO doses to monkeys (Truelove and Iverson, 1994; Truelove *et al.*, 1997), and recovery of unchanged DA in feces of rodents after oral dose (Iverson *et al*., 1990). Understanding the disposition processes of DA has been limited by lack of sensitive and selective assays to measure DA concentrations in biological specimens. LC-MS/MS based methods have been developed for measuring DA in seawater and in contaminated seafood (Wang *et al.*, 2012; Barbaro *et al.*, 2016),

but existing LC-MS/MS methods have lacked the sensitivity needed to quantify DA in samples from animals exposed to DA at doses below acute toxic doses (Frame and LeFebvre, 2013). A sensitive ELISA method has been developed that can measure DA at concentrations down to 0.4 ng/ml in biological specimens (Frame and LeFebvre, 2013), but ELISA assays can suffer from cross reactivity and lack of selectivity. In addition, the ELISA assay for DA also cross reacts with antibodies against DA in the exposed animals decreasing the usefulness of this assay in quantifying DA in situations with chronic exposures (Lefebvre *et al.*, 2012). Due to the lack of good bioanalytical methods, very limited data exists on DA plasma concentrations and pharmacokinetics following oral dosing. In fact, the only plasma concentration data available in a model species after oral consumption of DA is from monkeys dosed at 0.5 mg/kg/day from day 1 to 15 and 0.75 mg/kg/day from day 16-32 with single serum samples collected approximately 2 hours after dosing (Truelove et al., 1997). In the studies assessing DA pharmacokinetics in rats after oral administration (0.1mg/kg - 10 mg/kg DA), plasma concentrations were below limit of detection in all samples analyzed (Iverson *et al*., 1990; Truelove *et al.*, 1996).

As human and wildlife exposures to DA are exclusively via oral consumption, the aim of this study was to characterize DA toxicokinetics following oral administration to non-human primates at levels of exposure near and at the proposed TDI level, and to establish the key toxicokinetic parameters of DA following IV and PO dosing in monkeys. Using the determined and reported absorption, distribution, elimination and physicochemical data of DA, a physiological based pharmacokinetic (PBPK) model was developed to predict DA disposition in monkeys following a single IV dose and a single and multiple PO doses of DA.

4.3 MATERIALS AND METHODS

4.3.1 Chemicals and Reagents

DA was purchased from BioVectra (Charlottetown, PE, Canada). Certified calibration solution for DA was purchased from National Research Council Canada (Ottawa, Ontario, Canada). Optima grade water, methanol, acetonitrile and formic acid used for bioanalytical assays were purchased from Fisher Scientific (Pittsburgh, PA). β-glucuronidase from E. coli and ammonium acetate were purchased from Sigma-Aldrich (St. Louis, MO).

4.3.2 Animal Studies

Three healthy adult female cynomolgus monkeys weighing 5.2 ± 1.6 kg were enrolled in the study. Animals were housed in the Infant Primate Research Laboratory at the Washington National Primate Research Center. Animals were unsedated and unfasted for the duration of the study, with unrestricted access to food and water. Animals were fed with Lab Diet High Protein Monkey Diet biscuits twice a day, once approximately 2 hours before the DA dose and once approximately 5 hours after the dose of DA. All animal procedure guidelines followed the Animal Welfare Act and the Guide for Care and Use of Laboratory Animals of the National Research Council. All protocols were approved by the University of Washington Institutional Animal Care and Use Committee.

A single IV dose of 5 µg/kg DA dissolved in sterile saline was administered to fully conscious animals without restraint. Blood samples were collected from the saphenous vein before treatment (baseline) and 5, 10, 20, 30 and 45 minutes, and 1, 1.5, 2, 3, and 4 hours after treatment. Two repeated IV studies were conducted in these animals. Urine and feces samples were collected from cage pans after every blood draw during the study period and at 8, 12, and

24 hours post dose during the second IV study. The DA kinetics were also characterized in these animals following a single oral dose of 0.075 mg/kg or 0.15 mg/kg DA. DA oral dose was prepared using a concentration of 1 mg/ml DA dissolved in tap water with 5% sucrose and filtered with syringe filter (0.2 µM, 25mm). The dose was given to fully conscious animals without restraint. Blood samples were collected at baseline and at 1, 1.5, 2, 3, 5, 8, 12, 16, 24 and 48 hours post dose. Urine samples were collected from cage pans after every blood draw for 24 hours during the study with 0.075 mg/kg DA PO. At least two week washout period was given between each exposure.

Blood samples were collected into sodium heparin tubes and centrifuged at 3,000 x g for 15 minutes to isolate plasma for further analysis. Plasma, urine and feces samples were stored at −20 °C until analysis. For all studies, the dosing solution was analyzed for DA content as described below to confirm DA concentrations.

4.3.3 DA Plasma Protein Binding and Blood to Plasma Ratio

The protein binding of DA in plasma was determined by ultracentrifugation using mixed plasma samples from 8 healthy adult subjects. Plasma spiked with 100 nM DA was aliquoted into 6 tubes with 1ml plasma in each tube. Three plasma samples were incubated at 37 °C for 90 minutes and meanwhile another three samples were ultracentrifuged at 451,268 g for 90 mins at 37°C. After ultracentrifugation, the supernatant was collected and prepared together with incubated plasma samples using the method described below for LC-MS/MS analysis. The unbound fraction in plasma ($f_{u,p}$) was determined as DA concentration measured in the supernatant divided by the DA concentration in the incubated plasma samples.

The blood to plasma ratio (B/P) of DA was measured as previously described (Jing *et al.*, 2017) in fresh human blood. DA was spiked into 5 ml of blood with 100 nM final concentration. Samples were mixed and incubated at 37°C for up to 2 hours and blood samples were removed at 10 and 30 minutes, and 1, 1.5 and 2 hours during incubation. At each time point, 60 µl of blood in triplicate was removed, and protein was precipitated with 60 µl methanol. Additional 600 µl of blood was removed at the same time and centrifuged at 1,000 g for 10 minutes at 4°C to pellet red blood cells and isolate plasma. After centrifugation, plasma was aliquoted in triplicate with 60 µl/each and added to 60 µl of methanol, the samples prepared as described below and analyzed by LC-MS/MS.

4.3.4 Analysis of DA Concentrations in Biological Samples by LC-MS/MS

For DA measurement in plasma, 60 µl of methanol was added to 60 µl plasma, and the samples were centrifuged at 16,100 g for 40 minutes, set at 4 °C for 30 minutes and centrifuged again at 16,100g for 30 minutes. The supernatant was collected for analysis. For plasma samples that had concentrations beyond standard curves, supernatant was diluted 2-fold with water for analysis. For these samples, standard curves at 6-199 ng/ml (20-640 nM) spiked at $n \geq 6$ concentrations of DA were prepared the same way as the samples. For DA measurement in urine, 60 µl of methanol was added to 60 µl urine, the samples were centrifuged at 16,100 g for 20 minutes and the supernatant was collected and diluted 10-fold with water for analysis. For urine samples that had DA concentrations above the range of standard curves after dilution, the supernatant was collected and diluted 50-fold with water for analysis. For samples with undetectable/unquantifiable concentrations with 10-fold dilution, the samples were prepared and analyzed without further dilution by LC-MS/MS. Standard curves were prepared the same way as the urine samples at concentrations of 124-3985 ng/ml (400-12800 nM) for 1:50 dilution and

0.6-40 ng/ml (2-128 nM) for undiluted samples. For DA measurement in feces, 1 g of feces was first homogenized with 3 ml water using Omni tissue homogenizer (Omni International, Kennesaw, GA). After homogenization, 60 µl of methanol was added to 60 µl of sample and the mixture centrifuged for 20 minutes at 16,100 g. The supernatant was collected for LC-MS/MS analysis.

For method validation, standard curves were prepared using blank monkey plasma spiked with DA at concentrations 0.6-40 ng/ml (2-128 nM), blank monkeys urine spiked to concentrations 16-996 ng/ml (50-3200 nM) of DA and blank monkey feces spiked to concentrations 6-103 ng/ml (20-332 nM) of DA. All standard curves had ≥6 concentrations of DA. High, middle and low concentration quality control (QC) samples that were close to the lowest, middle and highest concentration within the standard curve were extracted along with standard curves and also included in all analyses. Low, middle and high QC samples were at DA concentrations of 0.9, 7 and 30 ng/ml (3, 24 and 96 nM) for plasma measurement, 16, 156 and 623 ng/ml (50, 500 and 2000 nM) for urine measurement and 6, 31 and 62 ng/ml (20, 100 and 200 nM) for feces measurement.

To determine the potential metabolic conjugation of DA in vivo, urine samples were prepared with and without β-glucuronidase hydrolysis treatment. Briefly, each urine sample was divided into three 200 µl aliquots. 46.1 µl ammonium acetate (1M) and 40 U β-glucuronidase (6.1 µl of 6.5 U/µl in 100mM ammonium acetate) were added to 200 µl urine and incubated at 37ºC for 24 hours. To compare with the samples treated with β-glucuronidase, 52.2 µl ammonium acetate (1M) was added to an additional 200 µl urine sample and incubated at 37ºC for 24 hours. To confirm the stability of DA in this assay, 52.2 µl ammonium acetate (1M) was

added to another 200 µl urine sample and stored at −20 °C until analysis. After 24 hours, samples were prepared as described above for analysis.

DA concentrations in plasma samples were measured by LC-MS/MS, using AB Sciex 5500 qTrap Q-LIT mass spectrometer (AB Sciex, Foster City, CA) equipped with an Agilent 1290 UHPLC (Agilent, Santa Clara, CA) and a Synergi™ Hydro-RP 100 Å LC Column (2.5 µm, 50 ×2 mm; Phenomenex). Compound dependent mass spectrometer parameters used for detection of DA were collision energy 26, collision cell exit potential 10, declustering potential 100 and entrance potential 10. Gradient elution with a flow rate of 0.5 ml/min using (A) water with 0.1% formic acid and (B) 95% acetonitrile with 5% water and 0.1% formic acid was used. The gradient was from an initial 95% A for 1 min to 0% A over 3 min and then to 95% A for 3 min. Analytes were detected using positive ion ESI mode. MS/MS transition monitored for DA were m/z 312.2>266. DA in the dosing solutions and in urine and feces samples was measured by LC-MS/MS, using AB Sciex 4500 mass spectrometer (AB Sciex, Foster City, CA) equipped with an Shimadzu UFLC XR DGU-20A5 (Shimadzu Scientific Instruments, Columbia, MD) and a Synergi™ Hydro-RP 100 Å LC Column (2.5 µm, 50 ×2 mm; Phenomenex). Compound dependent mass spectrometer parameters used for detection of DA were collision energy 20, collision cell exit potential 10, declustering potential 51 and entrance potential 10. Gradient elution and MS/MS transitions monitored for DA were as described above. Samples were kept in the autosampler at 4°C and 10 µl of sample was injected for analysis.

4.3.5 Pharmacokinetic Analysis

Pharmacokinetic parameters including area under plasma concentration time curve (AUC), volume of distribution at steady state (V_{ss}), systemic clearance (CL), half-life ($t_{1/2}$), maximum plasma concentration (C_{max}), time to reach (t_{max}), and linear terminal slope (k) were estimated by

standard non-compartmental analysis using Phoenix (St. Louis, MO). AUC was determined by the linear log trapezoidal method for IV data and linear trapezoidal method for PO data. Absolute bioavailability (F) was calculated using equation 4.1:

$$F = \frac{AUC_{\ p.o}}{AUC_{\ i.v}} \times \frac{Dose_{\ i.v}}{Dose_{\ p.o}} \qquad \text{Equation 4.1}$$

Renal clearance (CL_R) after IV and PO dose was obtained using equation 4.2:

$$CL_R = \frac{A_e}{AUC} \qquad \text{Equation 4.2}$$

in which A_e is the amount of DA excreted in urine in the same time period as AUC measurement (0 - 4 hour post IV dose and 0 to 24 hour post oral dose).

Creatinine clearance (CL_{cr}) in the monkeys was calculated using equation 4.3:

$$CL_{cr} = \frac{\frac{dA_e}{dt}}{C} \qquad \text{Equation 4.3}$$

in which A_e is the amount of creatinine excreted in the urine over a 4-hour interval (dt) and C is the concentration of creatinine measured in plasma. Blood and urine samples for creatinine clearance measurement were collected before the DA IV dose. Blood and urine creatinine concentrations were measured by clinical assays at Department of Laboratory Medicine, University of Washington Medical Center.

4.3.6 PBPK Model of DA disposition in Monkeys

A PBPK model of DA was constructed as a full PBPK model using Simcyp Monkey version 15 (Certara, Sheffield, UK). The absorption kinetics of DA was simulated with advanced dissolution, absorption and metabolism (ADAM) model. In brief, the fraction absorbed (F_a) and

F were predicted using a mechanistic P_{eff} model with a scaling factor of 0.45 applied to each part of the intestine to account for the multiple charges in the DA molecule. For DA distribution, a full PBPK model was used. A K_p value was assigned to brain according to the reported AUC_{brain} /AUC_{plasma} ratio in pregnant rats (Fuquay *et al.*, 2012a). For kidney, liver and heart, K_p values were estimated based on the reported concentrations in mice (Funk *et al.*, 2014). K_p value for the rest of the organs were independently predicted in Simcyp using the method described by Rodgers and Rowland (Rodgers and Rowland, 2006) with application of K_p scalar to obtain measured steady-state distribution volume (V_{ss}) that is consistent with the iv study. The elimination of DA was characterized based on the measured clearance after IV dosing by incorporating the measured renal clearance and assigning the rest of the systemic clearance to biliary clearance based on lack of observed metabolism of DA and the detection of unchanged DA in feces in monkeys and in bile of marine mammals. The details of the model input parameters are listed in Table 4.1.

The DA PBPK model was tested by simulating DA disposition in monkeys following IV and PO dosing and comparing the simulated results with the in-house toxicokinetic data and the reported data from the literature following higher doses of DA to monkeys. The observed concentration–time profiles from prior publications reporting DA plasma concentrations in monkeys (Truelove and Iverson, 1994; Truelove *et al.*, 1997)were digitized using Plot Digitizer software (http://plotdigitizer.sourceforge.net). For each study, 100 monkeys in virtual population were simulated at fed condition.

4.4 RESULTS

4.4.1 Development of a Sensitive and Specific LC-MS/MS Method to Measure DA in Biological Samples

In order to measure DA in biological samples including plasma and urine following IV and PO administration at a dose level near and at proposed TDI, a sensitive LC-MS/MS method was developed and validated. DA was detected in monkey plasma and urine using this method and the chromatograms of DA in the biological matrices are shown in Figure 4.2. The assay was validated according to the published guidelines for bioanalytical method validation (Shah *et al.*, 2000; Viswanathan *et al.*, 2007). The lower limits of quantification (LLOQ) in plasma and urine were 0.6 ng/ml (2 nM) and 1.6 ng/ml (5 nM) respectively based on a signal-to-noise ratio >9 and interday CV% < 15%. The accuracy and CV% of QC samples were <15% at all concentrations. The assay was determined sensitive enough to measure DA concentrations in plasma following oral exposures at the proposed TDI level of DA.

4.4.2 Toxicokinetics of DA Following Single IV and PO Dosing

The DA toxicokinetic study following IV and PO administration was conducted in three female monkeys. Following an IV dose of 5 µg/kg DA, DA was eliminated rapidly with a systemic clearance of 139 ± 70 ml/hr/kg and elimination half-life of 1.4 ± 1.0 hours (Table 4.2 and Figure 4.3a). On average, 42 ± 11% of the DA dose was recovered in urine over 24 hours after the IV dose. Based on urinary excretion (Figure 4.3b), the renal clearance of DA in these animals was 39 ± 39 ml/hr/kg which is 28% of systemic clearance and 25% of the creatinine clearance (155 ± 55 ml/hr/kg) in these monkeys. This suggests significant reabsorption of DA in the kidney and/or potential other elimination routes of DA including biliary secretion. In

accordance with some biliary secretion of DA, DA was also detected in feces after IV dosing, and the highest DA concentration in feces was 72 ng/g at 0.5 hours post IV dose. Based on this analysis, the maximum total amount of DA eliminated in 24-hour feces was calculated as 5% of the IV DA dose. Treatment of urine with β-glucuronidase to test potential glucuronidation of DA in vivo did not result in an increase in DA concentration (data not shown).

Administration of a single oral DA dose to the same monkeys at 0.075 mg/kg and 0.15 mg/kg showed flip-flop kinetics with an absorption rate constant smaller than the elimination rate constant (Figure 4.3c). Following oral administration of 0.075 mg/kg DA (proposed TDI), the maximum DA concentration of 1.9 ± 1.6 ng/ml was reached at 13.3 ± 4.6 hours post dose. DA reached a maximum concentration of 5.3 ± 3.4 ng/ml at 6.0 ± 1.7 hour after 0.15 mg/kg PO DA dose (2- fold of proposed TDI). The terminal half-life of DA following PO dosing of 0.075 mg/kg and 0.15 mg/kg DA was 11.3 ± 1.2 hours and 10.8 ± 5.8 hours, respectively, in contrast to the 1.4 ± 1.0 hours observed after IV dosing (Table 4.2). Based on the pharmacokinetic analysis, this indicated flip-flop kinetics with absorption rate constant (k_a) of 0.06 ± 0.01 1/hr and 0.08 ± 0.04 1/hr following an oral dose of 0.075 mg/kg and 0.15 mg/kg DA , respectively and elimination rate constant (k) of 0.5 ± 0.2 1/hr. The oral clearance of DA was 2.0 ± 0.7 l/hr/kg and 1.8 ± 0.9 l/hr/kg after a single oral dose of 0.075 mg/kg and 0.15 mg/kg DA, respectively, indicating liner kinetics. Based on the IV and PO dosing data, the absolute oral bioavailability of DA was calculated to be 6 ± 4 % and 8 ± 5 % after a single dose of 0.075 mg/kg and 0.15 mg/kg DA. After oral administration of 0.075 mg/kg DA, 4 ± 2 % of the DA dose was recovered in urine over 24 hours (Figure 4.3d). The renal clearance of DA measured after PO dosing was 104 ± 47 ml/hr/kg which was 75% of the systemic clearance of DA (139 ± 70 ml/hr/kg) and 67% of the creatinine clearance (155 ± 55 ml/hr/kg).

4.4.3 Simulation of DA Disposition in Monkeys Using PBPK Model

A PBPK model of DA disposition in the monkey was developed based on obtained experimental and literature data. To develop the PBPK model, the unbound fraction of DA in plasma and the blood to plasma ratio of DA were measured. The unbound fraction of DA in human plasma was 0.96, indicating low plasma protein binding of DA. Blood to plasma ratio of DA measured in human blood showed consistent values during the time of incubation with an average value of 0.51 ± 0.01, indicating no partitioning of DA into red blood cells. As this value is dependent on hematocrit in the individual a blood to plasma ratio of 0.615 was adapted in the PBPK model. The final model parameters are shown in Table 4.1.

To test developed DA PBPK monkey model, DA disposition was first simulated in monkeys following administration of a single IV dose at 5 µg/kg and 50 µg/kg of DA, and the simulations were compared to the observed plasma concentration data obtained in this study and in the previously published study (Truelove and Iverson, 1994) (Figure 4.4a, b). Majority of the observed data was within the simulated 2-fold range and all of the data was within the 5-fold range of the simulated mean. As summarized in Table 4.3, the simulated pharmacokinetic parameters were in good agreement with the observed data in the two IV dosing studies with 10-fold different doses, and all parameters were between 0.3 and 2.4- fold of the observed. DA disposition was also simulated in monkeys following single and multiple oral doses using the developed ADAM model for DA absorption in the monkey. The simulated DA concentration-time curves were in good agreement with the observed data after a single PO dose of 0.075 mg/kg and 0.15 mg/kg DA (Figure 4.4c, d). The PBPK model appropriately captured and predicted the flip-flop kinetics of DA with C_{max} values predicted within 2-fold of the observed and with the terminal half-life (absorption half-life) predicted with 0.8-fold of the observed. As

shown in Table 4.3, the mean simulated AUC was 0.8- and 0.6- fold of the observed values. In addition to the current study data, the plasma concentrations of DA following 15 days oral doses of 0.5 mg/kg/day DA were also simulated in accordance with the dosing in the prior study (Truelove *et al.*, 1997) which measured single time point concentrations of DA following multiple oral doses(Figure 4,4e). The PBPK model captured the multiple dose pharmacokinetics appropriately predicting the single time point plasma concentrations of DA accurately (Figure 4,4e).

DA is mainly eliminated via the renal route and hence the simulation accuracy of urinary excretion of DA was also evaluated. The excretion of DA into urine as a function of time was compared to the data collected in this study and to the previously reported data (Figure 4.5). Overall the simulated data of urinary excretion was in good agreement with the observed DA dose recovery in urine after both IV and PO dosing with both the rate and extent of urinary excretion captured appropriately by the model.

The predominant sites of DA toxicity appear to be the brain and possibly the kidney. Therefore the time courses of DA concentrations in the brain and kidney were simulated using the developed PBPK model that incorporated the K_p values for brain and kidney obtained from literature. As shown in Figure 4.6a, following a single IV dose of 5 µg/kg DA, DA rapidly distributed into brain and quickly equilibrated with plasma, while following a single PO dose of 0.075 mg/kg DA, maximum concentration was reached 2.3 hours post dose with prolonged DA exposure in the brain. In fact, despite the initial much higher brain concentrations of DA after IV dosing, the simulated brain concentrations of DA at later time points were higher following PO dosing than after IV dosing. Similarly, distribution pattern was also simulated in kidney

following IV and PO doses (Figure 4.6b). Overall, the predicted kidney tissue concentrations were higher than those predicted for the brain.

4.5 DISCUSSION

Over recent decades, there has been an increase in toxic algal blooms resulting in increased risk of DA poisoning in marine mammals and in humans who consume contaminated shellfish and fish (Mccabe *et al.*, 2016). Oral acute reference doses and a TDI for DA have been proposed for human consumption based on toxicity studies in non-human primates and estimated lowest observed adverse effect levels (LOAEL) in humans (Costa *et al.*, 2010). However, these values are derived without any knowledge of DA concentrations in human circulation following consumption of contaminated shellfish and without detailed characterization of the absorption kinetics (extent and rate of absorption) of DA in humans or non-human primates at oral dose levels that are at or close to the proposed TDI values. The lack of this information is largely due to the lack of reliable and sensitive bioanalytical methods that can accurately measure DA concentrations at low levels in biological samples. In fact, multiple methods have been developed for the measurement of DA in biological samples, including ELISA and LC-MS/MS methods which are most commonly used (Frame and LeFebvre, 2013; Lefebvre and Robertson, 2010; Wang et al., 2012). The ELISA method is generally reported to have higher sensitivity (minimum quantification level of 0.4 ng/ml in the original serum sample) than the LC-MS/MS methods (Frame and LeFebvre, 2013), and hence it has been used broadly for DA analysis in biological samples. However, ELISA detects both DA and DA-specific antibodies and can therefore result in inaccurate measurements of DA concentrations in serum, especially following chronic DA exposures (Lefebvre *et al.*, 2012). Despite the better reliability and specificity of LC-MS/MS, previously reported LC-MS/MS methods lack sufficient sensitivity compared with ELISA with a

quantification limit (defined by> 3 × background) above 7 ng/ml in serum (Frame and LeFebvre, 2013) and require large sample volumes (> 500 µl) for sample preparation through solid phase extraction (Wang *et al.*, 2012). In our study, we establish a novel LC-MS/MS method with sensitivity that is similar to the established ELISA assay and requires only small volumes of the biological samples with direct extraction. The developed LC-MS/MS method allows the detection of DA in biological samples and provides valuable information regarding the absorption kinetics and disposition of DA following oral and intravenous dosing to non-human primates. The developed method will be useful for future evaluation of DA kinetics and exposures in experimental animals, marine mammals and wildlife and in humans consuming potentially contaminated seafood, especially in situations where there is a concern of chronic exposure and development of DA antibodies.

A bioavailability of DA <10% has been proposed based on previous studies that showed in total approximately 71% and 4-7% of DA was recovered in 24-hour urine following IV and PO DA dose respectively in cynomolgus monkeys (Truelove and Iverson, 1994; Truelove *et al.*, 1997). The bioavailability of 7% determined in this study in a rigorous cross-over manner and based on plasma concentration data is in excellent agreement with the previous work. This low bioavailability is consistent with the high polarity and fully charged state of DA at physiological pH (Vera-avila *et al.*, 2011). Due to the lack of plasma concentration data in previous oral dosing studies the rate of absorption has not been previously determined. Surprisingly, the results of this study show that DA is subjects to flip-flop kinetics with slow absorption rate (absorption half-life of 11 hours) from the gut demonstrated by the significantly longer terminal half-life of DA following PO dosing when compared to IV dosing. Due to the flip-flop kinetics, the elimination

of DA following oral exposure is prolonged when compared to what would have been expected based on the IV data.

It is generally assumed that the majority of DA clearance is via the kidney. This is largely based on the findings that in rats DA was entirely eliminated via the kidney through glomerular filtration (Suzuki and Hierlihy, 1993). However, the data presented here shows a recovery of only 42% of the DA dose after IV dosing of DA. This less than complete urinary recovery is consistent with a previous study in cynomolgus monkeys with a higher IV dose (Truelove and Iverson, 1994) and suggests that at least in monkeys other elimination pathways of DA exist besides renal excretion. It is likely that the other elimination pathways involve biliary secretion as DA was detected in fecal samples in this study after IV dosing. DA has also been found in bile of stranded marine mammals including California sea lions (15- 344.7 ng/ml DA) and harbor porpoise (11.7 ng/ml DA) (Rust *et al.*, 2014), a finding in agreement with biliary secretion of DA in higher mammals. Further studies are needed to evaluate biliary secretion of DA and to identify potential transporters responsible for biliary secretion of DA. Such data would also be crucial for eventually predicting biliary secretion of DA in humans and to establish the importance of altered bile flow and biliary transport on human safety after consuming DA containing shellfish and fish. If biliary secretion of DA is significant in monkeys and other mammals, it is possible that enterohepatic recycling contributes to the toxicokinetics of DA. In fact, the plasma-concentration time curves of DA following oral dosing to monkeys (Figure 4.3) had a characteristic second peak for DA concentrations suggesting some extent of enterohepatic recycling.

The overall renal clearance of DA in monkeys was lower than the GFR suggesting that in addition to glomerular filtration significant DA reabsorption occurs. Due to its high charge state and polarity, passive diffusion and reabsorption of DA in the kidney tubule is not expected.

Consistent with this, in the rat the renal clearance of DA has been shown to be similar to the GFR (Suzuki and Hierlihy, 1993). However, the observation of apparent significant reabsorption is consistent with the previous studies after IV dosing of DA to monkeys also showing an estimated renal clearance less than GFR (Truelove and Iverson, 1994). This data suggest that active transport contributes to the reabsorption of DA in monkeys. A role of transporters in DA disposition is supported by a prior study in which apical-to-basolateral transport of DA in Caco-2 cells decreased by 31.5% when DA was incubated with probenecid (100 mM), a non-specific inhibitor of anion transport (Kimura *et al.*, 2011). However, the transporters involved in kidney transport of DA have not been identified and significant species differences are likely to complicate the interpretation of transporter contribution to renal handling of DA and uptake and efflux transporters likely affect DA disposition in the kidney in a concerted, species specific, manner. For example in rats in one study probenecid caused a significant increase in the plasma DA levels (Robertson *et al.*, 1992) while in a second study in rats probenecid did not alter DA renal clearance (Suzuki and Hierlihy, 1993). In mice probenecid significantly increased DA concentrations in the kidney tissue (Funk *et al.*, 2014) suggesting a role of efflux transporters in kidney distribution in the mouse. Taken together the observed species differences and the role of kidney transporters in DA disposition show that studies are needed to identify how DA is handled by human kidney and which human kidney transporters are involved in DA disposition.

To evaluate the absorption and distribution mechanisms of DA and to lay the foundation for modeling DA disposition in humans, a PBPK model was developed to characterize DA toxicokinetics in monkeys. Using the ADAM model to characterize DA absorption kinetics, the flip-flop kinetics of DA were accurately predicted based on in silico predictions of the absorption parameters. In addition, the PBPK model accurately predicted the bioavailability of DA observed

in this study and the toxicokinetics following oral dosing of DA in this study and in prior reported multiple dosing study with much higher doses. The fact that the PBPK model could be well extrapolated between different routes of administration and between different independent studies in different animals suggests that this study accurately characterized DA disposition in monkeys providing a powerful model for future evaluation of DA disposition in acute and chronic toxicology studies. The developed PBPK model can also be used as a basis to develop PBPK models for other species including humans to support extrapolation of toxicity data between species and exposure levels. The developed PBPK model was also used to simulate the brain and kidney concentrations of DA following IV and PO doses of DA. DA concentrations have been previously reported in the kidney, liver, heart and hippocampus of mice (Funk *et al.*, 2014), and in brain and cerebrospinal fluid in pregnant rats (Fuquay *et al.*, 2012a). The simulated brain and kidney distribution shown here is in excellent agreement with the prior data from rodents. The simulated fast partitioning of DA into brain following IV dose reflects the reported concentration-time profile measured in the brain of pregnant rats (Fuquay *et al.*, 2012a) with the brain concentrations reaching equilibrium with plasma rapidly after dosing. Similarly, the simulated fast distribution to the brain is in excellent agreement with the fast onset of vomiting (2-14 minutes) in monkeys dosed with 50 µg/kg IV and the duration of the vomiting restricted to the first 9-62 minutes after IV dosing (Truelove and Iverson, 1994). As such the developed PBPK model together with the observed toxicokinetics data provides a novel tool to evaluate exposure-toxicity relationships of DA that will be ultimately useful for predicting human toxicity of DA in different populations.

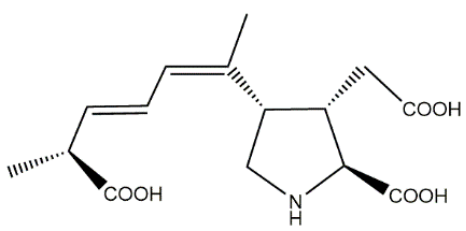

Domoic acid

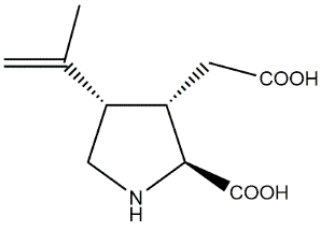

Kainic acid

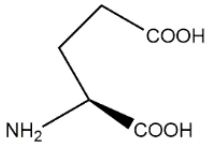

Glutamic acid

Figure 4.1. Structures of domoic acid, kainic acid and glutamic acid.

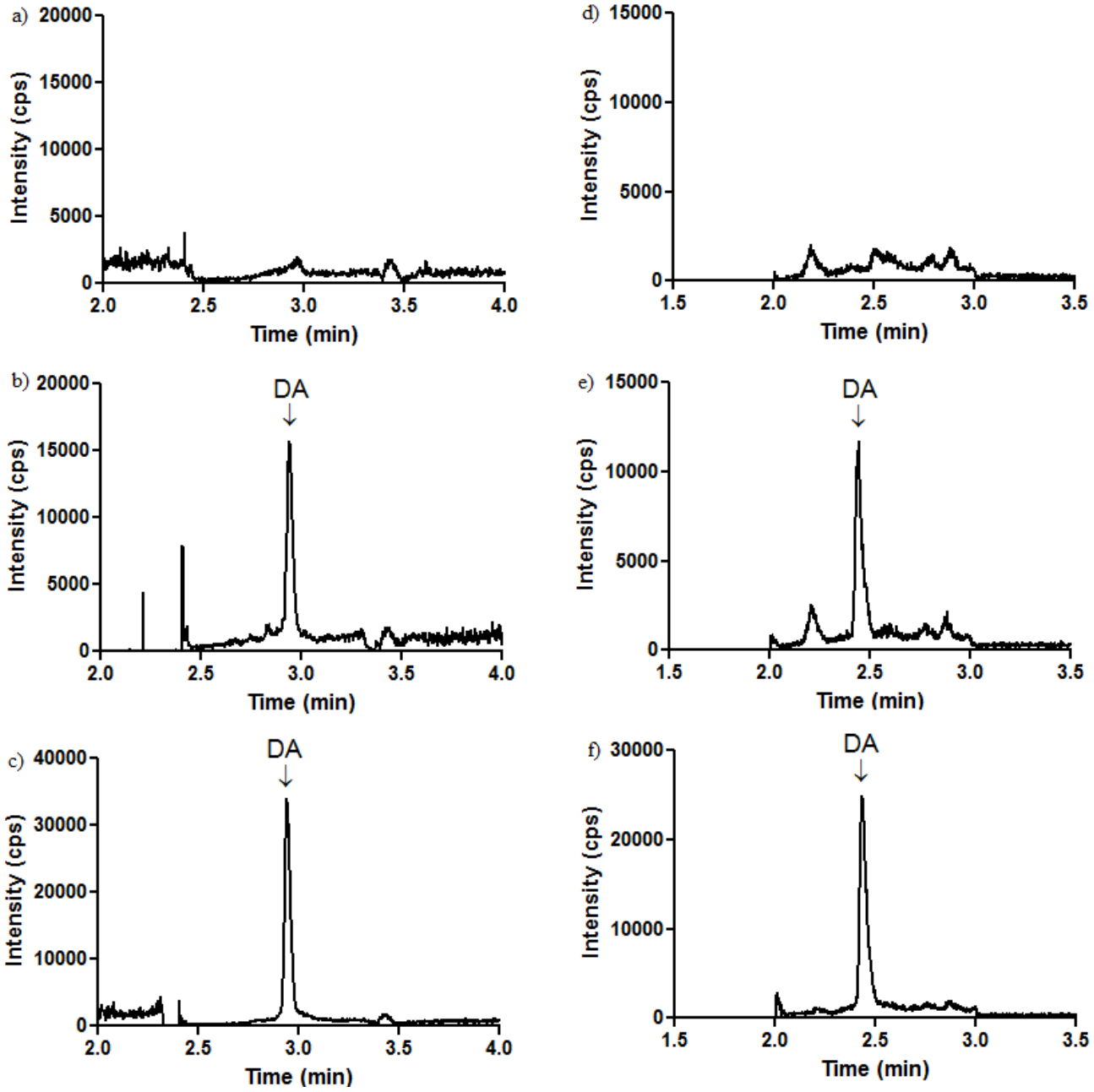

Figure 4.2. Detection of domoic acid (DA) by LC-MS/MS in monkey plasma and urine samples. a) Blank plasma. b) Plasma sample spiked with 0.6 ng/ml (2.0 nM) DA. c) Detection of DA in a plasma sample collected 24 hours after dosing with 0.15 mg/kg DA orally. The detected concentration of DA is 2.0 ng/ml (6.3 nM). d) Blank urine. e) Detection of DA in a urine sample spiked with 1.6 ng/ml (5.0 nM) DA. f) Detection of DA in a urine sample collected 24 hours after a 0.15 mg/kg DA dose PO to monkey. The concentration of DA is 3.7 ng/ml (11.8 nM). Samples were prepared and analyzed as described in materials and methods.

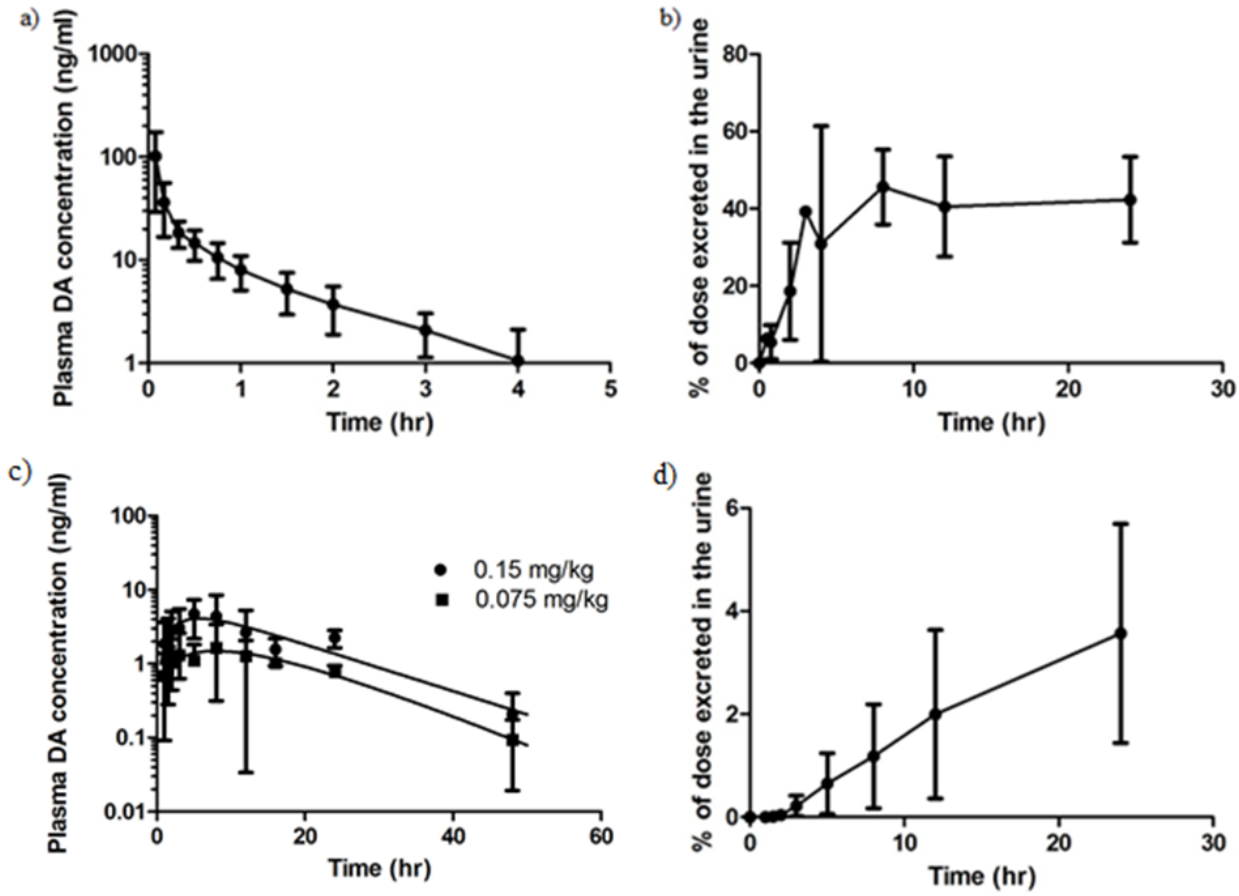

Figure 4.3. Toxicokinetics of DA in monkeys (n=3) following IV and PO administration. a) Mean plasma concentration-time profile of DA following a single IV dose of 5 µg/kg DA. Each data point represents the mean and standard deviation of the plasma concentrations measured in two different studies in three animals. b) Time course of DA excretion into urine following IV dosing. The percentage of the IV dose of DA (5 µg/kg) excreted in the urine as a function of time is shown. Each data point is the mean and standard deviation of three animals. c) Mean plasma concentration versus time curves of DA following a single oral dose of 0.075 mg/kg and 0.15 mg/kg DA. Each data point represents the mean and standard deviation of 3 monkeys. d) Time course of DA excretion into urine following p.o. dose of 0.075 mg/kg DA. The percentage of oral DA dose excreted in the urine as a function of time is shown as mean and standard deviation of 3 animals.

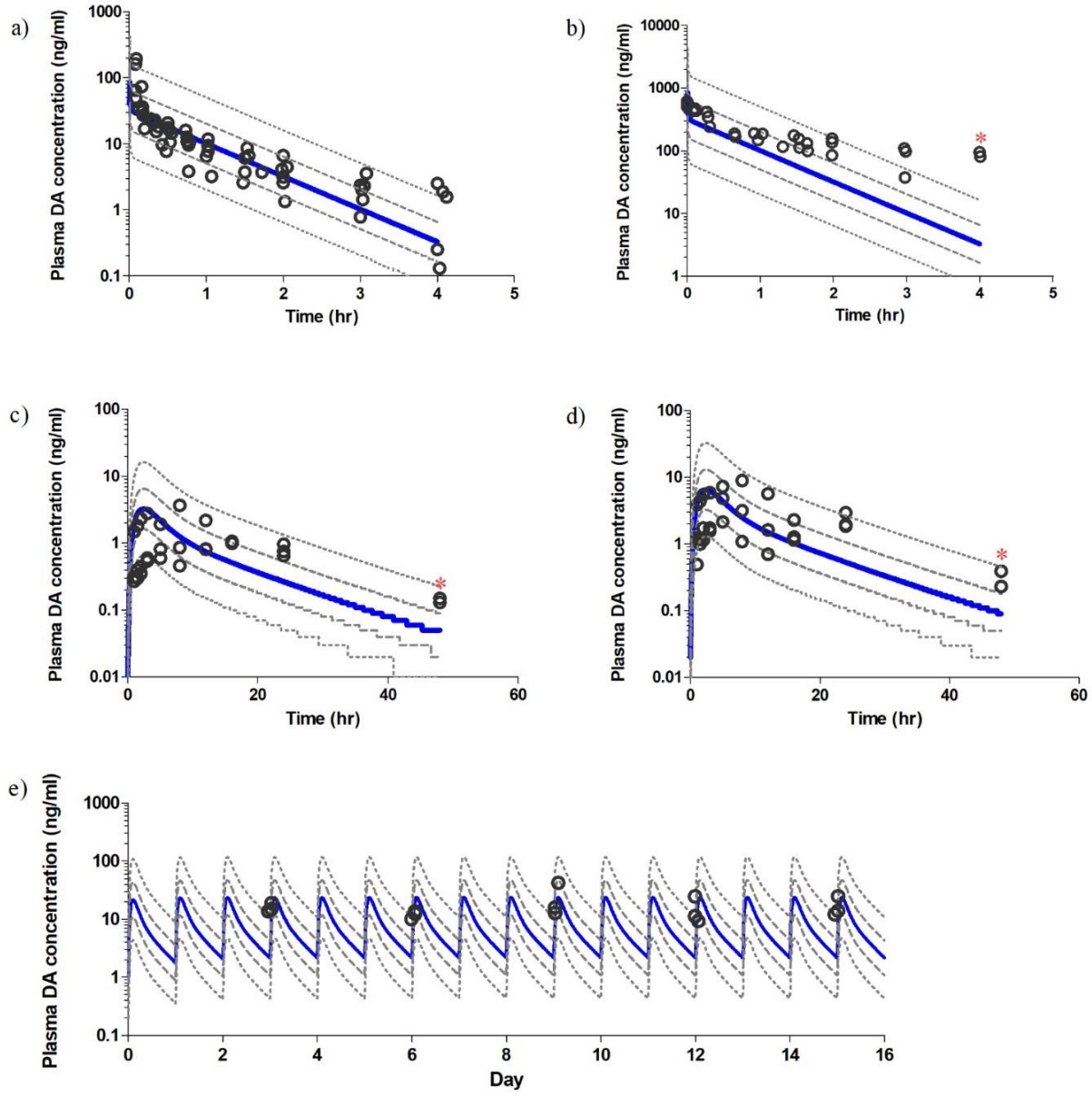

Figure 4.4. Predicted and observed plasma concentration–time profiles of DA in monkeys. The blue line in each panel depicts the mean simulated concentrations, the dashed lines depict the 2-fold range and the dotted lines represent the 5-fold range in simulated plasma concentrations. The black circles show the observed data from the current study (a, c and d) and from previous IV (Truelove and Iverson, 1994) (b) and PO studies (Truelove *et al.*, 1997) (e) The dosing simulated in the panels is a) Administration of 5 µg/kg DA IV b) Administration of 50 µg/kg DA IV c) Administration of 0.075 mg/kg DA PO d) Administration of 0.15 mg/kg DA PO e) Administration of 0.5 mg/kg/day DA PO for 15 days. *The plasma concentration in two animals was reported to be below detection and hence not reported in b. In c and d, DA concentration in one animal was below detection limit and hence data for this animal is not shown.

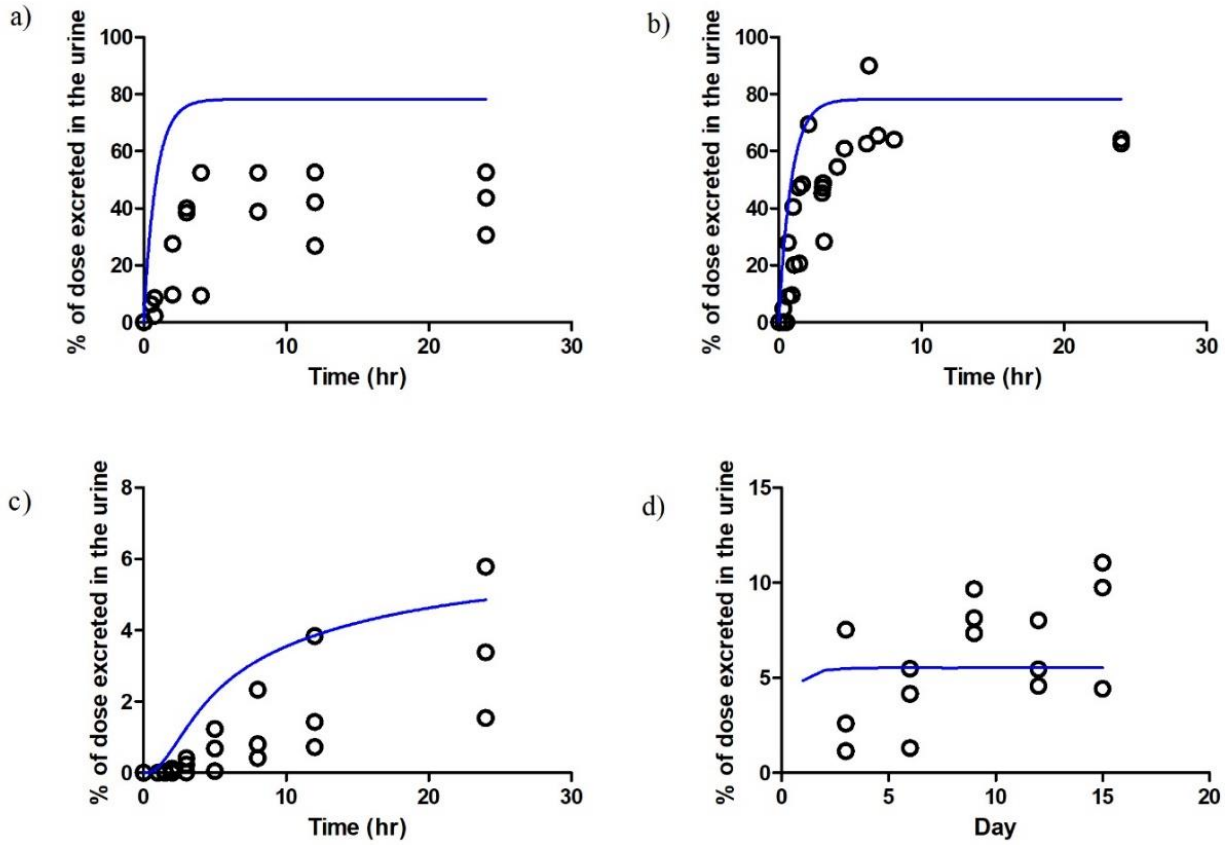

Figure 4.5. Predicted and observed time course of DA excretion into urine in monkeys. The blue line in each panel represents the mean simulated cumulative percentage of DA dose excreted in the urine. The black circles show the observed data from the current study (a and c) and from previous IV (Truelove and Iverson, 1994) (b) and PO studies (Truelove *et al.*, 1997) (d). In the PO study the % dose excreted is separately calculated for each dosing interval and the multiple dose excretion is shown. The percentage of DA dose excreted in the urine is simulated following a) administration of 5 µg/kg DA IV (a) Administration of 50 µg/kg DA IV (b), Administration of 0.075 mg/kg DA PO (c) Administration of 0.5 mg/kg/day DA orally for 15 days (d). The mean observed values for % excreted in urine were 42% in (a) 71% in (b) 4% in (c) and 6% in (d). In comparison the simulated % excreted in urine were 78% in (a) 78% in (b) 5% in (c) and 6% in (d).

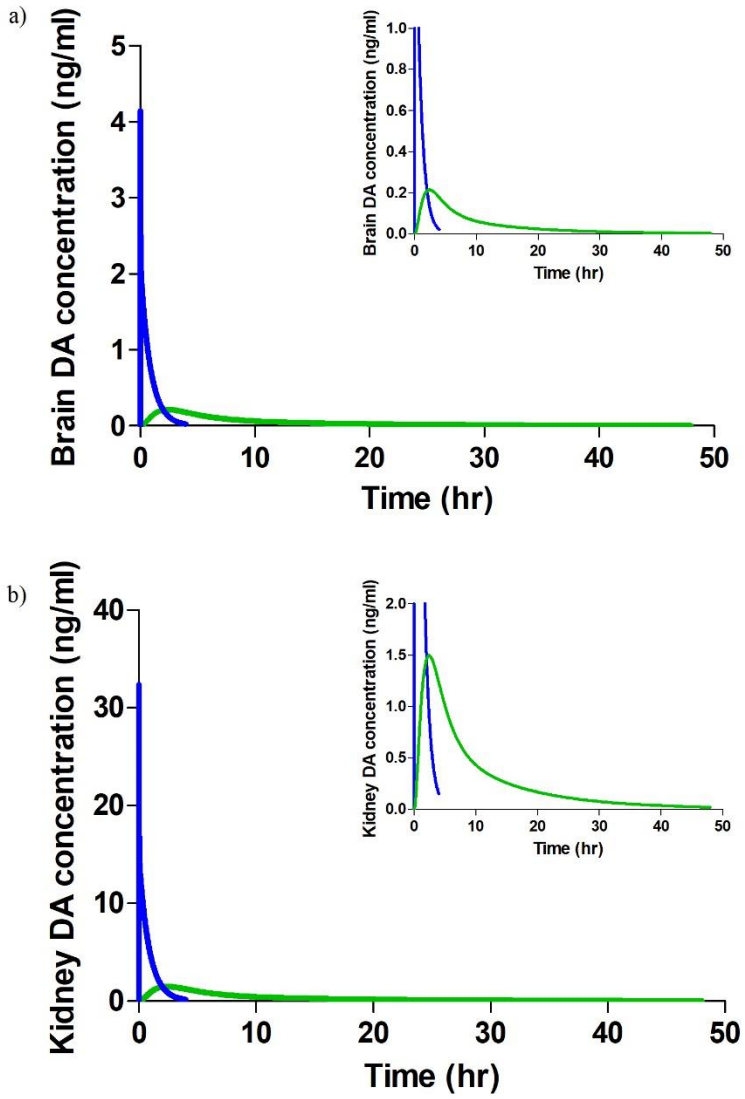

Figure 4.6. Predicted concentration–time profiles of DA in monkey brain and kidney. The blue line in each panel represents the mean simulated concentrations following IV dose of 5 µg/kg DA. The green line in each panel represents the mean simulated concentrations following PO dose of 0.075 mg/kg DA.

Table 4.1. Summary of parameter input values for DA PBPK model in monkeys

Parameters	Input values	Reference/comment
Molecular weight (g/mol)	311.33	PubChem
$logP_{o:w}$	-0.23	Drug bank
Compound type	Ampholyte	
pK_a 1	4.75	Walter et al., 1992
pKa 2	10.6	Walter et al., 1992
Blood-to-plasma ration (B/P)	0.615	Simcyp default value
$fu_{,p}$	0.96	Measured
Absorption	ADAM	
F_a	0.07	Predicted
P_{eff} (10^{-4} cm/s)	0.018	Predicted
Distribution	Full PBPK model	
V_{ss} (l/kg)	0.15	Measured
K_p – brain	0.066	Fuquay et al., 2012a
K_p – kidney	0.46	Funk et al., 2014
Kp – liver	0.13	Funk et al., 2014
Kp – heart	0.05	Funk et al., 2014
Kp – adipose	0.04	Predicted
Kp – bone	0.13	Predicted
Kp – gut	0.17	Predicted
Kp – lung	0.18	Predicted
Kp – muscle	0.17	Predicted
Kp – skin	0.14	Predicted
Kp – spleen	0.17	Predicted
Kp scalar	0.23	Assigned
Elimination		
Renal clearance (ml/min)	9.2	Measured
CL_{int} (Hep) µl/min/10^6 cells	0.28	Assigned (back-calculated from nonrenal clearance)

Table 4.2. Pharmacokinetic parameters in monkeys (n=3) following a single IV dose of 5 µg/kg DA and a single oral dose of 0.075 mg/kg and 0.15 mg/kg DA (mean ± S.D.)

Dose	$AUC_{0-\infty}$ (hr*ng/ml)	CL (mL/hr/kg)	V_{ss} (mL/kg)	$t_{1/2}$ (hr)	C_{max} (ng/ml)	t_{max} (hr)	F (%)
I.V. (5µg/kg)	45 ± 23	139 ± 70	145 ± 69	1.4 ±1.0	n/a	0	n/a
P.O. (0.075 mg/kg)	40 ± 14	n/a	n/a	11.3 ± 1.2	1.9 ± 1.6	13.3 ± 4.6	6 ± 4
P.O. (0.15 mg/kg)	100 ± 44	n/a	n/a	10.8 ± 5.8	5.3 ± 3.4	6.0 ± 1.7	8 ± 5

Table 4.3. Observed and predicted toxicokinetic parameters of DA in monkeys (mean ± S.D.) after single IV and PO doses

	$AUC_{0-\infty}$ (hr*ng/ml)	$t_{1/2}$ (hr)	V_{ss} (ml/kg)	CL (ml/hr/kg)
Observed IV 5 µg/kg	45 ± 23	1.4 ± 1.0	145 ± 69	139 ± 70
Predicted IV 5 µg/kg	28 ± 2 (14-56)	0.6 ± 0.04 (0.3-1.2)	151 (46- 302)	177 ± 12 (89-354)
[a]Observed IV 50 µg/kg	768 ±312	1.9 ± 1.0	159 ± 29	75 ± 29
Predicted IV 50 µg/kg	283 ± 19 (142-566)	0.6 ± 0.04 (0.3-1.2)	151 (46- 302)	177 ± 12 (89-354)
Observed PO 0.075 mg/kg	40 ± 14	11.3 ± 1.2	n/a	n/a
Predicted PO 0.075 mg/kg	30 ± 8.2 (15-60)	9.1 (4.6-18.2)	n/a	n/a
Observed PO 0.15 mg/kg	100 ± 44	10.8 ± 5.8	n/a	n/a
Predicted PO 0.15 mg/kg	60 ± 16 (30-90)	9.1 (4.6-18.2)	n/a	n/a

[a]Data from Truelove et al.,1994.

Chapter 5.

Toxicokinetics of Domoic Acid in Cynomolgus Monkeys during Pregnancy

5.1 ABSTRACT

Domoic acid (DA) is a potent neurotoxin that affects marine wildlife and human health. The impact of DA prenatal exposure has been evaluated in animal models with DA injections, and current data suggests that exposure to utero has negative consequences to the developing fetus. However, prenatal DA exposure following oral dose has not been investigated and little is known regarding the exposure levels that result in fetal harm. In this study, DA toxicokinetics were characterized in the same monkeys before and during pregancy following chronic dose of 0.15 mg/kg/day DA. Decreased AUC of DA and increased DA renal clearance were observed during pregnancy. DA was detected in both plasma and urine samples of the delivered infants. The results of this study indicate that exposure to DA in pregnant women is likely lower than that in non-pregnant women after similar consumption levels due to elevated DA renal clearance during pregnancy but even low level maternal exposure to DA results in detectable fetal exposures.

5.2 INTRODUCTION

Domoic acid (DA) is a water soluble, excitatory amino acid which is usually produced by the microscopic algae Pseudo-nitzschia in marine waters (Mos, 2001a). It is structurally similar to kainic acid, a toxin often used for study the effects of experimental ablation, and acts as a glutamate analog and is excitotoxic in the vertebrate central nervous system and other glutamate receptor-rich organs (Pulido, 2008). DA neurotoxicity is mediated by its interaction with glutamate receptors including N-methyl-D-aspartate (NMDA), alpha-amino-3-hydroxy-5-methylisoxazole-4-propionate (AMPA) and kainate receptors. It activates glutamate receptors causing increase of calcium ions (Ca^{2+}) and decrease of glutathione (GSH) levels and leading to apoptosis and cell death after series of celluar reactions (Giordano *et al.*, 2006).

DA poisoning has been known to affect various marine organisms including fish, sea birds, dolphins, and sea lions as well as humans through food web (Kathi A Lefebvre and Robertson, 2010). Syptoms of acute DA poisoning including vomiting, diarrhea, abdominal cramps, headache, memory loss, seizures, coma and death were reported in humans after consuming contaminated shellfish (Perl *et al.*, 1990). To protect humans from DA intoxication, oral acute reference doses and tolerable daily intake ranging from 0.018 to 0.1 mg/kg have been proposed (Lucio G Costa *et al.*, 2010). However, potential higher susceptibility of pregnant women and their fetuses was not taken into account to establish these values and studies addressing toxicokinetics of DA in pregnant animal models following oral dose and placental transfer of DA to the fetus upon oral exposure to dams are needed.

It is well established in humans that dynamic physiological alterations during pregnancy including changes of blood and body composition and organ systems such as cardiovascular, hepatic, renal and gastrointestinal systems (Costantine, 2014) can induce profound changes to pharmacokinetic properties of medications in pregnant women. Therefore, the impact of pregnancy on DA toxicokinetics needs to be investigated to protect pregnant women and their babies from DA toxicity. However, limited studies have been conducted to characterzie DA toxicokinetics during pregnancy. In one study, DA toxicokinetics was evaluated in pregnant rats given a single i.v dose of 1.0 mg/kg DA on GD 20. The systemic clearance of DA was 6.5 ml/hr/kg, steady-state volume of distribution was 494.1 ml/kg and terminal half-life of 29.5 min in pregnant rats (Maucher Fuquay et al., 2012). These values are silghtly different than the clearance of 7.8 ± 2.7 ml/hr/kg, steady-state volume of distribution of 229 ±88 ml/kg and half-life of 21 ± 3.2 reported in non-pregnant rats dosed with 1.0 mg/kg DA i.v.(Truelove J, 1994). It was proposed that the slower elimination of DA in pregnant rats may be caused by the fetal

elimation of DA through first placental then maternal plasma elimination and amniotic fluid circulation of DA in the fetal compartment without considering the effect of physiolgoical changes during pregnancy. However, the fact that the two studies used different analytical methods and were conducted independently makes evaluation of the effects of pregnanvy on DA disposition challenging. Moreover, the partioning of DA to brain and cerebrospinal fluid (CSF) was observed in pregnant rats upon given 1.0 mg DA/kg intravenously at GD 20. The estimated half-life of 4 hr and 19 hr was reported for CSF and brain respectively (Maucher Fuquay *et al.*, 2012a).

Effects of pre-natal DA exposure have been studied in rodents with DA injections. Upon injection of 0.6 mg/kg DA intravenously to pregnant female mice on gestational day (GD) 13, age related developmental neurotoxicity was observed in the intrauterine DA exposed mice with reduced seizure thresholds and morphological alterations in hippocampus (Dakshinamurti *et al.*, 1993). Moreover, subcutaneously injection of 1.2 mg/kg DA in pregnant rat on GD13 caused no effects in dams, but significantly increased the response latency in T-maze spontaneous alternation test and rate of habituation in Figure-8 locomotor task in pups (Levin *et al.*, 2005). In addtion, a study conducted in pregnant female mice on GD 11.5, 14.5 or 17.5 following a single intraperitoneal dose of 1mg/kg DA revealed severe impairment of learning and memory with serious deviances of anxiety-related behaviors and myelination failure and the overgrowth of neuronal processes of the limbic cortex neurons in exposed pups (Tanemura *et al.*, 2009). Similar findings of behavioral changes following prenatal DA exposure were also reported in recent studies in mice(Mills *et al.*, 2016; Zuloaga *et al.*, 2016). Taken together, these studies suggest that DA passes the placental barrier and affect the development of pups which is supported by the existence of DA in fetuses of rodents and sea lions.

DA has been shown in fetal brains and amniotic fluid in rats upon i.v. injection of 0.6 mg/kg and 1.6 mg/kg DA in pregnant rats on GD13 and GD20 (Maucher and Ramsdell, 2007). In a diffent study in rats, DA was measured in fetal plasma, fetal brain, placenta and amniotic fluid following i.v. dose of 1.0 mg /kg DA on GD 20 in pregnant rats (Maucher Fuquay *et al.*, 2012b). In addtion, DA was also detected in fetal urine, feces and gastric fluid as well as amniotic fluid in sea lions (Brodie *et al.*, 2006). However, the knowledge of dose-response and exposure levels of DA in pups given oral DA pre-natally is not available in any animal models.

This study was conducted to compare DA toxicokinetics before and during pregnancy following chronic oral dose of 0.15 mg/kg/day DA across pregancy. It is the first time that DA toxicokinetic parameters have been reported in non-pregnant and pregnant monkeys following chronic low oral exposure to DA. Results of our study will help understanding DA disposition during pregnancy and protect pregnant women and their fetuses from DA intoxication.

5.3 MATERIALS AND METHODS

5.3.1 Chemicals and Reagents

DA was purchased from BioVectra (Charlottetown, PE, Canada). Certified calibration solution for DA was purchased from National Research Council Canada (Ottawa, Ontario, Canada). Optima grade water, methanol, acetonitrile and formic acid used for bioanalytical assays were purchased from Fisher Scientific (Pittsburgh, PA).

5.3.2 Animal Studies

Six healthy adult female cynomolgus monkeys were enrolled in the study. Animals were housed in the Infant Primate Research Laboratory at the Washington National Primate Research Center. Animals were unsedated and unfasted for the duration of the study, with unrestricted access to food and water. Animals were fed with Lab Diet High Protein Monkey Diet biscuits twice a day, once approximately 2 hours before the DA dose and once approximately 5 hours after the dose of DA. All animal procedure guidelines followed the Animal Welfare Act and the Guide for Care and Use of Laboratory Animals of the National Research Council. All protocols were approved by the University of Washington Institutional Animal Care and Use Committee.

The DA kinetics on day 1 and day 56 were characterized in six animals following daily oral dose of 0.15 mg/kg DA. Three of the six animals were dosed 0.15 mg/kg DA daily until two weeks after delivery and DA kinetics were characterized before pregnancy (day 1 and day 56), on two separate days (55 days apart) during pregnancy and two weeks after delivery. DA oral dose was prepared using a concentration of 1 mg/ml DA dissolved in tap water with 5% sucrose and filtered with syringe filter (0.2 µM, 25mm). The dose was given to fully conscious animals without restraint. Blood samples were collected at baseline and at 1, 2, 4, 6, 8, 10, 12 and 24 hours post dose. Urine samples were collected from cage pans after every blood draw during the study for 24 hours. To design the study of monitoring DA exposure levels in infants, one blood sample (3 days post-delivery), two urine samples (3 days and 6 days post-delivery) were collected from two delivered infants. Blood samples were collected into sodium heparin tubes and centrifuged at 3,000 x g for 15 minutes to isolate plasma for further analysis. Plasma and urine samples were stored at −20 °C until analysis. For all studies, the dosing solution was analyzed for DA content as described below to confirm DA concentrations.

5.3.3 Analysis of DA Concentrations in Biological Samples by LC-MS/MS

For DA measurement in plasma, 60 µl of methanol was added to 60 µl plasma, and the samples were centrifuged at 16,100 g for 40 minutes, set at 4 °C for 30 minutes and centrifuged again at 16,100g for 30 minutes. The supernatant was collected for analysis. Standard curves were prepared using blank monkey plasma 0.3-20 ng/ml (1- 64 nM) spiked at n≥6 concentrations of DA with high, middle and low quality control (QC) samples at 0.9, 3.7 and 14.9 ng/ml (3, 12 and 48 nM).

For DA measurement in urine, urine samples were first diluted 50-fold with water and then 60 µl of methanol was added to 60 µl diluted urine, the samples were centrifuged at 16,100 g for 20 minutes and supernatant was collected and for analysis. Standard curves were prepared using blank monkey urine 7.8-996.3 ng/ml (25 - 3200 nM) spiked at n≥6 concentrations of DA with high, middle and low QC samples at 15.6, 155.7 and 622.7 ng/ml (50, 500 and 2000 nM).

DA concentrations in plasma and urine samples were measured by LC-MS/MS, using AB Sciex 6500 QTRAP mass spectrometer (AB Sciex, Foster City, CA) equipped with a Shimadzu UFLC XR DGU-20A5 (Shimadzu Scientific Instruments, Columbia, MD) and a Synergi™ Hydro-RP 100 Å LC Column (2.5 µm, 50 ×2 mm; Phenomenex). Compound dependent mass spectrometer parameters used for detection of DA were collision energy 24, collision cell exit potential 10, declustering potential 15 and entrance potential 10. Gradient elution with a flow rate of 0.5 ml/min using (A) water with 0.1% formic acid and (B) 95% acetonitrile with 5% water and 0.1% formic acid was used. The gradient was from an initial 95% A for 1 min to 0% A over 3 min and then to 95% A for 5 min. Analytes were detected using positive ion ESI mode. MS/MS transitions monitored for DA were m/z 312.1>266.2. Samples were kept in the autosampler at 4°C and 10 µl of sample was injected for analysis.

5.3.4 Pharmacokinetic Analysis

Area under plasma concentration-time curve (AUC) after oral dose was determined with linear trapezoidal method in standard non-compartmental analysis using Phoenix (St. Louis, MO). Renal clearance (CL_R) after oral dose was obtained using equation:

$$CL_R = \frac{A_e}{AUC} \quad (1)$$

in which A_e is the amount of DA excreted in urine in the same time period as AUC measurement (0 to 24 hour post oral dose).

Creatinine clearance (CL_{cr}) after oral dose was calculated using equation:

$$CL_{cr} = \frac{\frac{dA_e}{dt}}{C} \quad (2)$$

in which A_e is the amount of creatinine excreted in the urine over a 12-hour interval (dt) and C is the concentration of creatinine measured in plasma. Blood and urine creatinine concentrations were measured by clinical assays at Department of Laboratory Medicine, University of Washington Medical Center.

5.3.5 Statistical Analysis

Results presented in the figures and tables are mean ± SD values. Nonparametric correlation was used to evaluate the association of DA renal clearance and creatinine clearance. Wilcoxon matched-pairs signed rank test was conducted to DA renal clearance and creatinine clearance between day 1 and day 56 in non-pregnant monkeys (n=6). Paired T-test was used to evaluate the changes of AUC, creatinine clearance, DA renal clearance and weight of monkeys (n=3) between k2 and pk1 and pk2 with log transformed values. The p values were two-tailed ($\alpha = 0.05$) and p value <0.05 was considered significant. Analyses were performed using Prism

software (GraphPad, La Jolla, CA, USA). Potential presence of outliers of the study were tested using Grubbs' test.

5.4 RESULTS

5.4.1 Toxicokinetics of DA under Chronic Oral Exposure

To evaluate toxicokinetics of DA following chronic dosing, kinetic studies were conducted in 6 female monkeys dosed with 0.15 mg/kg DA PO daily before pregnancy. The plasma concentration- time curves of DA in these animals on day 1 and day 56 (steady-state) are shown in Figure 5.1A. One animal was detected to be an outlier and the data was analyzed also with exclusion of this animal. The $AUC_{0\text{-}24hr}$ (98 ± 27 ng*hr/ml) of DA on 56 days was similar to the $AUC_{0\text{-}\infty}$ (100 ± 44 ng*hr/ml) observed in previous studies (Chapter 4) in monkeys after single dose of 0.15 mg/kg DA, indicating linear kinetics and lack of time dependent changes in DA disposition. Trough concentration ratio between day 56 and day 1 was 0.9 ± 0.4 indicating that DA dose not accumulate in the plasma following chronic exposure. DA renal clearance was 0.44 ± 0.32 l/hr on day 1 and 0.32 ± 0.22 l/hr on day 56 (Table 5.1). Renal clearance on day 56 was not significantly different from that on day 1 ($p = 0.125$) (Figure 5.1B). The creatinine clearance was 0.69 ± 0.2 l/hr on day 1 and 0.66 ± 0.18 l/hr on day 56, respectively. Statistical analysis showed no significant difference ($p = 1$) of creatinine clearance between day 1 and day 56 indicating that kidney function was not affected by chronic DA exposure (Figure 5.1C). There was no correlation ($p = 0.6$) between DA renal clearance and the measured creatinine clearance in the 6 monkeys on day 1 or day 56 (Figure 5.1D) and DA renal clearance was 64% and 48% of creatinine clearance on day 1 and 56 respectively, indicating the existence of renal reabsorption of DA.

5.4.2 Toxicokinetics of DA during pregnancy

To investigate toxicokinetics of DA during pregnancy and compare it with DA disposition in non-pregnant monkeys, five kinetic studies including on day 1 and day 56 post dose before pregnancy (k1 and k2), two studies during pregnancy (55 days apart, pk1 and pk2), and one postpartum study (two weeks after delivery, ppk) were conducted in 3 female monkeys dosed with 0.15 mg/kg DA PO daily. The plasma concentration- time curves of DA in these animals on each kinetic day are shown in Figure 5.2A. The average AUC was 40 ± 23 ng*hr/ml and 69 ± 27 ng*hr/ml on day 1 and 56 in non-pregnant monkeys. During pregnancy, the average AUC was 48 ± 13 ng*hr/ml and 38 ± 23 ng*hr/ml on two different kinetic day. Two weeks after delivery, the AUC increased to 59 ± 20 ng*hr/ml in same monkeys. As shown in Figure 5.2B, compared with AUC on day 1 and day 56 before pregnancy, AUC of DA slightly decreased during pregnancy and increased to similar level as pre-pregnancy AUC two weeks after delivery.

The time course of DA excretion in urine is presented in Figure 5.2C. The 24 -hour urine collection showed 3 ± 1.4 % and 4 ± 2% of the DA dose were excreted in urine on day 1 and day 56 before pregnancy, 3.5% and 4.6 % of the DA dose were recovered during pregnancy on two different kinetic days and 4.9 ± 0.6 % of the DA dose was measured in postpartum urine collection. This result is consistent with previous studies, in which 4 ± 2% of the DA dose was recovered in the 24 hour-urine collections after oral administration of 0.075 mg/kg DA. DA renal clearance of 0.47 ± 0.21 l/hr and 0.33 ± 0.12 l/hr was observed on day 1 and day 56 respectively before pregnancy. During pregnancy, DA renal clearance increased to 0.6 ± 0.22 l/hr and 0.69 ± 0.27 l/hr on two different kinetic days. After delivery, DA renal clearance was measured as 0.55 ± 0.27 l/hr. The trend of increased DA renal clearance during pregnancy is shown in Figure 5.2E. The elevated DA renal clearance in pregnant monkeys may be explained by the increased

creatinine clearance during pregnancy (Figure 5.2D). During pregnancy, creatinine clearance was 1.2 ± 0.03 l/hr and 1.16 ± 0.13 l/hr on two different kinetic days, which is higher than the creatinine clearance of 0.81 ± 0.25 l/hr and 0.72 ± 0.22 l/hr measured before pregnancy and creatinine clearance of 1.05 ± 0.26 l/hr obtained postpartum. DA renal clearance was 58%, 46%,50%,59% and 52% of creatinine clearance measured on day 1 and day 56 before pregnancy, during pregnancy and postpartum. Besides increased creatinine clearance, the increased body weight was also observed in these monkeys during pregnancy (Figure 5.2F). The body weight was increased from 3.9 ± 0.5 kg and 3.9 ± 0.7 kg before pregnancy to 4.4 ± 0.8 kg and 5.1 ± 0.8 kg during pregnancy. After delivery, the body weight was 4.7 ± 0.9 kg and similar to pregnancy weight. DA was detected in the infant plasma sample collected 3 days after delivery and infant urine samples collected 3 days and 6 days after delivery.

5.5 DISCUSSION

The toxicokinetics of DA in non-pregnant and pregnant monkeys following chronic low oral dose of DA have been determined here for the first time. Despite the previously observed flip-flop kinetics in non-pregnant monkeys with 10- 11 hr terminal half-life after oral DA dose, no accumulation of DA was observed in monkeys following 56 days daily oral dose of 0.15 mg/kg DA. DA has been reported to preferentially accumulate in the kidney in mice given a single dose of 2.5 mg/kg DA intraperitoneally (Funk *et al.*, 2014). Kidney injury molecule-1 (uKIM-1), acute kidney injury biomarker, was shown to be elevated given 0.1 mg/kg DA intraperitoneally for 3 consecutive days, a dose level that was considered below the limit of toxicity (Funk *et al.*, 2014). Due to the suspect of the effect of chronic oral DA exposure on kidney function, creatinine clearance and DA renal clearance were monitored in the study. The creatinine clearance and DA renal clearance were not significantly changed after 56 days of daily

oral doses of 0.15 mg/kg DA suggesting that kidney function is unaffected at this exposure level. Previously we have shown that DA renal clearance was 25% of the creatinine clearance in monkeys given a single i.v. injection of 5 µg/kg DA, which suggested significant reabsorption of DA in the kidney. The finding of DA renal clearance accounting for 64% and 48% of creatinine clearance on day 1 and 56 respectively given 0.15 mg/kg/day of DA and no correction between DA renal clearance and creatinine clearance confirmed previous conclusion of reabsorption of DA in the kidney.

In humans, changed physiological parameters such as increase of glomerular filtration rate (GFR), body fat, total body water and cardiac output during pregnancy are well documented (Tasnif *et al.*, 2016). In our study animals, creatinine clearance increased approximately 54% during pregnancy in comparison to average creatinine clearance measured before pregnancy suggesting the increase of GFR. In addition, monkey body weight also increased with time during pregnancy. Since DA is cleared through kidney, the increase of GFR likely leads to increased DA renal clearance. As we expected, average DA renal clearance increased 61% during pregnancy compared with the value obtained before pregnancy. The elevated body weight likely contributes to increased apparent volume of distribution as reported in previous studies in rats (Truelove J, 1994; Maucher Fuquay et al., 2012). The increase of DA renal clearance caused decrease of AUC at steady-state during pregnancy (pk1 and pk2) in comparison to AUC obtained at steady-state before pregnancy (k2) and slight increase in the percentage of DA excreted in the urine during pregnancy. These findings suggested upon exposure to same levels of DA, pregnant women likely have lower exposures compared to non-pregnant women since DA renal clearance is elevated during pregnancy. However, only 3 monkeys were included in this study and more animals are needed to draw a conclusion with statistical power.

Another question that remains and requires further investigation is the placental transfer of DA to fetus during pregnancy. To design a study in the infants delivered by these female monkeys dosed with 0.15 mg/kg/day DA across pregnancy, a plasma sample on day 3 post-delivery and two urine samples on day 3 and day 6 post-delivery were collected from two infants and DA was detected in all 3 samples. The dose of 0.15 mg/kg/day given in the study animals is close to the proposed oral acute reference doses and tolerable daily intake (ranging from 0.018 to 0.1 mg/kg) (Costa *et al.*, 2010). Even under such dose level, DA was still detected in the infants which indicates that infants may be threatened by DA toxicity due to the maternal exposure to chronic low oral dose of DA. However, the quantitative analysis of these infant samples and behavioral and neurological tests are needed to better evaluate fetal DA exposure and potential DA toxicity in fetus.

This study suggested changed toxicokinetics of DA during pregnancy in monkeys exposed to chronic oral dose of 0.15 mg/kg/day DA and placental transfer of DA to fetus. Future studies with more animals are undergoing and will contribute to statistical solid conclusion on our findings. The behavioral and neurological changes caused by the chronic low level of oral DA exposure will also be evaluated on both dams and pups in the future study.

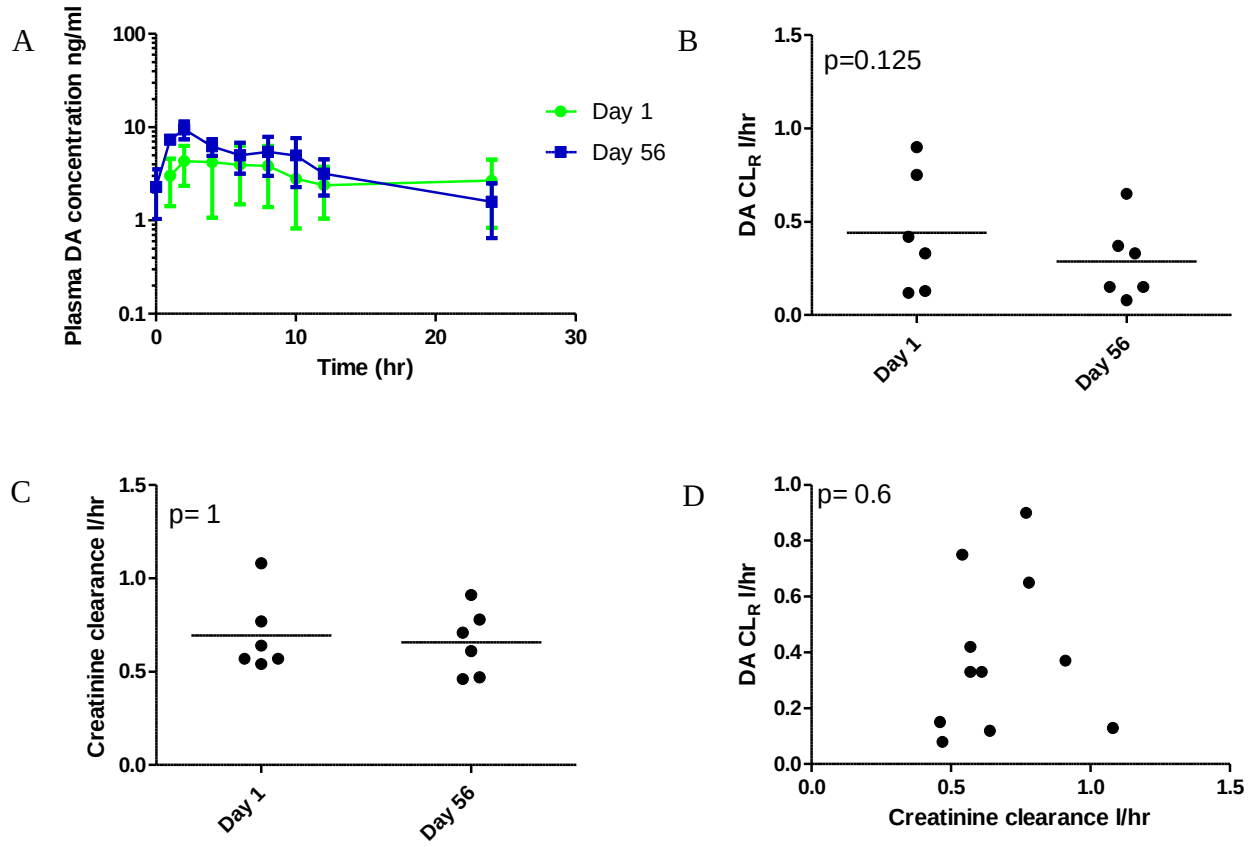

Figure 5.1. Pharmacokinetics of DA in non-pregnant monkeys (n=6) following oral administration of 0.15 mg/kg/day DA for 56 days. (A) Plasma DA concentration-time curve on day 1 and day 56 after DA dose. (B) The comparison of DA renal clearance between day 1 and day 56 (C)The comparison of creatinine clearance between day 1 and day 56. (D) The correlation between DA renal clearance and creatinine clearance on both day 1 and day 56. One animal was detected to be an outlier and the data was analyzed with outlier.

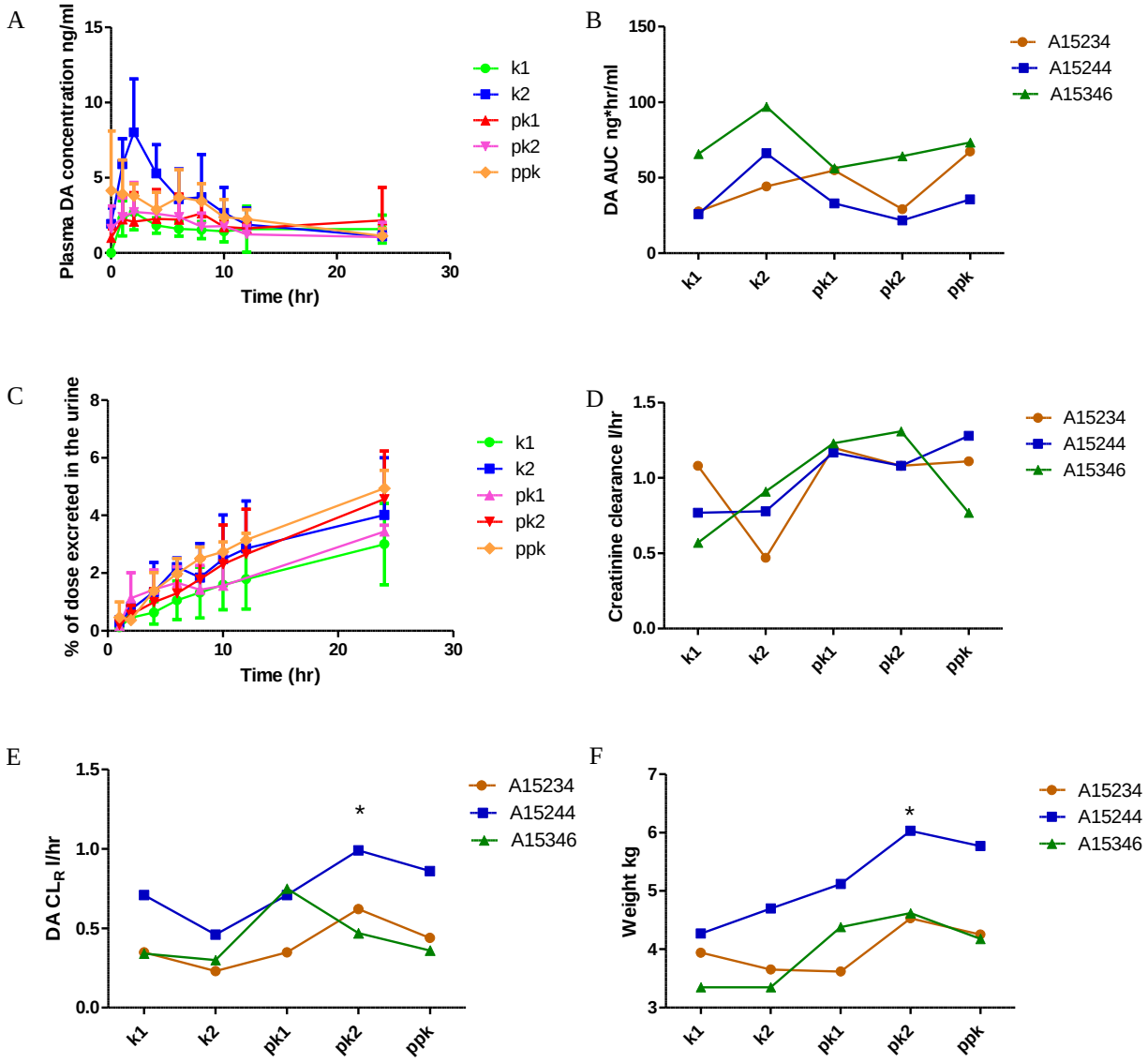

Figure 5.2. Pharmacokinetics of DA following oral administration of 0.15 mg/kg/day DA in monkeys(n=3) on day 1 (k1) and day 56 (k2) before pregnancy, on two days (pk1 and pk2) during pregnancy and two weeks after delivery (ppk) (A) Plasma DA concentration-time curves is shown as mean and standard deviation of three animals (B) DA $AUC_{0\text{-}24hr}$ in the three animals studied in the 5 study days (C) Time course of DA excretion into urine. The percentage of oral DA dose excreted in the urine as a function of time is shown as mean and standard deviation of three animals (D) Creatinine clearance in the three animals studied in the 5 study days (E) DA renal clearance in the three animals studied in the 5 study days (F) Body weight in the three animals studied in the 5 study days

* Paired t test $p<0.05$ between k2 and pk2

Table 5.1 . Pharmacokinetic parameters in monkeys (n=6) on day 1 and day 56 following chronic oral administration of 0.15 mg/kg DA once daily

	Day 1 $AUC_{0\text{-}24hr}$ (h*ng/mL)	Day 56 $AUC_{0\text{-}24hr}$ (h*ng/mL)	[c]Trough concentration ratio	Day 1 CL_R (l/hr)	Day 56 CL_R (l/hr)
[a]Mean ± SD	72 ± 31	155 ± 143	1.0 ± 0.5	0.44 ± 0.32	0.29 ± 0.19
[b]Mean ± SD	72 ± 31	98 ± 27	0.9 ± 0.4	0.44 ± 0.32	0.32 ± 0.22

Significant outlier p< 0.05, [a] with outlier, [b] without outlier, [c] concentration between day 56 and day 1 measured at 24 hour post dose

Chapter 6.

Conclusions

The thesis projects demonstrate that the disposition of xenobiotics such as *at*RA and DA changed in patients with CKD and cancer as well as during pregnancy and PBPK model can be used to simulate the disposition of xenobiotics and help better understand ADME of xenobiotics in special populations.

Vitamin A homeostasis was shown to be altered in patients with CKD in comparison to healthy subjects. The increased hepatic RBP4 synthesis, retinyl ester hydrolysis, and/or hepatic secretion of RBP4-retinol may be responsible for the changed vitamin A homeostasis. This study highlights the necessity to redefine CKD not as an isolated disease, but as a global condition that affects many organ systems.

Using the in vitro and in vivo data, *at*RA PBPK model was built and this PBPK model successfully simulated the dose- and time- dependent pharmacokinetics of *at*RA in healthy humans and in cancer patients including adult and pediatric patients in the absence and presence of *at*RA metabolism inhibitors.

Despite the short half-life of DA following IV dosing, flip-flop kinetics with prolonged terminal half-life was observed following oral administration of DA. The absolute bioavailability of DA is about 7% and DA is mainly cleared through kidneys. The developed PBPK model of DA successfully simulated DA plasma concentration-time profiles, urinary excretion and tissue concentration-time profiles following IV and PO dosing.

Following multiple oral doses of DA, DA did not accumulate in the body. DA renal clearance and creatinine clearance were not changed following chronic low oral exposure to DA. During pregnancy, the increase of body weight and creatinine clearance were observed. The AUC of DA decreased and DA renal clearance increased during pregnancy which were likely

caused by the increase of GFR in monkeys during pregnancy. DA was detected in the plasma and urine of the delivered infants.

Taken together, the novel findings from these thesis projects greatly enhance the understanding of *at*RA and DA disposition in patients with CKD and cancer as well as during pregnancy. The similar study approach can be applied to investigate the disposition of other xenobiotics in special populations.

REFERENCES

Abduljalil K, Cain T, Humphries H, and Rostami-Hodjegan A (2014) Deciding on success criteria for predictability of pharmacokinetic parameters from in vitro studies: An analysis based on in vivo observations. *Drug Metab Dispos* **42**:1478–1484.

Ablain J, and De The H (2011) Revisiting the differentiation paradigm in acute promyelocytic leukemia.

Adamson P (1996) All-Trans-Retinoic Acid Pharmacology and Its Impact on the Treatment of Acute Promyelocytic Leukemia. *Oncologist* **1**:305–314.

Adamson P, Bailey J, Pluda J, Poplack D, Bauza S, Murphy R, Yarchoan R, and Balis F (1995) Pharmacokinetics of all-trans-retinoic acid administered on an intermittent schedule. *J Clin Oncol* **13**:1238–1241.

Argilés J (2005) Cancer-associated malnutrition. *Eur J Oncol Nurs* **9**.

Arnold S, Amory J, Walsh T, and Isoherranen N (2012) A sensitive and specific method for measurement of multiple retinoids in human serum with UHPLC-MS/MS. *J Lipid Res* **53**:587–598.

Arnold S, Kent T, Hogarth C, Griswold M, Amory J, and Isoherranen N (2015) Pharmacological inhibition of ALDH1A in mice decreases all-trans retinoic acid concentrations in a tissue specific manner. *Biochem Pharmacol* **95**:177–192, Elsevier Inc.

Arnouts P, Bolignano D, Nistor I, Bilo H, Gnudi L, Heaf J, and Biesen W (2014) Glucose-lowering drugs in patients with chronic kidney disease: a narrative review on pharmacokinetic properties. *Nephrol Dial Transplant* **29**:1284–1300.

Arrieta O, González-De la Rosa C, Aréchaga-Ocampo E, Villanueva-Rodríguez G, Cerón-Lizárraga T, Martínez-Barrera L, Vázquez-Manríquez M, Ríos-Trejo M, Alvarez-Avitia M, Hernández-Pedro N, Rojas-Marín C, and De la Garza J (2010) Randomized phase II trial of All-trans-retinoic acid with chemotherapy based on paclitaxel and cisplatin as first-line treatment in patients with advanced non-small-cell lung cancer. *J Clin Oncol* **28**:3463–71.

Barazzoni R, Zanetti M, Semolic A, Pirulli A, Cattin MR, Biolo G, Bosutti A, Panzetta G, Bernardi A, and Guarnieri G (2011) High plasma retinol binding protein 4 (RBP4) is associated with systemic inflammation independently of low RBP4 adipose expression and is normalized by transplantation in nonobese, nondiabetic patients with chronic kidney disease. *Clin Endocrinol (Oxf)* **75**:56–63, Blackwell Publishing Ltd.

Barbaro E, Zangrando R, Barbante C, and Gambaro A (2016) Fast and Sensitive Method for Determination of Domoic Acid in Mussel Tissue. *Sci World J* **2016**:1–6.

Barnes K, Rowland A, Polasek T, and Miners J (2014) Inhibition of human drug-metabolising cytochrome P450 and UDP-glucuronosyltransferase enzyme activities in vitro by uremic toxins. *Eur J Clin Pharmacol* **70**:1097–1106.

Baxter J, Brass C, Schentag J, and Slaughter R (1986) Pharmacokinetics of Ketoconazole Administered Intravenously to Dogs and Orally as Tablet and Solution to Humans and

Dogs. *J Pharm Sci* **75**:443–447.

Bendich A O (1989) Biological actions of carotenoids. **3**:1927–1932.

Bhat P and Samaha H (1999) Kinetic properties of the human liver cytosolic aldehyde dehydrogenase for retinal isomers. *Biochem Pharmacol* **57**:195–197.

Bosworth C, and de Boer I (2013) Impaired Vitamin D Metabolism in CKD. *Semin Nephrol* **33**:158–168.

Bosworth C, Levin G, Robinson-Cohen C, Hoofnagle A, Ruzinski J, Young B, Schwartz S, Himmelfarb J, Kestenbaum B, and de Boer I (2012) The serum 24,25-dihydroxyvitamin D concentration, a marker of vitamin D catabolism, is reduced in chronic kidney disease. *Kidney Int* **82**:693–700.

Brelsford, M. & Beute T (2008) Preventing and managing the side effects of isotretinoin. *Semin Cutan Med Surg* **27**:197–206.

Brodie E, Gulland F, Greig D, Hunter M, Jaakola J, Leger J St., Leighfield T, and Van Dolah F (2006) Domoic acid causes reproductive failure in California sea lions (Zalophus Californianus). *Mar Mammal Sci* **22**:700–707, Blackwell Publishing Inc.

Bryson H, and Wagstaff A (1996) Liarozole. *Drugs {&} Aging* **9**:478–484.

Nelson C, Buttrick B and Isoherranen N (2013) Therapeutic Potential of the Inhibition of the Retinoic Acid Hydroxylases CYP26A1 and CYP26B1 by Xenobiotics. *Curr Top Med Chem* **13**:1402–28.

Yeung C, Shen D, Thummel K, and Himmelfarb J (2014) Effects of chronic kidney disease and uremia on hepatic drug metabolism and transport. *Kidney Int* **85**:522-8.

Cheeti S, Budha N, Rajan S, Dresser M, and Jin J (2013) A physiologically based pharmacokinetic (PBPK) approach to evaluate pharmacokinetics in patients with cancer. *Biopharm Drug Dispos* **34**:141–54.

Chen C, Mistry G, Jensen B, Heizmann P, Timm U, Van Brummelen P, and Rakhit A (1996) Pharmacokinetics of Retinoids in Women after Meal Consumption or Vitamin A Supplementation. *J Clin Pharmacol* **36**:799–808, Blackwell Publishing Ltd.

Cho Y, Youn B-S, Lee H, Lee N, Min S-S, Kwak S, Lee H, and Park K (2006) Plasma Retinol-Binding Protein-4 Concentrations Are Elevated in Human Subjects With Impaired Glucose Tolerance and Type 2 Diabetes. *Diabetes Care* **29**.

Clewell H, Andersen M, Wills R, and Latriano L (1997) A physiologically based pharmacokinetic model for retinoic acid and its metabolites. *J Am Acad Dermatol* **36**:S77-85.

Conaway H, Henning P, and Lerner U (2013) Vitamin a metabolism, action, and role in skeletal homeostasis. *Endocr Rev* **34**:766–797.

Conley B, Egorin M, Sridhara R, Finley R, Hemady R, Wu S, Tait N, and Van Echo D (1997)

Phase I clinical trial of all-trans-retinoic acid with correlation of its pharmacokinetics and pharmacodynamics. *Cancer Chemother Pharmacol* **39**:291–299.

Coombs C, Tavakkoli M, and Tallman M (2015) Acute promyelocytic leukemia: where did we start, where are we now, and the future. *Blood Cancer J* **5**:e304.

Costa L, Giordano G, and Faustman E (2010) Domoic acid as a developmental neurotoxin. *Neurotoxicology* **31**:409–423.

Costa L, Giordano G, and Faustman E (2010) Domoic acid as a developmental neurotoxin. *Neurotoxicology* **31**:409–23.

Costantine M (2014) Physiologic and pharmacokinetic changes in pregnancy. *Front Pharmacol* **5 APR**:1–5.

D'Ambrosio D, Clugston R, and Blaner W (2011) Vitamin A metabolism: An update. *Nutrients* **3**:63–103.

Dakshinamurti K, Sharma S, Sundaram M, and Watanabe T (1993) Hippocampal changes in developing postnatal mice following intrauterine exposure to domoic acid. *J Neurosci* **13**.

Daneshmend T, Warnock D, Ene M, Johnson E, Potten M, Richardson M, and Williamson P (1984) Influence of food on the pharmacokinetics of ketoconazole. *Antimicrob Agents Chemother* **25**:1–3.

Daneshmend T, Warnock D and Roberts A (1981) Pharmacokinetics of ketoconazole in normal subjects. *J Antimicrob Chemother* **8**:299–304.

De Buck S, Sinha V, Fenu L, Gilissen R, Mackie C, and Nijsen M (2007) The prediction of drug metabolism, tissue distribution, and bioavailability of 50 structurally diverse compounds in rat using mechanism-based absorption, distribution, and metabolism prediction tools. *Drug Metab Dispos* **35**:649–59.

Denis L, Debruyne F, De Porre P, and Bruynseels J (1998) Early clinical experience with liarozole (Liazal^{TM}) in patients with progressive prostate cancer. *Eur J Cancer* **34**:469–475.

Desai C, Huang J, Lokhandwala A, Fernandez A, Riaz I Bin, and Alpert J (2014) The Role of Vitamin Supplementation in the Prevention of Cardiovascular Disease Events. *Clin Cardiol* **37**:n/a-n/a, Wiley Periodicals, Inc.

Dreisbach A, Japa S, Gebrekal A, Mowry S, Lertora J, Kamath L, and Rettie A (2003) Cytochrome P4502C9 activity in end-stage renal disease. *Clin Pharmacol Ther* **73**:475–477.

Du X, Peterson W, Fisher J, Hunter M, and Peterson J (2016) Initiation and development of a toxic and persistent Pseudo-nitzschia bloom off the Oregon coast in spring/summer2015. *PLoS One* **11**.

Erikstrup C, Mortensen O, Nielsen A, Fischer C, Plomgaard P, Petersen A, Krogh-Madsen R, Lindegaard B, Erhardt J, Ullum H, Benn C, and Pedersen B (2009) RBP-to-retinol ratio, but not total RBP, is elevated in patients with type 2 diabetes. *Diabetes, Obes Metab* **11**:204–212, Blackwell Publishing Ltd.

FDA (2016) Clinical Pharmacology Section of Labeling for Human Prescription Drug and

Biological Products — Content and Format Guidance for Industry. *Fda*.

FDA (2010) Guidance for Industry Pharmacokinetics in Patients with Impaired Renal Function — Study Design , Data Analysis , and Impact on Dosing and Labeling. *Clin Pharmacol*.

Fernandez E, Perez R, Hernandez A, Tejada P, Arteta M, and Ramos J (2011) Factors and mechanisms for pharmacokinetic differences between pediatrie population and adults. *Pharmaceutics* **3**:53–72.

Frame E, and LeFebvre K (2013) *ELISA Methods for Domoic Acid Quantification in Multiple Marine Mammal Species and Sample Matrices*.

Frey S, Nagl B, Henze A, Raila J, Schlosser B, Berg T, Tepel M, Zidek W, Weickert M, Pfeiffer A, and Schweigert F (2008) Isoforms of retinol binding protein 4 (RBP4) are increased in chronic diseases of the kidney but not of the liver. *Lipids Health Dis* **7**:29.

Funk J , Janech M, Dillon J, Bissler J, Siroky B, and Bell P (2014) Characterization of Renal Toxicity in Mice Administered the Marine Biotoxin Domoic Acid. *J Am Soc Nephrol* 1–11.

Fuquay J, Muha N, Wang Z, and Ramsdell JS (2012a) Elimination kinetics of domoic acid from the brain and cerebrospinal fluid of the pregnant rat. *Chem Res Toxicol* **25**:2805–2809.

Fuquay J, Muha N, Wang Z, and Ramsdell JS (2012b) Toxicokinetics of domoic acid in the fetal rat. *Toxicology* **294**:36–41.

Giordano G, White C, McConnachie L, Fernandez C, Kavanagh T, and Costa L (2006) Neurotoxicity of Domoic Acid in Cerebellar Granule Neurons in a Genetic Model of Glutathione Deficiency. *Mol Pharmacol* **70**.

Graham T, Wason C, Blüher M, and Kahn B (2007) Shortcomings in methodology complicate measurements of serum retinol binding protein (RBP4) in insulin-resistant human subjects. *Diabetologia* **50**:814–823.

Henze A, Frey S, Raila J, Scholze A, Spranger J, Weickert M, Tepel M, Zidek W, and Schweigert F (2010) *Alterations of retinol-binding protein 4 species in patients with different stages of chronic kidney disease and their relation to lipid parameters*.

Henze A, Frey S, Raila J, Tepel M, Scholze A, Pfeiffer A, Weickert M, Spranger J, and Schweigert F (2008) Evidence That Kidney Function but Not Type 2 Diabetes Determines Retinol-Binding Protein 4 Serum Levels. *Diabetes* **57**.

Hiolski E, Kendrick P, Frame E, Myers M, Bammler T, Beyer R, Farin F, Wilkerson H, Smith D, Marcinek D, and Lefebvre K (2014) Chronic low-level domoic acid exposure alters gene transcription and impairs mitochondrial function in the CNS. *Aquat Toxicol* **155**:151–159.

Huang Y, Colaizzi J, Bierman R, Woestenborghs R, and Heykants J (1986) Pharmacokinetics and dose proportionality of ketoconazole in normal volunteers. *Antimicrob Agents Chemother* **30**:206–210.

Iland H, Bradstock K, Supple S, Catalano A, Collins M, Hertzberg M, Browett P, Grigg A, Firkin F, Hugman A, Reynolds J, Di Iulio J, Tiley C, Taylor K, Filshie R, Seldon M, Taper J, Szer J, Moore J, Bashford J, and Seymour J (2012) All-trans-retinoic acid, idarubicin, and

IV arsenic trioxide as initial therapy in acute promyelocytic leukemia (APML4). *Blood* **120**.

Isoherranen N, and Thummel K (2013) Drug metabolism and transport during pregnancy: How does drug disposition change during pregnancy and what are the mechanisms that cause such changes? *Drug Metab Dispos* **41**:256–262.

Iverson F, Truelove J, Tryphonas L N (1990) The toxicology of domoic acid administered systemically to rodents and primates. *Can Dis Wkly Rep* **16**:Suppl 1E:15-8; discussion 18-9.

Jing J, Isoherranen N, Robinson-Cohen C, Petrie I, Kestenbaum B, and Yeung C (2016) Chronic Kidney Disease Alters Vitamin A Homeostasis via Effects on Hepatic RBP4 Protein Expression and Metabolic Enzymes. *Clin Transl Sci* **9**:207–15.

Jing J, Nelson C, Paik J, Shirasaka Y, Amory J, and Isoherranen N (2017) Physiologically Based Pharmacokinetic Model of All- *trans* -Retinoic Acid with Application to Cancer Populations and Drug Interactions. *J Pharmacol Exp Ther* **361**:246–258.

Jones H, Chen Y, Gibson C, Heimbach T, Parrott N, Peters S, Snoeys J, Upreti V, Zheng M, and Hall S (2015) Physiologically based pharmacokinetic modeling in drug discovery and development: a pharmaceutical industry perspective.

Kane M (2012) Analysis, occurrence, and function of 9-cis-retinoic acid. *Biochim Biophys Acta - Mol Cell Biol Lipids* **1821**:10–20.

Kedishvili N (2013) Enzymology of retinoic acid biosynthesis and degradation: Thematic Review Series: Fat-Soluble Vitamins: Vitamin A. *J Lipid Res* **54**:1744–1760.

Kimura O, Kotaki Y, Hamaue N, Haraguchi K, and Endo T (2011) Transcellular transport of domoic acid across intestinal Caco-2 cell monolayers. *Food Chem Toxicol* **49**:2167–2171.

Klammt S, Wojak H, Mitzner A, Koball S, Rychly J, Reisinger E, and Mitzner S (2012) Albumin-binding capacity (ABiC) is reduced in patients with chronic kidney disease along with an accumulation of protein-bound uraemic toxins. *Nephrol Dial Transplant* **27**:2377–2383.

Lambadiari V, Kadoglou N, Stasinos V, Maratou E, Antoniadis A, Kolokathis F, Parissis J, Hatziagelaki E, Iliodromitis E, and Dimitriadis G (2014) Serum levels of retinol-binding protein-4 are associated with the presence and severity of coronary artery disease. *Cardiovasc Diabetol* **13**:121.

Lee J, Newman R, Lippman S, Fossella F, Calayag M, Raber M, Krakoff I, and Hong W (1995) Phase I evaluation of all-trans retinoic acid with and without ketoconazole in adults with solid tumors. *J Clin Oncol* **13**:1501–1508.

Lefebvre K, Bargu S, Kieckhefer T, and Silver M (2002) From sanddabs to blue whales: the pervasiveness of domoic acid. *Toxicon* **40**:971–977.

Lefebvre K, Frame E, Gulland F, Hansen J, Kendrick P, Beyer R, Bammler T, Farin F, Hiolski E, Smith D, and Marcinek D (2012) A Novel Antibody-Based Biomarker for Chronic Algal Toxin Exposure and Sub-Acute Neurotoxicity. *PLoS One* **7**:e36213, The University of Southern Mississippi.

Lefebvre K, Kendrick P, Ladiges W, Hiolski E, Ferriss B, Smith D, and Marcinek D (2017) Chronic low-level exposure to the common seafood toxin domoic acid causes cognitive deficits in mice. *Harmful Algae* **64**:20–29.

Lefebvre K, and Robertson A (2010) Domoic acid and human exposure risks: A review. *Toxicon* **56**:218–230.

Lefebvre K, and Robertson A (2010) Domoic acid and human exposure risks: a review. *Toxicon* **56**:218–30.

Levey A, Eckardt K, Tsukamoto Y, Levin A, Coresh J, Rossert J, De Z, Hostetter T, Lameire N, and Eknoyan G (2005) Definition and classification of chronic kidney disease: a position statement from Kidney Disease: Improving Global Outcomes (KDIGO). *Kidney Int* **67**:2089–2100.

Levey A, Stevens L, Schmid C, Zhang Y, Feldman H, Kusek J, Eggers P, Lente F, and Greene T (2006) A New Equation to Estimate Glomerular Filtration Rate. *Ann Intern Med*.

Levin E, Pizarro K, Pang W, Harrison J, and Ramsdell J (2005) Persisting behavioral consequences of prenatal domoic acid exposure in rats. *Neurotoxicol Teratol* **27**:719–725.

Lewitus A, Horner R, Caron D, Garcia-Mendoza E, Hickey B, Hunter M, Huppert D, Kudela R, Langlois G, Largier J, Lessard E, RaLonde R, Rensel J, Strutton P, Trainer V, and Tweddle J (2012) Harmful algal blooms along the North American west coast region: History, trends, causes, and impacts. *Harmful Algae* **19**:133–159.

Lim Y, Kang H, Kim Y, and Choi E (2012) All-trans-retinoic acid inhibits growth of head and neck cancer stem cells by suppression of Wnt/β-catenin pathway. *Eur J Cancer* **48**:3310–8.

Liu Y, Chen H, Wang J, Zhou W, Sun R, and Xia M (2015) Association of serum retinoic acid with hepatic steatosis and liver injury in nonalcoholic fatty liver disease. *Am J Clin Nutr* **102**:130–137, American Society for Nutrition.

Louisse J, Bosgra S, Blaauboer B, Rietjens I and Verwei M (2015) Prediction of in vivo developmental toxicity of all-trans-retinoic acid based on in vitro toxicity data and in silico physiologically based kinetic modeling. *Arch Toxicol* **89**:1135–1148, Springer Berlin Heidelberg.

Lu H, and Rosenbaum S (2014) Developmental pharmacokinetics in pediatric populations. *J Pediatr Pharmacol Ther* **19**:262–76.

Lutz J, Dixit V, Yeung C, Dickmann J, Zelter A, Thatcher J, Nelson W, and Isoherranen N (2009) Expression and functional characterization of cytochrome P450 26A1, a retinoic acid hydroxylase. *Biochem Pharmacol* **77**:258–68.

Lutz J, and Isoherranen N (2012) In vitro-to-in vivo predictions of drug-drug interactions involving multiple reversible inhibitors. *Expert Opin Drug Metab Toxicol* **8**:449–466.

Maharaj A, and Edginton A (2014) Physiologically based pharmacokinetic modeling and simulation in pediatric drug development. *CPT pharmacometrics Syst Pharmacol* **3**:e150.

Feghali M, Venkataramanan R (2015) Pharmacokinetics of drugs in pregnancy. **39**:512–519.

Makimura H, Wei J, Dolan-Looby S, Ricchiuti V, and Grinspoon S (2009) Retinol-binding protein levels are increased in association with gonadotropin levels in healthy women. *Metabolism* **58**:479–487.

Manickavasagar B, McArdle A, Yadav P, Shaw V, Dixon M, Blomhoff R, O'Connor G, Rees L, Ledermann S, van't Hoff W, and Shroff R (2014) Hypervitaminosis A is prevalent in children with CKD and contributes to hypercalcemia. *Pediatr Nephrol* **30**:317–325.

Mariën K (1996) Establishing tolerable dungeness crab (Cancer magister) and razor clam (Siliqua patula) domoic acid contaminant levels. *Environ Health Perspect* **104**:1230–1236.

Matzke G, Aronoff G, Atkinson A, Bennett W, Decker B, Eckardt K, Golper T, Grabe D, Kasiske B, Keller F, Kielstein J, Mehta R, Mueller B, Pasko D, Schaefer F, Sica D, Inker L, Umans J, and Murray P (2011) Drug dosing consideration in patients with acute and chronic kidney disease—a clinical update from Kidney Disease: Improving Global Outcomes (KDIGO). *Kidney Int* **80**:1122–1137.

Maucher J, and Ramsdell J (2007) Maternal-fetal transfer of domoic acid in rats at two gestational time points. *Environ Health Perspect* **115**:1743–1746.

Mccabe R, Hickey B, Kudela R, Lefebvre K, Adams N, Bill B, Gulland F, Thomson R, Cochlan W, and Trainer V (2016) An unprecedented coastwide toxic algal bloom linked to anomalous ocean conditions. 366–376.

Mckibben S, Peterson W, Wood A, Trainer V, Hunter M, and White A (2017) Climatic regulation of the neurotoxin domoic acid. **114**.

Michaëlsson K, Lithell H, Vessby B, and Melhus H (2003) Serum Retinol Levels and the Risk of Fracture. *N Engl J Med* **348**:287–294.

Miller V, Rigas J, Muindi J, Tong W, Venkatraman E, Kris M, and Warrell R (1994) Modulation of all-trans retinoic acid pharmacokinetics by liarozole. *Cancer Chemother Pharmacol* **34**:522–526.

Mills B, Pearce H, Khan O, Jarrett B, Fair D, and Lahvis G (2016) Prenatal domoic acid exposure disrupts mouse pro-social behavior and functional connectivity MRI. *Behav Brain Res* **308**:14–23, Elsevier B.V.

Mills J, Furr H, and Tanumihardjo S (2008) Retinol to Retinol-Binding Protein (RBP) Is Low in Obese Adults due to Elevated apo-RBP. *Exp Biol Med* **233**:1255–1261, SAGE PublicationsSage UK: London, England.

Mitchell A, Gilboa S, Werler M, Kelley K, Louik C, and Hernández-Díaz S (2011) Medication use during pregnancy, with particular focus on prescription drugs: 1976-2008. *Am J Obstet Gynecol* **205**:51.e1-51.e8, Elsevier Inc.

Mos L (2001) Domoic acid: a fascinating marine toxin. *Environ Toxicol Pharmacol* **9**:79–85.

Muindi J, Frankel S, Miller W, Jakubowski A, Scheinberg D, Young C, Dmitrovsky E, and Warrell R (1992) Continuous treatment with all-trans retinoic acid causes a progressive reduction in plasma drug concentrations: implications for relapse and retinoid "resistance" in patients with acute promyelocytic leukemia. *Blood* **79**:299–303, American Society of

Hematology.

Muindi J, Frankel S, Huselton C, DeGrazia F, Garland W a, Young C, and Warrell R (1992) Clinical pharmacology of oral all-trans retinoic acid in patients with acute promyelocytic leukemia. *Cancer Res* **52**:2138–2142.

Muindi J, Young C, and Warrell R (1994) Clinical pharmacology of all-trans retinoic acid. *Leukemia* **8**:1807–1812.

Nakai D, Kumamoto K, Sakikawa C, Kosaka T, and Tokui T (2004) Evaluation of the Protein Binding Ratio of Drugs by A Micro-Scale Ultracentrifugation Method. *J Pharm Sci* **93**:847–854.

Nielsen R, Christensen E, and Birn H (2016) Megalin and cubilin in proximal tubule protein reabsorption: from experimental models to human disease. *Kidney Int* **89**:58–67.

Njar V, Gediya L, Purushottamachar P, Chopra P, Vasaitis T, Khandelwal A, Mehta J, Huynh C, Belosay A, and Patel J (2006) Retinoic acid metabolism blocking agents (RAMBAs) for treatment of cancer and dermatological diseases.

Obi Y, Hamano T, and Isaka Y (2015) Prevalence and prognostic implications of vitamin d deficiency in chronic kidney disease. *Dis Markers* **2015**.

Ozpolat B, Lopez-Berestein G, Adamson P, Fu C, and Williams A (2003) Pharmacokinetics of intravenously administered liposomal all-trans-retinoic acid (atra) and orally administered atra in healthy volunteers. *J Pharm Pharm Sci* **6**:292–301.

Peng J-B, Luo C-H, Wang Y-C, Huang W-H, Chen Y, Zhou H-H, and Tan Z-R (2014) Validation of a Liquid Chromatography-Electrospray Ionization-Tandem Mass Spectrometry Method for Determination of All-Trans Retinoic Acid in Human Plasma and Its Application to a Bioequivalence Study. *Molecules* **19**:1189–1200.

Penniston K, and Tanumihardjo S (2006) The acute and chronic toxic effects of vitamin A 1 – 4. *Am J Clin Nutr* **83**:191–201.

Perl T, Bédard L, Kosatsky T, Hockin J, Todd E, and Remis R (1990) An outbreak of toxic encephalopathy caused by eating mussels contaminated with domoic acid. *N Engl J Med* **322**:1775–80, Massachusetts Medical Society.

Phuphanich S, Scott C, Fischbach A, Langer C, and Yung W (1997) All-trans-retinoic acid: a phase II Radiation Therapy Oncology Group study (RTOG 91-13) in patients with recurrent malignant astrocytoma.

Prasad B, Gaedigk A, Vrana M, Gaedigk R, Leeder JS, Salphati L, Chu X, Xiao G, Hop C, Evers R, Gan L, and Unadkat J (2016) Ontogeny of Hepatic Drug Transporters as Quantified by LC-MS/MS Proteomics. *Clin Pharmacol Ther* **100**:362–370.

Pulido O (2008) Domoic acid toxicologic pathology: A review. *Mar Drugs* **6**:180–219.

Raghu P and Sivakumar B (2004) Interactions amongst plasma retinol-binding protein, transthyretin and their ligands: implications in vitamin A homeostasis and transthyretin amyloidosis. *Biochim Biophys Acta - Proteins Proteomics* **1703**:1–9.

Raila, Willnow T, and Schweigert F (2005) Megalin-mediated reuptake of retinol in the kidneys of mice is essential for vitamin A homeostasis. *J Nutr* **135**:2512–2516.

Regazzi M, Iacona I, Gervasutti C, Lazzarino M, and Toma S (1997) Clinical pharmacokinetics of tretinoin. **32**:382–402.

Rigas J, Miller V, Zhang Z, Klimstra D, Tong W, Kris M, and Warrell R (1996) Metabolic phenotypes of retinoic acid and the risk of lung cancer.

Rigas J, Francis P, Muindi J, Kris M, Huselton C, DeGrazia F, Orazem J, Young C and Warrell R (1993) Constitutive variability in the pharmacokinetics of the natural retinoid, all-trans-retinoic acid, and its modulation by ketoconazole. *J Natl Cancer Inst* **85**:1921–6.

Robertson H, Renton K , Kohn J and White T (1992) Patterns of Fos Expression Suggest Similar Mechanisms of Action for the Excitotoxins Domoic and Kainic Acid. *Ann N Y Acad Sci* **648**:330–334.

Rodgers T, and Rowland M (2006) Physiologically based pharmacokinetic modelling 2: predicting the tissue distribution of acids, very weak bases, neutrals and zwitterions. *J Pharm Sci* **95**:1238–57.

Rowland M, Peck C, and Tucker G (2011) Physiologically-Based Pharmacokinetics in Drug Development and Regulatory Science. *Annu Rev Pharmacol Toxicol* **51**:45–73.

Russo D, Regazzi M, Sacchi S, Visani G, Lazzarino M, Avvisati G, Pelicci P, Dastoli G, Grandi C, Iacona I, Candoni A, Grattoni R, Galieni P, Rupoli S, Liberati A, and Maiolo A (1998) All-trans retinoic acid (ATRA) in patients with chronic myeloid leukemia in the chronic phase. *Leukemia* **12**:449–54.

Rust L, Gulland F, Frame E, and Lefebvre K (2014) Domoic acid in milk of free living California marine mammals indicates lactational exposure occurs. *Mar Mammal Sci* **30**:1272–1278.

Saadeddin A, Torres-Molina F, Cárcel-Trullols J, Araico A and Peris JE (2004) Pharmacokinetics of the time-dependent elimination of all-trans-retinoic acid in rats. *AAPS J* **6**:1–9.

Sager J, Yu J, Ragueneau-majlessi I, and Isoherranen N (2015) Physiologically Based Pharmacokinetic (PBPK) Modeling and Simulation Approaches: A systematic review of published models, applications and model verification. *Dmd*, doi: 10.1124/dmd.115.065920.

Saiag P, Pavlovic M, Clerici T, Feauveau V, Nicolas J, Emile D and Chastang C (1998) Treatment of early AIDS-related Kaposi's sarcoma with oral all-trans-retinoic acid: results of a sequential non-randomized phase II trial. Kaposi's Sarcoma ANRS Study Group. Agence Nationale de Recherches sur le SIDA. *AIDS* **12**:2169–2176.

Sandberg J, Eckhoff C, Nau H, and Slikker W (1994) Pharmacokinetics of 13-cis-, all-trans-, 13-cis-4-oxo-, and all-trans-4-oxo retinoic acid after intravenous administration in the cynomolgus monkey. *Drug Metab Dispos* **22**:154–60.

Scholin C, Gulland F, Doucette G, Benson S, Busman M, Chavez F, Cordaro J, DeLong R, De Vogelaere, Harvey J, Haulena M, Lefebvre K, Lipscomb T, Loscutoff S, Lowenstine L,

Marin R, Miller PE, McLellan W, Moeller P, Powell C, Rowles T, Silvagni P, Silver M, Spraker T, Trainer V, and Van Dolah F (2000) Mortality of sea lions along the central California coast linked to a toxic diatom bloom. *Nature* **403**:80–84.

Shah V, Midha K, Findlay J, Hill H, Hulse J, McGilveray I, McKay G, Miller K, Patnaik R, Powell M, Tonelli A, Viswanathan C, and Yacobi A (2000) Bioanalytical method validation — A revisit with a decade of progress. *Pharm Res* **17**:1551–1557.

Shirasaka Y, Sager J, Lutz J, Davis C, and Isoherranen N (2013) Inhibition of CYP2C19 and CYP3A4 by omeprazole metabolites and their contribution to drug-drug interactionss. *Drug Metab Dispos* **41**:1414–1424.

Silvagni P, Lowenstine L, Spraker T, Lipscomb T, and Gulland F (2005) Pathology of domoic acid toxicity in California sea lions (Zalophus californianus). *Vet Pathol* **42**:184–91, SAGE PublicationsSage CA: Los Angeles, CA.

Suzuki C, and Hierlihy S (1993) Renal clearance of domoic acid in the rat. *Food Chem Toxicol* **31**:701–706.

Takemoto F, Shinki T, Yokoyama K, Inokami T, Hara S, Yamada A, Kurokawa K, and Uchida S (2003) Gene expression of vitamin D hydroxylase and megalin in the remnant kidney of nephrectomized rats. *Kidney Int* **64**:414–420.

Tanemura K, Igarashi K, Matsugami T, Aisaki K, Kitajima S, and Kanno J (2009) Intrauterine environment-genome interaction and children's development (2): Brain structure impairment and behavioral disturbance induced in male mice offspring by a single intraperitoneal administration of domoic acid (DA) to their dams. *J Toxicol Sci* **34 Suppl 2**:SP279-86.

Tasnif Y, Morado J, and Hebert M (2016) Pregnancy-related pharmacokinetic changes. *Clin Pharmacol Ther* **100**:53–62.

Tay S, Dickmann L, Dixit V, and Isoherranen N (2010) A comparison of the roles of peroxisome proliferator-activated receptor and retinoic acid receptor on CYP26 regulation. *Mol Pharmacol* **77**:218–27.

Thatcher J, Buttrick B, Shaffer S, Shimshoni J, Goodlett D, Nelson W, and Isoherranen N (2011) Substrate specificity and ligand interactions of CYP26A1, the human liver retinoic acid hydroxylase. *Mol Pharmacol* **80**:228–39.

Thatcher J, and Isoherranen N (2009) The role of CYP26 enzymes in retinoic acid clearance. *Expert Opin Drug Metab Toxicol* **5**:875–886.

Thatcher J, Zelter A, and Isoherranen N (2010) The relative importance of CYP26A1 in hepatic clearance of all-trans retinoic acid. *Biochem Pharmacol* **80**:903–12.

Thomas S and Yates L (2012) Prescribing without evidence - pregnancy. *Br J Clin Pharmacol* **74**:691–697.

Thudi N, Shrivastav V, Monif T, Khuroo A, Gurule S, Partani P, Tandon M, and Mathur R (2011) Pharmacokinetic and bioequivalence study of endogenous compound tretinoin 10 mg capsules in healthy volunteers by base line correction approach. *Clin Res Regul Aff* **28**:68–

73, Taylor & Francis.

Todd E (1993) Domoic acid and amnesic shellfish poisoning - a review. *J Food Prot* **56**:69–83.

Topletz A, Thatcher J, Zelter A, Lutz J, Tay S, Nelson W, and Isoherranen N (2012) Comparison of the function and expression of CYP26A1 and CYP26B1, the two retinoic acid hydroxylases. *Biochem Pharmacol* **83**:149–63.

Topletz A, Tripathy S, Foti R, Shimshoni J, Nelson W, and Isoherranen N (2015) Induction of CYP26A1 by metabolites of retinoic acid: evidence that CYP26A1 is an important enzyme in the elimination of active retinoids. *Mol Pharmacol* **87**:430–41.

Truelove J, Mueller R, Pulido O, and Iverson F (1996) Subchronic toxicity study of domoic acid in the rat. *Food Chem Toxicol* **34**:525–529.

Truelove J, Mueller R, Pulido O, Martin L, Fernie S, and Iverson F (1997) 30-day oral toxicity study of domoic acid in cynomolgus monkeys: Lack of overt toxicity at doses approaching the acute toxic dose. *Nat Toxins* **5**:111–114.

Truelove and Iverson (1994) Serum domoic acid clearance and clinical observations in the cynomolgus monkey and Sprague-Dawley rat following a single i.v. dose. *Bull Env Contam Toxicol* **52**:479–86.

Tsutsumi C, Okuno M, Tannous L, Piantedosi R, Allan M, Goodman D, and Blaner W (1992) Retinoids and retinoid-binding protein expression in rat adipocytes. *J Biol Chem* **267**:1805–1810.

US Renal Data System, USRDS 2013 Annual Data Report: Atlas of End-Stage Renal Disease in the United States (n.d.) . *Natl Institutes Heal Natl Inst Diabetes Dig Kidney Dis Bethesda, MD*.

Velenosi T, Feere D, Sohi G, Hardy D, and Urquhart B (2014) Decreased nuclear receptor activity and epigenetic modulation associates with down-regulation of hepatic drug-metabolizing enzymes in chronic kidney disease. *FASEB J* **28**:5388–97, Federation of American Societies for Experimental Biology.

Vera-avila L, Marín-pérez D, and Covarrubias-herrera R (2011) Trace Level Determination of Domoic Acid in Seawater by Off-line / on-line Solid-phase Extraction Coupled to HPLC-UV. *J Mex Chem Soc* **55**:65–71.

Verbeeck R (2008) Pharmacokinetics and dosage adjustment in patients with renal dysfunction. *Eur J Clin Pharmacol* **12**:1147–61.

Verbeeck R, and Musuamba F (2009) Pharmacokinetics and dosage adjustment in patients with renal dysfunction. *Eur J Clin Pharmacol* **65**:757–773.

Viswanathan C, Bansal S, Booth B, DeStefano A, Rose M, Sailstad J, Shah V, Skelly J, Swann P, and Weiner R (2007) Quantitative bioanalytical methods validation and implementation: Best practices for chromatographic and ligand binding assays. *Pharm Res* **24**:1962–1973.

Wagner C, Zhao P, Pan Y, Hsu V, Grillo J, Huang S, and Sinha V (2015) Application of Physiologically Based Pharmacokinetic (PBPK) Modeling to Support Dose Selection:

Report of an FDA Public Workshop on PBPK. *CPT Pharmacometrics Syst Pharmacol* **433**:226–230.

Walter J, Leek D, and Falk M (1992) NMR study of the protonation of domoic acid. *Can J Chem* **70**:1156–1161.

Wang C, Campbell S, Furner R, and Hill D (1980) Disposition of all-trans- and 13-cis-retinoic acids and n- hydroxyethylretinamide in mice after intravenous administration. *Drug Metab Dispos* **8**:8–11.

Wang Z, Maucher-Fuquay J, Fire S, Mikulski C, Haynes B, Doucette G, and Ramsdell J (2012) Optimization of solid-phase extraction and liquid chromatography-tandem mass spectrometry for the determination of domoic acid in seawater, phytoplankton, and mammalian fluids and tissues. *Anal Chim Acta* **715**:71–79, Elsevier B.V.

Yang Q, Graham T, Mody N, Preitner F, Peroni O, Zabolotny J, Kotani K, Quadro L, and Kahn B (2005) Serum retinol binding protein 4 contributes to insulin resistance in obesity and type 2 diabetes. *Nature* **436**:356–362.

Zuloaga D, Lahvis G, Mills B, Pearce H, Turner J, and Raber J (2016) Fetal domoic acid exposure affects lateral amygdala neurons, diminishes social investigation and alters sensory-motor gating. *Neurotoxicology* **53**:132–140, Elsevier B.V.

VITA

Jing Jing was born in Luoyang, China in 1987. She obtained her Bachelor of Science in Biotechnology from Henan Agricultural University, Zhengzhou, China in 2010, and then received her Master of Science in Biochemistry from George Washington University, Washington DC in 2012. She joined the Department of Pharmaceutics at the University of Washington in 2012, and then worked as a doctoral student under the guidance of Dr. Nina Isoherranen.